PHYSIOLOGICAL RADAR SYSTEM FOR DIAGNOSING SLEEP DISORDERS

A DISSERTATION SUBMITTED TO THE GRADUATE DIVISION OF THE UNIVERSITY OF HAWAII AT MANOA IN PARTIAL FULFILLMENT OF THE REQUIREMENTS FOR THE DEGREE OF

DOCTOR OF PHILOSOPHY
IN
ELECTRICAL ENGINEERING

AUGUST 2014

By
Mehran Baboli

Dissertation committee:
Victor M. Lubecke, Chairperson
Olga Borić-Lubecke
Aaron Ohta
David Garmire
Marguerite Butler

We certify that we have read this dissertation and that, in our opinion, it is satisfactory in scope and quality as a dissertation for the degree of Doctor of Philosophy in Electrical Engineering.

Dissertation Committee:

Victor M. Lubecke, Chairperson _____

Olga Boric-Lubecke, _____

David G. Garmire _____

Aaron Ohta _____

Marguerite Butler _____

To my parents

Acknowledgements

I would like to express my deep appreciation and gratitude to my advisor, Dr. Victor M. Lubecke, for the patient guidance and mentorship he provided to me, all the way from the first day I applied to the PhD program in Electrical Engineering, through to completion of this degree. I am truly fortunate to have had the opportunity to work closely with him. I would also like to thank my committee members, Olga Borić-Lubecke, Aaron Ohta, David Garmire, and Marguerite Butler for the friendly guidance, thought provoking suggestions, and the general collegiality that each of them offered to me. I'd also like to recognize Dr. Bruce Soll for the contributions and help with the medical and biological aspects of my research as well as the assistance of sleep center technicians, Kristin Une. Thanks to my colleagues at our lab for their help and fruitful technical discussions throughout my research: Aditya, Xiaomeng, Noah, Ehsan, Bryson, Ehsaneh, Ashikur, Bob and Chenyan. Finally, I'd like to thank my friends Shaun Kindred and Lisa Widdison for their help.

Abstract

Sleep disorders are a class of medical disorders where typical sleep behavior is disrupted or abnormal, which leads to physical, mental, and emotional dysfunction. Often, sleep disorders go undiagnosed at the source of these symptoms. Sleep apnea and hypopnea are the most common sleep disorders. They are classified by a recurring interruption of breathing during sleep or abnormally shallow breathing as a result of the obstruction of the upper airway or neurological malfunction. Statistics show that about 15 million Americans suffer from obstructive sleep apnea (OSA), one type of sleep apnea. Currently, polysomnography (PSG) is considered the gold standard test for detecting sleep disorders. During this test a subject with a suspected disorder spends a night in a sleep lab, and several physiological parameters are recorded during their sleep using sensors attached to the body. All of this makes PSG time consuming, complicated, inconvenient, and expensive. Therefore, the development of more simple, accurate, comfortable, and affordable devices for sleep monitoring is desired to improve the efficacy of sleep tests and improve accessibility. In this dissertation, a non-contact physiological radar monitoring system (PRMS) is introduced for sleep disorder monitoring. This PRMS utilizes continuous-wave Doppler radar and a real-time algorithm which recognizes paradoxical breathing to diagnose OSA and hypopnea. The PRMS was integrated with a standard PSG system to evaluate the efficacy for supplementing or replacing a standard PSG test for some applications. A clinical study was carried out using the PRMS on 10 subjects with known sleep apnea. In this study, the PRMS accurately diagnosed the occurrence of either an OSA or hypopnea event, but was less effective for differentiating between them. As a compliment to a standard PSG test, the PRMS results provided a clear way to quickly identify the occurrence of an obstructive apnea/hypopnea event, with the PSG measurements then used to further analyze the event. Recognition of the occurrence of a general obstructive sleep disorders also makes the system attractive as a stand-alone screening device that could be conveniently used, perhaps at home, on a broad population to identify patients that should be considered for further sleep medicine treatment.

Contents

List of Figures

List of Tables

Chapter 1

Overview

In remote health care, research in the design of affordable and reliable non-contact physiological monitoring systems is a very important goal for extending monitoring beyond the sleep clinic. Remote monitoring and analysing of physiological parameters allows early detection of critical health conditions and as result can decreases the number of visits to hospital emergency rooms and to reduce the duration of hospital stays [1].

1.1. Research Problem and Scope

With about 15 million Americans suffering from obstructive sleep apnea [1] it is one of the most common health disorders. Studies show a relationship between sleep apnea and cardiovascular diseases. Many patients with heart failure have central apnea [2-7]. Obstructive sleep apnea is commonly seen in patients with hypertension, atrial fibrillation, coronary artery disease, and stroke [2, 8-13]. Hence, diagnosing and treating sleep apnea more effectively could play an important role in preventing cardiovascular disease. Development of a remote non-invasive sleep monitoring system to automatically detect sleep apnea could be a very valuable contribution to improvement of healthcare cost and efficacy.

1.2. Research Motivations

Polysomnography (PSG) is the gold standard, most accurate test, for detecting sleep apnea. A complete PSG test includes simultaneous monitoring of respiratory signals and electrophysiological signals such as electrocardiogram (ECG) and electroencephalogram (EEG). The test lasts a whole night and patient must stay in a specially-equipped sleep laboratory in which multiple different sensors are attached to a patient to measure different physiological parameters. All of this makes PSG a complicated, expensive, and time consuming procedure [14] which leads to diagnosis and treatment of only a small population of sleep apnea cases. Hence,

developing a new simple, accurate and cheap device for sleep monitoring is needed and can help diagnosing more patients. In this dissertation, a non-contact physiological radar monitoring system (PRMS) is designed, based on CW Doppler radar, for sleep disorder monitoring. The hardware system includes radars with two different frequencies. Real time sleep monitoring software is also developed to accompany the hardware. The proposed system potentially can be utilized in sleep centers to augment current monitoring devices. It also has the potential to serve as a simple and unique portable monitoring system to be used at home. Since it requires no patient contact it may be less invasive and more convenient than current portable systems that require contact sensors.

1.3. Scope of this dissertation

Chapter 2 explains the theory behind Doppler radar and its application in physiological monitoring. The effect of radar's parameters on accuracy of measurement in physiological monitoring is investigated and the optimum design for sleep monitoring application is presented.

A background about sleep disorder monitoring methods is described in Chapter 4. Next, the structure of a PRMS is presented based on Doppler radar structure. A new sleep disorder monitoring algorithm is presented which is able to track respirator motion and detect apnea and hypopnea using the Doppler radar. A method of integrating the outputs of the PRMS to a gold standard monitoring system is also explained.

The experimental setup and protocol as well as relevant subject physical characteristics are outlined in Chapter 5, following the results of using the PRMS along with a Sandman Elite system as a gold standard to detect apnea and hypopnea.

Chapter 6 describes the steps of developing scoring rules for the PRMS and gold standard. After that, the results of comparing the two systems are presented.

Finally a Summary of the results and future work are outlined in Chapter 7.

Chapter 2

Doppler for physiological measurement

There is currently a need in medicine for detecting vital signs such as heart beat and respiration without directly contacting the patient. There are situations where physically contacting a patient is difficult or unwanted – where it is preferable to avoid problems of skin irritation, airway restriction, and use of electrodes. Some potential applications of remote physiological sensing are rescue operations, burn patients, and monitoring patients at home, for fatigue, or for neonatal purposes. Measurements of cardiopulmonary movements in men and animals was proven successful with microwaves in the 1970's [15]. There have been great advances in the medical use of microwave monitoring since that time [16-23].Yanming *et al.*[16] presented a low power Ka-band Doppler to detect a heartbeat. Their results show an accuracy of more than 80% at a distance of 2m. In [17], Li *et al.* described development of non-contact physiological motion sensor chips using CMOS technology based on a design buit initially at Bell lab in the early 2000's [24-27] for military and commercial applications. In another work, Mostov *et al.* [22] successfully measured human heart and respiration rate using short range FM radar. Very recently, Qiao *et al.* [23] proposed a non-contact physiological monitoring system to measure respiratory and heart rate by means of a 24GHz CW Doppler radar.

However, the application of microwaves for long-term monitoring is not yet well developed, particularly for cardiopulmonary measures beyond rate. The following chapter will cover the fundamentals of radar, techniques for demodulation of a quadrature Doppler radar signal, the use of Doppler radar for sensing physiological parameters, and the specific radar architecture used for this sensing research.

2.1. Radar System

Radar is the acronym for RAdio Detection and Ranging, which highlights the original two main purposes of radio wave reflectometry – detecting and locating a target. It was

originally developed as a device to detect the approach of enemy aircraft and antiaircraft weapons during WWII. RADAR was the code word officially adopted by the United State Navy in November 1940 [28]. While having many different names, such as radio position finding, RDF (radio direction finding), and DEM (Detection Electromagn Etique), RADAR was adopted nearly universally in the post-war years. Radar today is used much more broadly and in more sophisticated applications such as identifying, producing images of, and tracking objects such as military weapons, wildlife, and topography [29].

Simply, radar is a transmitter that sends out a signal in the radar wavelength, which then scatters off or around all objects it encounters. Some of this scattered energy returns to the receiver – usually beside the transmitter. Then, this signal is processed to filter out the noise using electronic signal processing with hardware and data processing with computer software. The distance to the object is found by measuring the time taken for the radar signal to travel to the object from the transmitting antenna and return to the receiver. Direction of the object is found by the direction of the arrival of the scattered energy onto the receiver. If the target or the origins of the radar signal are moving in relation to one another, there is a shift in the frequency of the reflected wave – called the Doppler effect – which can be used to measure the target's relative velocity and separate moving and stationary objects.

Depending on the system hardware and type of radar signal, it may be possible to detect the range, angle, size, shape, and linear and rotational velocity of the target [30]. However, all of these features can not necessarily be detected at the same time as different radar topologies serve different purposes.

2.2. Radar Equation

The radar equation [31] shows the dependency of the performance of the radar as well as its working range to the radar parameters such as the transmitter and receiver antenna gains, power and pattern. This equation also shows the effect of the environment (e.g. noise) and the target (e.g by its cross section) on the radar performance.

As mentioned before radar detects the objects by transmitting energy to the environment and receive the partial of that energy which is scatter back from the target. Hence; to derive the simplest form of radar equation we start with the transmitted power radiated from the antenna.

Assuming that this power is radiated isotropically from the antenna, the power density at distance R from the radar is calculated by [32]:

$$P_D = \frac{P_t}{4\pi R^2} \tag{2-1}$$

Where P_t is the transmitted power and $4\pi R^2$ is the area of a sphere of radius R.

If the antenna is directive, then the Eq. (2-1) becomes [32]:

$$PF_t = \frac{P_t G_t}{4\pi R^2} \tag{2-2}$$

Where G is the transmitting gain.

The amount of power that scatters back from the target to the radar's direction depends on the radar cross section (RCS) of the target which is defined as [29]:

$$\sigma = (\textit{Project cross section}) \times (\textit{Reflectivity}) \times (\textit{Directivity}) \tag{2-3}$$

RCS depends on different parameters of the object, such as its size and geometry and it position and angular orientation relative to the radar antennas.

The power received by antenna is then given by [32]:

$$P_r = \frac{P_t G_t}{4\pi R^2} \cdot \frac{\sigma}{4\pi R^2} A_e = \frac{P_t G_t \sigma \ A_e}{(4\pi)^2 R^4} \tag{2-4}$$

Where A_e is the effective area of the receiving antenna.

From the Eq. 2-4 the maximum distance in which the target is detectable cab be calculated as [32]:

$$R_{\max} = \left(\frac{P_t G_t \sigma A_e}{(4\pi)^2 S_{\min}} \right)^{\frac{1}{4}} \tag{2-5}$$

Where S_{min} is the minimum detectable signal at the receiver.

Eq. 2-5 is the simplest form of the radar equation. All the parameters in this equation is related to the radar design except the radar cross section which is depended to the target.

2.3. Radar Topologies

2.3.1. Continuous-wave (CW) Radar

CW radar uses the Doppler Effect to detect a moving target. It transmits a continuous wave signal with constant energy. The frequency of the received signal scattered back from the target has a shift which is proportional to the target velocity. Assuming the distance between the target and the radar is *R,* The phase changes in the propagation path is calculated by [28]:

$$\phi = 2\pi \times \frac{2R}{\lambda} = \frac{4\pi R}{\lambda} \tag{2-6}$$

Where, λ is the transmitted signal wavelength.

The rate change of the phase as a result of moving target (i.e variable *R*) is given by:

$$\omega_d = \frac{d\phi}{dt} = \frac{4\pi}{\lambda}.\frac{dR}{t} = \frac{4\pi v_r}{\lambda} = 2\pi f_d \tag{2-7}$$

Where $v_r = \frac{dR}{dt}$ is the radial velocity of the target [30].

The Doppler frequency shift can be calculated the angular frequency:

$$f_d = \frac{\omega_d}{2\pi} = \frac{2v_r}{\lambda} = \frac{2f_t v_r}{c} \tag{2-8}$$

Where f_t is the frequency of transmitted signal, c is the velocity of wave propagation [30].

Figure 2-1 illustrates a homodyne single-channel CW Doppler radar system. The transmitted signal can be represented as:

$$S_t(t) = \cos(2\pi f(t) + \varphi(t)) \tag{2-9}$$

Where $\varphi(t)$ is the phase noise of the oscillator. Assuming that the target nominal distance between the target and the radar is d_0 and target has a time varying displacement (x(t)).In physiological monitoring $x(t)$ could be the chest displacement of the target with varies with time because of respirations.

$$R(t) = d_0 + x(t) \tag{2-10}$$

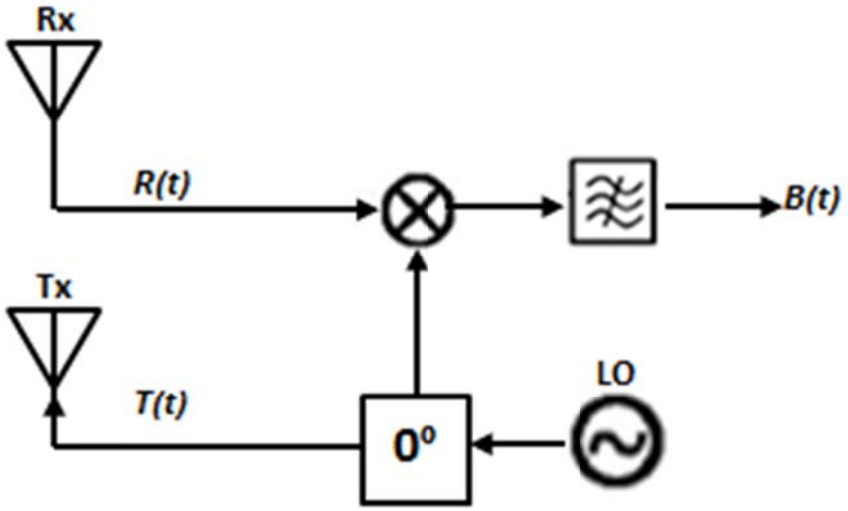

Figure 2-1 A single channel doppler radar system

Having the Doppler phase shift from the moving target (Eq. 2-6), the received signal becomes:

$$\begin{aligned} S_r(t) &= A_R \cos(2\pi f(t) + \frac{4\pi R(t)}{\lambda} + \varphi(t) + \phi_0) \\ &= A_R \cos(2\pi f(t) + \frac{4\pi(d_0 + x(t))}{\lambda} + \varphi(t) + \phi_0) \\ &= A_R \cos\left[2\pi f t - \frac{4\pi d_0}{\lambda} - \frac{4\pi x(t)}{\lambda} + \varphi(t) + \phi_0\right] \end{aligned} \tag{2-11}$$

Where A_R is the amplitude attenuation and ϕ_0 is the constant phase shift.

A homodyne receiver (a.k.a. direct-conversion or zero-IF receiver) is likely the simplest receiver architecture that can be used for any purpose. It mixes the received signal $S_r(t)$ with a local oscillator at the frequency of the carrier. The Radio Frequency (RF) is therefore converted directly to baseband. A heterodyne receiver is another commonly used architecture. It mixes the received signal with a local oscillator (LO) at a different frequency. Unlike the homodyne receiver, which converts the signal directly to baseband, the information is modulated on a non-zero intermediate frequency (IF). The homodyne receiver has been selected for this study because of its simplicity [29].

The information about the periodic motion of the target can be demodulated from a CW Doppler radar with a homodyne receiver. The baseband signal after demodulation is given by:

$$B(t) = A_B \cos\left[\phi t - \frac{4\pi x(t)}{\lambda} + \Delta\varphi(t)\right] \tag{2-12}$$

Where $A_B = A_R\sqrt{G_{RX}G_{CL}}$ represents the baseband amplitude with the receiver gain of GRX and the mixer conversion gain of G_{CL}. $\Delta\varphi(t)$ is the residue phase noise and $\phi = \frac{4\pi d_0}{\lambda} - \phi_0$ is the constant phase shift due to the nominal distance to the target [29].

A continuous-wave (CW) system can detect moving targets and measure only the target velocity. Adding FM modulation makes the radar system capable of detecting the range by measuring the propagation delay at the signal source [32, 33].

The transmitted signal of a FMCW radar is given by [33]:

$$S_t(t) = A_t \cos(2\pi f(t)t) = A_t \cos(2\pi f_0 + 2\pi k t^2) \tag{2-13}$$

Where A_t is the amplitude and $f(t) = f_0 + kt$ is the frequency modulated term.

The received signal is calculated by:

$$S_r(t) = A_r \cos(2\pi(f_0 + f_d)(t - \Delta t) + 2\pi k(t - \Delta t)^2) \tag{2-14}$$

Where Δt is the propagation delay and f_d is Doppler shift [33].

The received signal is converted to the baseband using a down-conversion mixer. Target range and velocity is the calculated using fast Fourier transform from the intermediate frequency (IF) [33].

2.3.2. Pulsed radar

Pulsed radar is another type that allows transmitting and receiving radar signals at different times [34]. It is typically used in situations where the return signal is much smaller than the transmitted one or when the peak power of the transmitted signal is much higher than the average [32]. Pulsed radar can be further subdivided into three groups:

1- pulse compression, moving target indicator (MTI),
2- pulse Doppler radar [34].

2.4. System Design considerations

There are two significant limitations of directly converting a single-channel radar [35].

1- Intrinsic channel noise and extrinsic artifacts from body movements and fluctuations in clutter in the surrounding environment degrade the performance and reliability of this system.
2- The occurrence of dead spots because of the null points of the standing wave pattern.

The noise problems of the former may be partially lessened by using clutter cancellation circuitry [36] or extracting the signal from noisy measurements [37] or other appropriate signal processing methods. The latter problem may be lessened by avoiding placing the detector in a null spot in relation to the target. However, a quadrature detection scheme is a much more reliable way to eliminate the dead spot.

In the following sections the structure of quadrature receiver system and the demodulation techniques on its base-band signal are explained. Then the effect of radar parameters on measuring the respiratory signals is investigated.

2.4.1. Quadrature receiver system

This structure splits the received signal into two orthogonal components, which when analyzed together, helps to eliminate the null point. According to the baseband output equation

above in Eq. 2-12 if $x(t) << \lambda$ and ϕ is an odd multiple of $\pi/2$, then the small angle approximation will be valid. The baseband output equation could then be simplified to [29]:

$$B(t) \approx A_B\left(\frac{4\pi x(t)}{\lambda} + \Delta\varphi(t)\right) \tag{2-15}$$

This is the case where the optimum phase demodulation sensitivity can be achieved. The baseband output is proportional to sum of the target's periodic displacement *x(t)*, and the residual phase noise $\Delta\varphi(t)$.

If ϕ is an odd multiple of π, then the baseband output could then be approximated to:

$$B(t) \approx A_B\left(1 - \left[\frac{4\pi x(t)}{\lambda} + \Delta\varphi(t)\right]^2\right) \tag{2-16}$$

In this case, the baseband output is no longer linearly proportional to the time-varying displacement and the sensitivity of the receiver decreases. As shown in [38] this squared relationship affects the perceived frequency of the target's movements, which can result in error above 100%.

The null point occurs when the received signals are either in phase or 180^o out of phase. Because of the constant phase shift θ, depends on the variable d_0, the null point occurs at every quarter wavelength from the radar. The antithesis of the null point, where the amplitude of the signal is zero is the optimal point, where the amplitude of the signal at the receiver is the same as the source reflection from the target. These two wave types alternate at every eighth wavelength to each other or every quarter wavelength to themselves. As an example, a radio frequency signal of 2.4GHz will cycle between an optimal to null state every 1.5625cm. As such, the quadrature receiver is able to improve this radar sensitivity problem. The main problem with a single channel radar system – as opposed to a quadrature radar system – is the variation in the accuracy of phase demodulation depending on the range of the radar to its target. The baseband signal is proportional to the target motion at the optimal point (Eq. 2-15) and proportional to the square of the target motion (Eq. 2-16) at the null point. This problem created by the difference in these two

equations could be avoided by using the quadrature detection scheme. It has two receiver chains with the local oscillator separated into two signals with a 90^o phase difference (Figure 2-2). This scheme ensures that every output has at least one utilizable point, regardless of the presence of a null point. Two LO signals differ in phase by $\pi/2$.

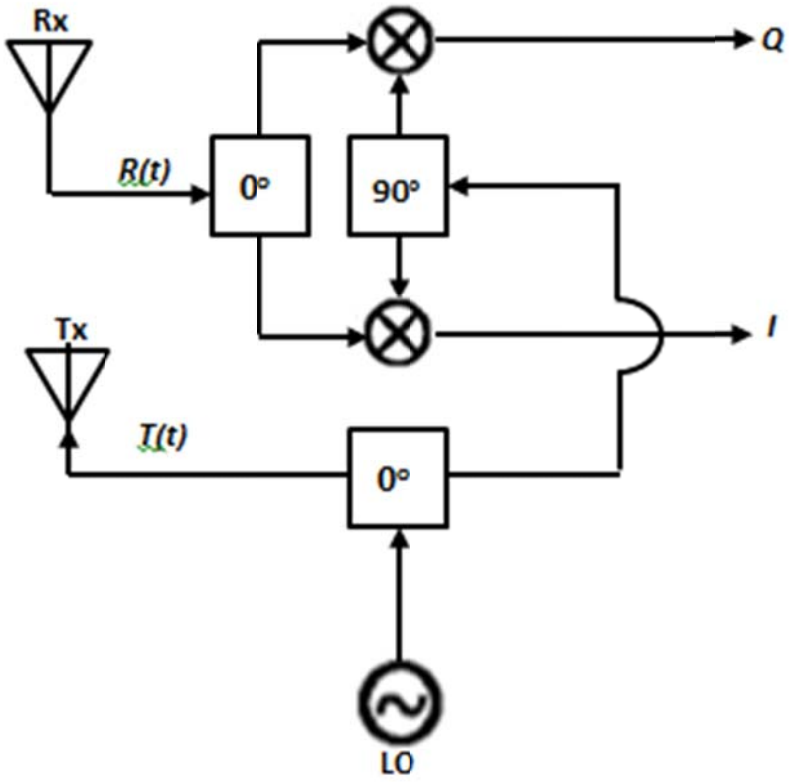

Figure 2-2 A quadrature CW Doppler radar system.

Thus, the two receiver baseband outputs are given by [29]:

$$I(t) = A_B \cos\left(\phi + \frac{\pi}{4} + \frac{4\pi x(t)}{\lambda} + \Delta\varphi(t)\right) \tag{2-17}$$

and

$$Q(t) = A_B \cos\left(\phi - \frac{\pi}{4} + \frac{4\pi x(t)}{\lambda} + \Delta\varphi(t)\right) = A_B \sin\left(\phi + \frac{\pi}{4} + \frac{4\pi x(t)}{\lambda} + \Delta\varphi(t)\right) \tag{2-18}$$

The signal output *I* is at a null point when $\phi + \frac{\pi}{4}$ is an integer multiple of π. On the other hand, the output *Q* is at an optimum point because $\phi - \frac{\pi}{4}$ is an odd multiple of π/2. The quadrature receiver gives the ability to avoid null phase demodulation points by choosing the larger of the two signals, which will always be at the optimal point when a null point is present. The worst case occurs when ϕ is an integer multiple of π, making both $\phi + \frac{\pi}{4}$ (for the null point) and $\phi - \frac{\pi}{4}$ (for the optimum point) odd multiples of π/4. Neither *I* nor *Q* is at an optimum phase demodulation point here and the baseband outputs become:

$$I(t) = Q(t)$$
$$\approx \pm A_B \left[\frac{1}{\sqrt{2}} - \frac{1}{\sqrt{2}} \left[\left(\frac{4\pi x(t)}{\lambda} + \Delta\varphi(t) \right) + \left(\frac{4\pi x(t)}{\lambda} + \Delta\varphi(t) \right)^2 \right] \right] \quad (2\text{-}19)$$

However, if $x(t) << \lambda$, the linear term is much larger than the squared term and so the target motion can still be detected [29].

2.4.2. Demodulation Methods

When the baseband signal is obtained by the quadrature receiver, it can be further processed to give information about the physiological parameters such as respiration rate and heart rate by analyzing the subject's chest displacement. These parameters change over time so it is imperative to track them over time. Baseband signals I and Q can be processed individually, which risks getting a null point, or combined. Various methods have been proposed on how to combine I and Q channels which includes linear (or Eigen) demodulation [29] Non-linear (or arctangent) demodulation [36] and complex demodulation [39] Linear demodulation is a method that transposes multi-dimensional data into a single dimension by suppressing redundant information and maximizing variance. As linear demodulation is usually used to simplify multi-dimensional data to lower dimensions for analysis, it is a helpful way to identify patterns in data

and make the similarities and differences in the data more apparent. Since graphical representation of high dimensional data is often unavailable and difficult to implement, linear demodulation is a useful tool for analyzing data. Its algorithm can be fundamentally summarized as the following:

1. Subtract the mean from each of the data dimensions.
2. Calculate the covariance matrix.
3. Calculate the eigenvectors and eigenvalues of the covariance matrix.
4. Choose the components to form a feature vector.

Taking the quadrature receiver as an example, any and all dc offsets are removed from the data, and the covariance matrix between the I and Q channels becomes apparent. The arc between I and Q is rotated so that it will parallel the Q-axis by multiplying the received signal by the transpose of the covariance matrix's eigenvector. After this rotation, the Q-component will always be at an optimum point and the I-component will always be at a null point. This allows the Q-component to be used as the demodulation signal. The benefit of this technique is that the strongest signal pattern will be selected. However, there is a always a chance that the strongest signal could be noise or motion artifacts rather than the desired physiological signatures, and when this is the case, the output of the Eigen decomposition will be distorted. One additional advantage of linear modulation, however, is that sudden changes in the eigenvector and eigenvalue can be used to identify motion artifacts.

The next type of demodulation – non-linear or arctangent demodulation – uses the features of the quadrature receiver. The phase information is recovered directly using both *I* and *Q* outputs [29]:

$$\theta(t) = \arctan\left(\frac{I(t)}{Q(t)}\right) = \arctan\left(\frac{A_B \sin\left(\phi + \frac{\pi}{4} + \frac{4\pi x(t)}{\lambda} + \Delta\varphi(t)\right)}{A_B \cos\left(\phi + \frac{\pi}{4} + \frac{4\pi x(t)}{\lambda} + \Delta\varphi(t)\right)}\right) \tag{2-20}$$

$$\phi(t) = \phi + \frac{\pi}{4} + \frac{4\pi x(t)}{\lambda} + \delta\varphi(t) \tag{2-21}$$

The phase information is demodulated without using the small angle approximation, which is a more reliable than the linear method. However, dc offsets make the arctangent demodulation difficult to use reliably. To be applied correctly, this demodulation method requires methods to accurately cancel out the clutter created by the dc offsets or by using center tracking dc information estimation [36].

In the case that the channels are balanced, there is no signal distortion, and there is only one source of periodic motion, the complex plot of *Q* versus *I* channel forms an arc on a circle with a radius of A_B and its center offsets by the dc offset in each channel. The dc offset is then can be cancelled using the center tracking method in [36]. This allows accurate signal demodulation. When the dc components of the signal are eliminated with analog high-pass filtration, the phase delay inserted into the system by the filter will also cause signal distortion. If the target motion signal *x(t)* is sinusoidal, such as a respiratory signal, after the high-pass filter is applied, the chest is at the maximum displacement, and Eq. 2-20 and 2-21 becomes:

$$I(t) = \left[A_B \cos\left(\phi + \frac{\pi}{4} + \frac{4\pi}{\lambda} x(t)\middle|\max/\min \right) - \overline{I(t)} \right] . e^{-t/\tau} \tag{2-22}$$

$$Q(t) = \left[A_B \sin\left(\phi + \frac{\pi}{4} + \frac{4\pi}{\lambda} x(t)\middle|\max/\min \right) - \overline{Q(t)} \right] . e^{-t/\tau} \tag{2-23}$$

Assuming the sinusoidal breathing the means of the baseband outputs, $\overline{I(t)}$ and $\overline{Q(t)}$ can be represented as $A_B.\cos\phi$ and $A_B.\sin\phi$ respectively. The equations then become [29]:

$$I(t) = \left[A_B \cos\left(\phi + \frac{\pi}{4} + \frac{4\pi}{\lambda} x(t)\middle|\max/\min \right) - \cos\phi \right] . e^{-t/\tau} \tag{2-24}$$

$$I(t) = -2A_B \sin\left(\phi + \frac{2\pi}{\lambda} x(t)\middle|\max/\min \right) . \sin\left(\frac{2\pi}{\lambda} x(t)\middle|\max/\min \right) . e^{-t/\tau} \tag{2-25}$$

$$Q(t) = \left[A_B \sin\left(\phi + \frac{\pi}{4} + \frac{4\pi}{\lambda} x(t)\middle|\max/\min \right) - \sin\phi \right] . . e^{-t/\tau} \tag{2-26}$$

$$Q(t) = 2A_B \cos\left(\phi + \frac{2\pi}{\lambda} x(t)\Big|\max/\min\right).\sin\left(\frac{2\pi}{\lambda} x(t)\Big|\max/\min\right).e^{-t/\tau} \tag{2-27}$$

These equations are based on the assumption that the exponential decrease only occurs at the maximum and minimum of the chest displacement. However, because the lower frequency signals are also affected by the filters, they are not entirely accurate. By dividing Eq. 2-25 by Eq. 2-27 we have:

$$Q(t) = \arctan\left(\phi + \frac{2\pi}{\lambda} x(t)\Big|\max/\min\right).I(t) \tag{2-28}$$

Eq. 2-28 shows that the baseband outputs after applying the high-pass filter are a linear combination with a constant slope.

If the length of arc forming by plotting *Q*(t) versus *I(t)* is small, it can be approximated with a linear line using the linear demodulation method. If the signal to noise ratio is low (giving a thicker arc) or when ac coupling is used, the signal traces can fit onto a single axis, which may allow it to be more accurate.

For the long-term measurement of Doppler radar, dc drift poses a significant and common problem. While it could be overcome using the techniques in [40] in this study the signal was ac-coupled to increase resolution and decrease drift. However, when using such a method, the lack of dc information makes it impossible to use the arctangent method to combine *I* and *Q* for demodulation. In general, linear demodulation is better than arctangent methods when the arc length is low.

The last demodulation technique is to consider *I* and *Q* data together as a complex signal and perform signal processing on that signal. The main advantage of this technique is the large variety of signal processing algorithms that can be directly applied to the complex signals and their simple representation in exponential form. Some of the processing techniques that could be used for rate estimation are auto correlation, Fast Fourier Transform (FFT), Short time Fourier transform (STFT), peak detection, and wavelet analysis [41]. These techniques are well known and described in signal processing texts [42]. Recent advances in signal processing technology

have brought about newer techniques such as the Hilbert Huang transform and empirical mode decomposition that overcome some of the limitations of older techniques [43]. However, the research conducted for this dissertation primarily relies upon using Fast Fourier Transform techniques.

2.4.3. Radar parameters

Doppler radar systems consist of physical and logical layers. The physical layer includes the RF domain where the Doppler Effect occurs as well as parts for baseband and signal acquisition. The logical layer is represented by digital signal processing that is applied in real-time and post measurement. The design parameters of each layer determine the performance of the system and suitability to its target applications. Doppler radar systems fundamentally start at the physical layer where all of the RF and baseband components connect. These components include the transmitter chain and quadrature receiver with a dc cancellation. As the baseband signal is digitally acquired, a logical layer is introduced where the digital signal processing is performed. This section presents the actual system deployed to characterize the radar for physiological monitoring application. Design considerations for this application are:

1. Signal to Noise ratio (for subjects measured at a distance), affecting antenna selection, transmit power, and receiver architecture.

2. Phase sensitivity (for small motion associated with cardiopulmonary activity), affecting frequency choice and demodulation scheme.

3. Discrimination of motion for different parts of a target (for assessing respiratory effort), affecting demodulation scheme and frequency choice.

2.4.3.1. Experiment setup

Quadrature Doppler radars at 2.45 GHz were used for this study [44]. Two types of the transmitting and receiving antenna used for experiment, 1) PA24-16, 380700279 panel antennas (29 cm x 29 cm x 2.5 cm) from Laird Technologies having 16 dBi gain and 26° E plane beam width, 2) ASPPT 2998 from Antenna Specialist™ (10.5 cm x 10 cm x 4 cm) having 8 dBi gain and 60° E plane beam width. The radar was constructed using connectorised parts from Mini-Circuits (ZFSC 2-2500 splitters, ZFM-4212 mixers and a ZX10Q-2-27 90splitter). An Agilent E4433B RF signal generator provided the LO and transmit power. The baseband data obtained

from radar was passed through a low noise amplifier after which an NI USB-6009 data acquisition card was used with a computer and Labview software to record the data at a sampling rate of 100 Hz.

Figure 2-3 shows the difference in the physical size of the two antennas used for experiments and the radar system arrangement is shown in Figure 2-4

Figure 2-3 PA24-16 (29 × 29 × 2.5 cm^3) and ASPPT 2998 (10.5 × 10 × 4 cm^3) radar .The figure shows the size difference between two radars [44].

Experiments were performed in the hallway of college of engineering building of University of Hawaii at Mānoa to facilitate greater radar–target ranges

Figure 2-5). Experiments were performed mostly during night time to reduce clutter motion from other people nearby. Subject was located at 1, 3, 6, 9, 12, 15, 18, 21 and 24 meters from the radar and his heart rate was measured with a finger pulse sensor for reference. The subject was in a seated position and was asked to hold his breath for the duration of the experiment. The duration of measurements was 30 seconds.

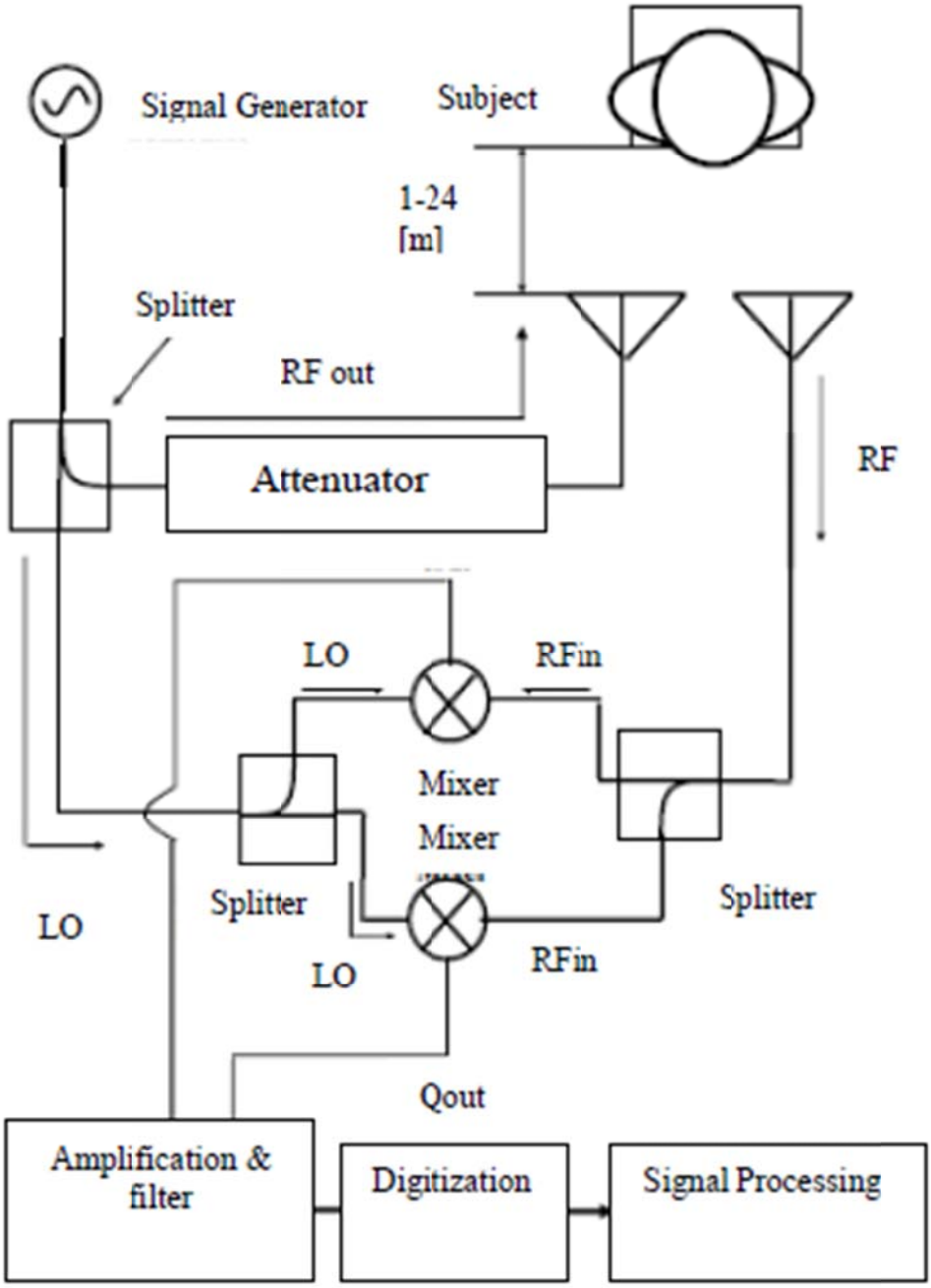

Figure 2-4 Block diagram of Doppler radar system with long rang approach [44].

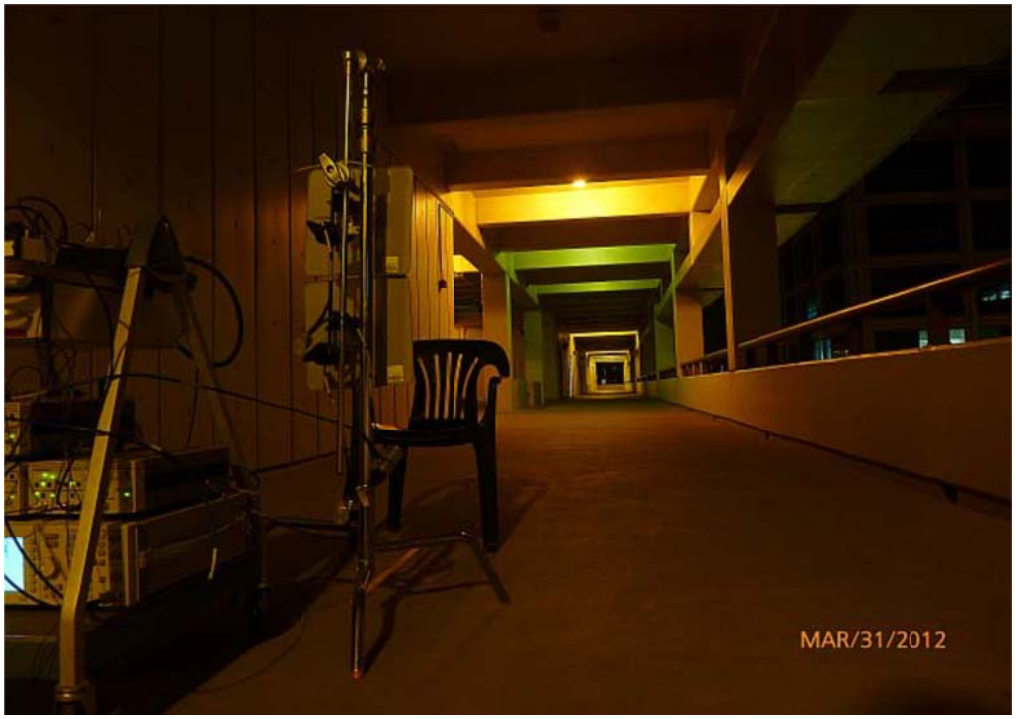

Figure 2-5. Experiment setup at night in the hallway of college of engineering. Note that the building is not completely isolated from variations in weather outside [44].

The data obtained from radar was filtered using a bandpass filter with cutoff frequencies between 0.5 and 3.5 Hz for heart rate detection. After performing a Fast Fourier Transform on the data, a peak detection algorithm was used to find peaks. An assumption was made to consider the maximum signal content in the frequency range to be originating from cardiac activity of the subject. This was verified against the reference pulse pressure sensor. The detection algorithm is shown in Fig.4. The radar data was analyzed using MATLAB.

2.4.3.1. Results

The transmitted power from signal generator was set to 13 dBm keeping in mind 16 dBi gain of the antenna. With PA24-16 antenna, the system was able to detect respiration at 69 m and heart rates at a distance of 18 m Figure 2-7 and Figure 2-8. Figure 2-8 shows the FFT of the linear demodulated data at 1m and 18 m respectively. Table 2-1 shows the result of the detection algorithm for different ranges. The algorithm failed to detect a heart rate at distances of 12 and 15 meters for one set of data. However, repeated measurements indicated that as an isolated

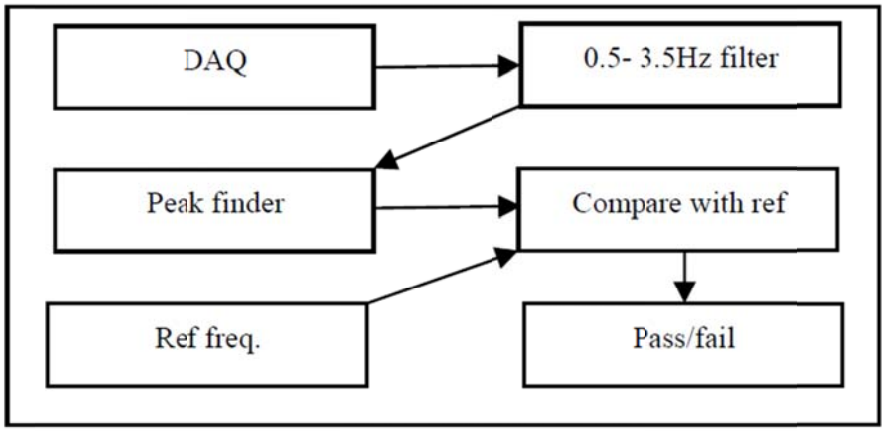

Figure 2-6 Motion detection and grading algorithm for heart rate detection [44].

problem since heart rates were detected successfully. This again highlights the usefulness of a phantom to characterize a system before human testing. Part of the problem could also be attributed to the use of bistatic radar system with large antennas having narrow beam-width.

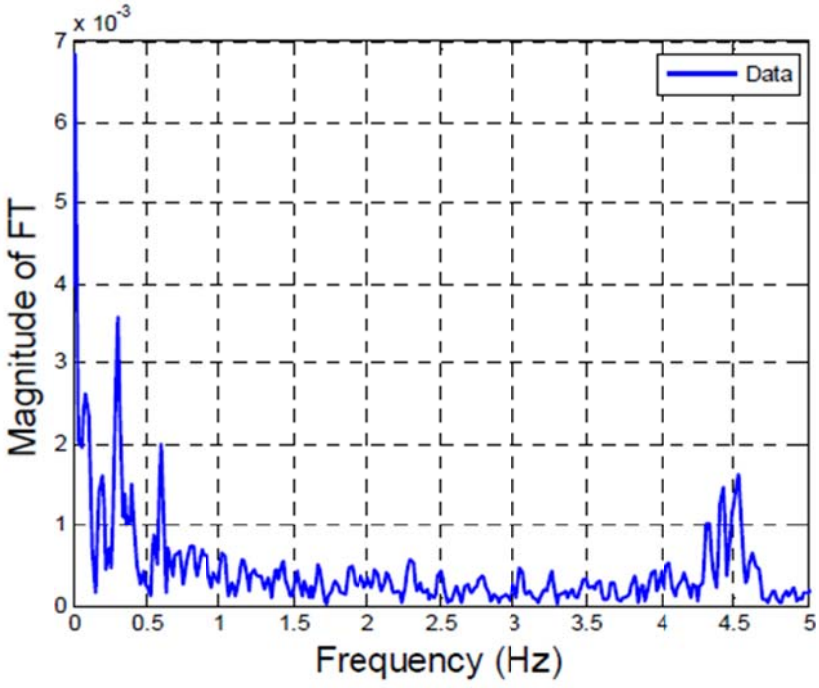

Figure 2-7 FFT of linear demodulated data showing detected respiration rate at approximately .27 Hz for 69m distance [44].

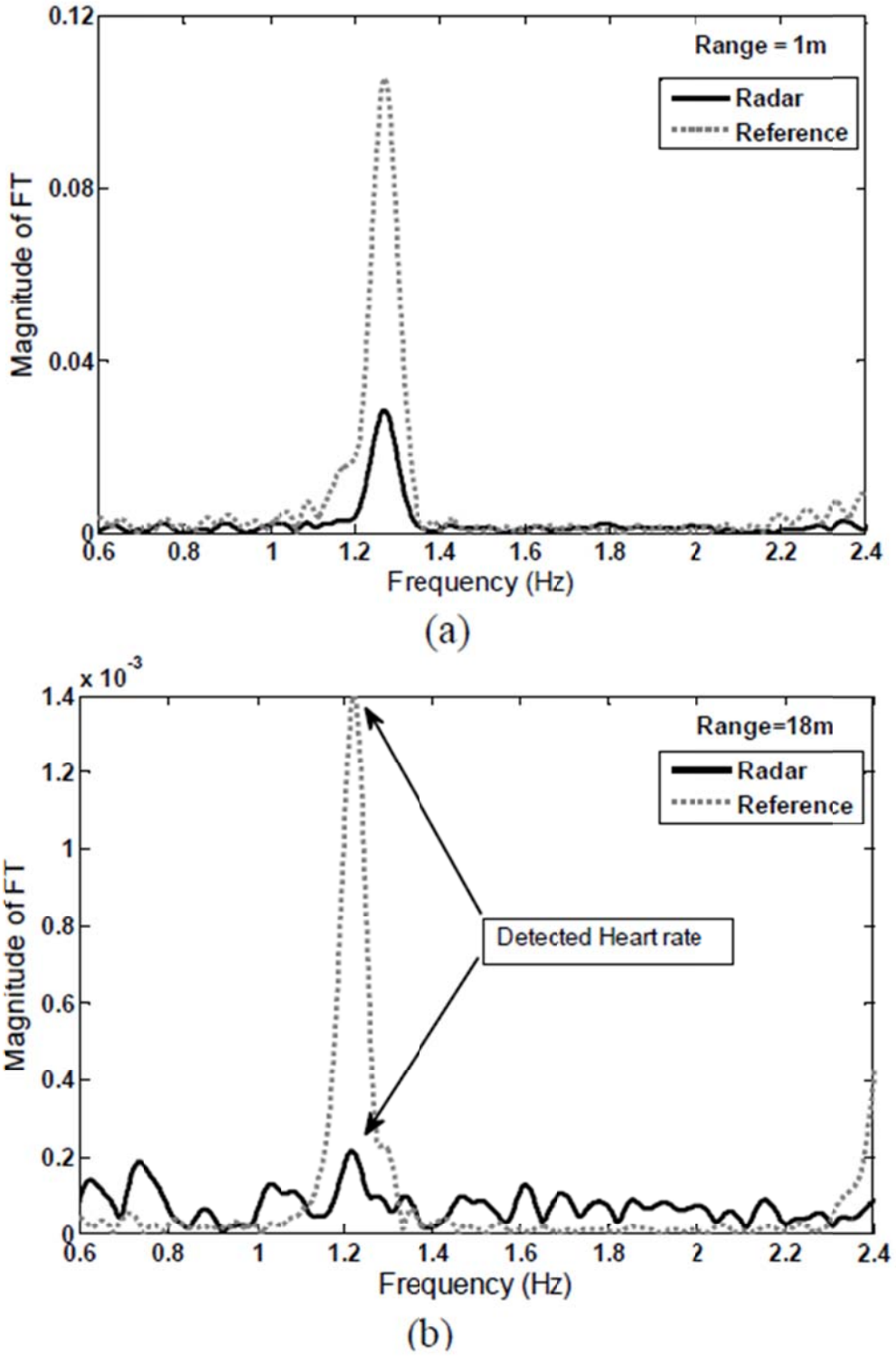

Figure 2-8 FFT of linear demodulated data showing detected heart rate at approximately 1.3 Hz for 1m distance (a) and for 18 m distance (b). Note that for 18 m distance, the reference FFT amplitude was divided by 100 in order to clearly display radar data [44].

The measurements were repeated with ASPPT 2998 (Antenna B) that had a different radiation pattern and gain. Since the gain of the antenna is only 8 dBi, the transmitted power from the signal generator was increased to 18 dBm. Use of antenna B increased the maximum range to21 m as shown in Figure 2-9. The results of the motion gradient algorithm for ASPPT 2998 at different distances are also shown in Table 2-1. Again, the detection algorithm failed to detect heart rate at 12 meters for one set of data but was successfully detected in subsequent measurements.

Table 2-1 Output from heart rate detection grading module [44].

Range(m)	Antenna Type A	Antenna Type B
1	Pass	Pass
3	Pass	Pass
6	Pass	Pass
9	Pass	Pass
12	Fail/Pass	Fail/Pass
15	Fail/Pass	Fail/ Pass
18	Pass	Pass
21	Fail	Pass
24	Fail	Fail

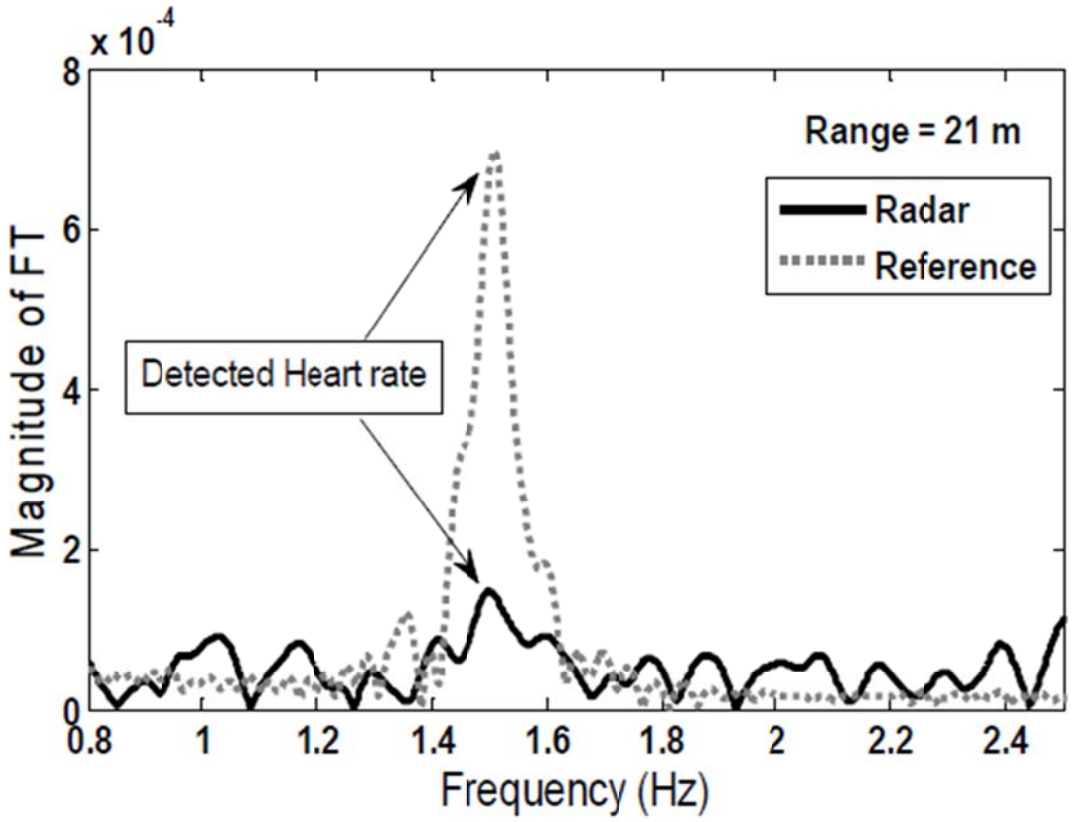

Figure 2-9 Detected heart rate at a range of 21m for ASPPT based system. The Reference amplitude was scaled down by 100 to display the data together with radar data [44].

Based on the result, it was observed that using a large antenna with narrow beamwidth does provide some challenge in obtaining proper measurements with a bistatic radar system. The signal processing technique used to detect the presence of heart rate was very basic involving frequency analysis. Improvements in signal processing techniques could significantly improve the detection accuracy of the algorithm and may also help in extending the range of the radar. It would also be interesting to study long range heart rate detection system using a monostatic radar system with antenna A and antenna B.

The trade-off in using a smaller antenna with a smaller gain is the availability of a higher power signal source or the inclusion of an RF amplifier in the transmitting chain. With PCB fabrication technology and surface mount components, circuits can be made very small and hence the size of antenna becomes an important factor. This study shows that smaller antennas could be positioned better for long range cardiac activity monitoring.

Chapter 3

Sleep Disorder Monitoring

Sleep is an essential condition for human life, driven by the body's natural circadian rhythms and driven by a circadian clock. Sleep is necessary for the proper functioning of the body and health. It helps the body heal itself, helps the brain to develop, to process memories and other important functions. During sleep, the heart rate slows down, hormones and blood pressure fluctuates, muscles and other tissues relax, and metabolism slows down, allowing the body and mind time to rest and repair. People who cannot sleep well or at all are plagued with multiple difficulties such as a weaker immune system and lower cognitive function [45].

Sleeping disorders are medical disorders where typical sleep behavior is disrupted or otherwise abnormal to various degrees, which damages normal physical, mental, and emotional function. Sleeping disorders include dyssomnias, where sleep is difficult to enter or maintain, – or in the case of hypersomnias – difficult to stay awake. They also include parasomnias, which relate to abnormal behaviors and actions that occur throughout the various sleep stages, and circadian rhythm sleep disorders, which affect the timing of the body's circadian clock. Of all sleep disorders, one of the most widespread among the general population and serious is sleep apnea (SA).

In this chapter first, different kinds of sleep apnea are described along with methods presented in the literature for sleep disorder monitoring. Next a new Physiological Radar Monitoring System (PRMS) for detecting sleep apnea is presented.

3.1. Sleep disorder definitions and classifications

3.1.1. Obstructive Sleep Apnea

Obstructive Sleep Apnea (OSA) is a type of sleep apnea classified by a recurring interruption of ventilation during sleep as a result of collapsing the pharyngeal airway. This interruption consists of a pause in respiration equal to or greater than 10 seconds in length [2].

Related to OSA, obstructive hyperpnoea consist of significant decreases in ventilation and a fall in oxygen saturation but do not have a complete cessation of ventilation. These conditions are diagnosed when a patient has over 5 apneas or hypopneas per hour of sleep (apnea-hyperpnoea index > 5) as well as showing signs of excessive sleepiness during the day [2] [46] (

Figure 3-1).

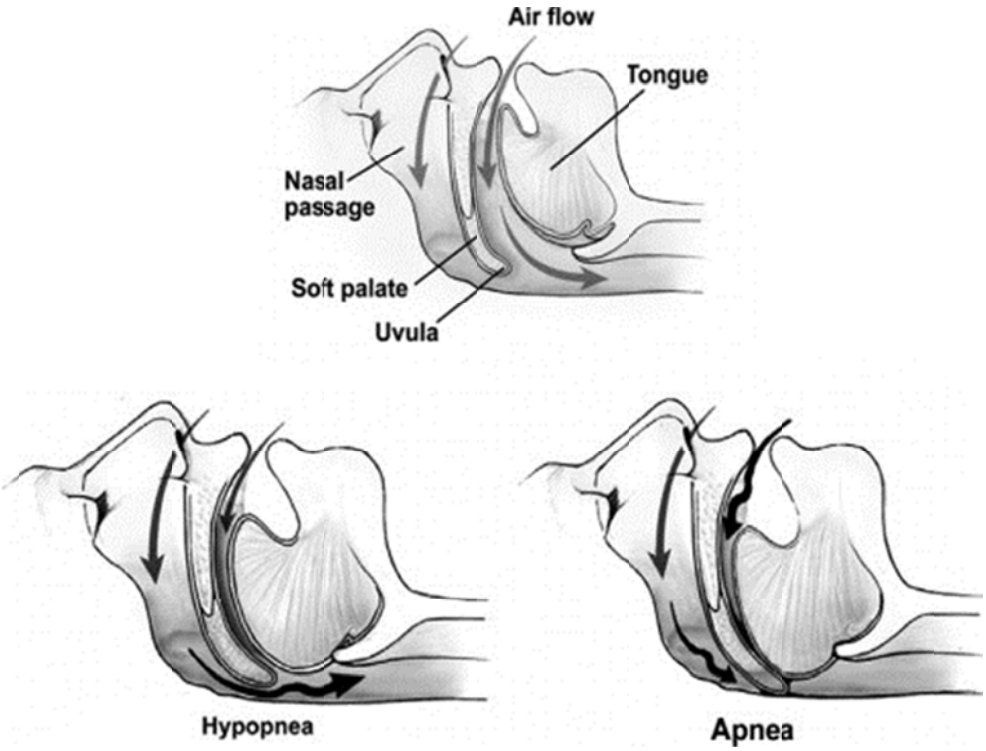

Figure 3-1 Partial and complete airway obstruction during hypopnea and apnea respectively Reprinted from Hahn PY, Somers VK. Sleep apnea and hypertension. In: Lip GYH, Hall JE, eds. Comprehensive hypertension. St. Louis, MO: Mosby; 2007:201–207. Copyright Elsevier

OSA is both highly prevalent and has a wide range of severity in adults according to many studies conducted around world. Although conducted under different circumstances, most of these studies have shown that approximately one in five adults has mild to severe sleep apnea [2].

At least 1 in 5 adults has at least mild OSA, which is defined by an apnea-hypopnea index (AHI) of 5 or more. 1 in 15 people have moderate to severe cases of sleep apnea (e.g. AHI > 15). Two longitudinal population studies conducted have shown that OSA progresses over time. In [47] showed an increase in AHI over 8 years, particularly for habitual snorers, those with a body mass index (BMI) of over 30, and those between 45 and 60 years old. In [48] the

median AHI increased the most for those 41-54 years old. However, the vast majority (>85%) of patients with treatable OSA have never been diagnosed [2].

3.1.2. Central Sleep Apnea

Central Sleep Apnea (CSA) can be defined as the repetitive cessation of ventilation during sleep due to the loss of the ventilatory drive [2]. A central apnea must have ventilatory pauses equal to or greater than 10 seconds whereby there is no respiration. In most situations, anything beyond 5 of these events per hour of sleep is considered abnormal and is diagnosed by this frequency as well as the presence of associated symptoms such as frequent arousals during sleep and hypersomnolence [46] Some individuals may have both central and obstructive apneas and in such cases CSA is only diagnosed as the primary problem if it occurs more than 50% of the time [2].

There is no single common cause of CSA, and so a few different syndromes have appeared which are triggered by different underlying physiological conditions [2].

3.1.3. Mixed Sleep Apnea

Mixed apnea is the combination of both obstructive and central apnea. In which the central apnea is developed as a result of severe and longstanding episode of obstructive apnea [49].

3.2. Sleep disorder monitoring techniques

For Obstructive Sleep Apnea (OSA), a final diagnosis is usually obtained by a medical examination using a Polysomnography (PSG) test which is records the biophysiological changes that happen during sleep at a sleep lab. This test is difficult, time consuming, and labor intensive as a human observer is required to monitor the patient overnight [50]. There is much need to improve the efficiency, diagnosis time, and accuracy of the PSG. New techniques are currently being developed and tested by bioengineers to improve upon the weaknesses of the PSG and help diagnose more patients more quickly.

Many studies show that OSA can be detected by the use of an Electrocardiogram (ECG), which measures cyclic variations in the length of heartbeats. During SA, the bradycardia (slow heart rate) normal during sleep is always followed by tachycardia (abnormally fast heart rate)

upon its cessation [50]. Chazal *et al.*[51] presented an automated classification algorithm to determine sleep disorder period using the short-duration epochs of surface electrocardiogram data which were recorded during a polysomnography studies [51]. Later they proposed an automatic method of detecting sleep disorder including obstructive, mixed and central apneas, and obstructive, mixed and central hypopneas by analysing the heart variability, an ECG based respiration signal and blood oxygen level with a pattern recognition system [52].

In another work, Yilmaz *et al.* [53] proposed a method to detect paradoxical breathing epochs by extracting some features from only a single-lead electrocardiography (ECG) signal. A beat-to-beat (RR interval) event was computed using an R-peak detection algorithm. Then the sleep stages are classified using k-nearest-neighbor (KNN), quadratic discriminant analysis (QDA), and support vector machines (SVM) methods based on the features (e.g. the median value, the difference between the 75 and 25 percentile values, and mean absolute deviations of the RR intervals) extracted from RR intervals. Their result showed the feasibility of using only single-lead ECG data for sleep disorder detection [53]. Almazaydeh *et al.* [54] presented an automated classification algorithm based on support vector machine. The methodology processes short duration of the electrocardiogram (ECG) data by combining the RR-interval based features of ECG signal based on the methods presented in [51] and [53]. It is showed in [54] that this automated method is able to detect sleep disorders very accurately. Mendez et al [55] explores the application of time varying autoregressive models and KNN linear classifier to evaluate the probability of being in apnea or not during each minute. The accuracy of the classifications using these methods usually exceeds 85%, and may be further increased by using different time resolutions to extract features other than the very low frequency that defines the rhythm of apnea and normal respiration.

Many studies have shown that an Electroencephalogram (EEG) - a monitor of brain wave activity – can diagnose SA [56]. Electroencephalographic (EEG) arousal happens in EEG recordings when patient awakes from sleep. Sleep apnea events usually cause an arousal as a result of stoppage in respiration. Hence; the respiratory-related arousals is visible EEG recording. Hence; in [57] Sugi *et al*. presented a method to automatically detect EEG arousals in the EEG data recorded during PSG test. The method is based on comparing with a threshold values that were calculated based on pathological events as sleep apnea and electromyogram (EMG). The result shows that this method is sensitive enough and can assist in common visual inspection

method. In another work, wavelet transforms and an artificial neural network (ANN) algorithm is applied to the EEG signal [58] to identify the EEG arousals. The results show the sensitivity of 69.64% and a specificity of approximately 44.44%. However, one major flaw of the EEG signal is that it is easily contaminated by artifacts [50].Hence; a preprocessor circuit is necessary to eliminate artifacts and enable the EEG to more reliably recognize SA events [50, 59].

Snoring is always almost happens with obstructive sleep apnea as OSA is generally caused by the blocking of the airway. This functional and structural changes disturbs the sites spatially and temporally which leads to snoring [60, 61]. Several snore-based methods have also proven promising for the detection of SA [46, 61-66]. Abeyratne *et al.* [61] presented a snore-based multi-feature class OSA screening tool. The method uses snore parameters that are related to the voiced parts of snore with the a sensitivity of 93±9% with specificity 93±9% for females and sensitivity of 92±6% with specificity 93±7% for males at an AHI decision threshold of 15 events/h the proposed method can potentially be used for screening of OSA at home. Karunajeewa *et al.* [62] presented a logistic regression model that uses some snore features to detect OSA. The features include pitch and total airway response (TAR) which depends on the airway vibration in time-domain and acoustical changes as a result of airway obstruction respectively. The result showed 89.3% sensitivity with 92.3% specificity which proved the feasibility of using this non contacted method for sleep disorder monitoring. Yeh-Liang *et al.* [63] developed a portable device to monitor snore at home. The device calculates total snoring count, average number of snores per hour, and number of intermittent snores by processing the temporal feature of the snoring sounds. The results show the average success rate of over 85% in a lab environment and around 70% at home [63]. Formant estimation method was also used to detect OSA based on snoring data [64-66].

Using an ultrasonic device for the non-invasive detection of obstructive sleep apnea/hypopnea (OSAH) is presented in [67]. The proposed method is safe, non-invasive, cheap and portable. The preliminary results of an in vivo study for the detection of airway occlusion during apnea/hypopnea events using the spectral features of the ultrasonic waves presented in this study shows the feasibility of developing an ultrasonic detection device for low cost diagnosis of Sleep Disordered Breathing.

Pulse oximetry measuring Arterial oxygen saturation (SpO2) can also help diagnose OSA as clinical experience indicates that SA events are often accompanied by oxygen desaturation, or

a fall in the SpO2 signal [50, 68]. Schlotthauer *et al.* [69] presented a recognition method based on the empirical mode decomposition of the pulse oximetry signal. The pattern of saturation during OSA is extracted and the oxygen desaturation thresholds were set. The results show a high sensitivity (84%) and specificity (85%).

3.3. The Gold Standard

There are a few ways to record body activity during sleep. The current gold standard and arguably best way to study sleep apnea is Polysomnography (PSG). Polysomnography makes comprehensive recordings of the biophysiological changes that happen during sleep. The PSG monitors many body functions during sleep such as: brain activity (EEG), eye movements (EOG), muscle activity (EMG), heart rhythm (ECG), respiratory airflow and respiratory effort.

Several systems available in the market for sleep studies such as SomnoStar® z4 Sleep System, from CareFusion (http://www.carefusion.com), Sapphire PSG™ with its complementary software Cyrstal PSG™ Software from Cleveland Medical Devices Inc, (http://www.clevemed.com) and Sandman Elite PSG Software with its complementary hardware from Embla (http://www.embla.com/).

In our project, all the tests were carried out in Queens Medical Center (http://queensmedicalcenter.org/) which uses Sandman for sleep studies. Hence, we consider it as a gold standard for our project.

3.4. Doppler radar design for sleep monitoring

The schematic in Figure 3-2 shows the basic concept of integrating PRMS with the Sandman as a gold standard sleep monitoring device.

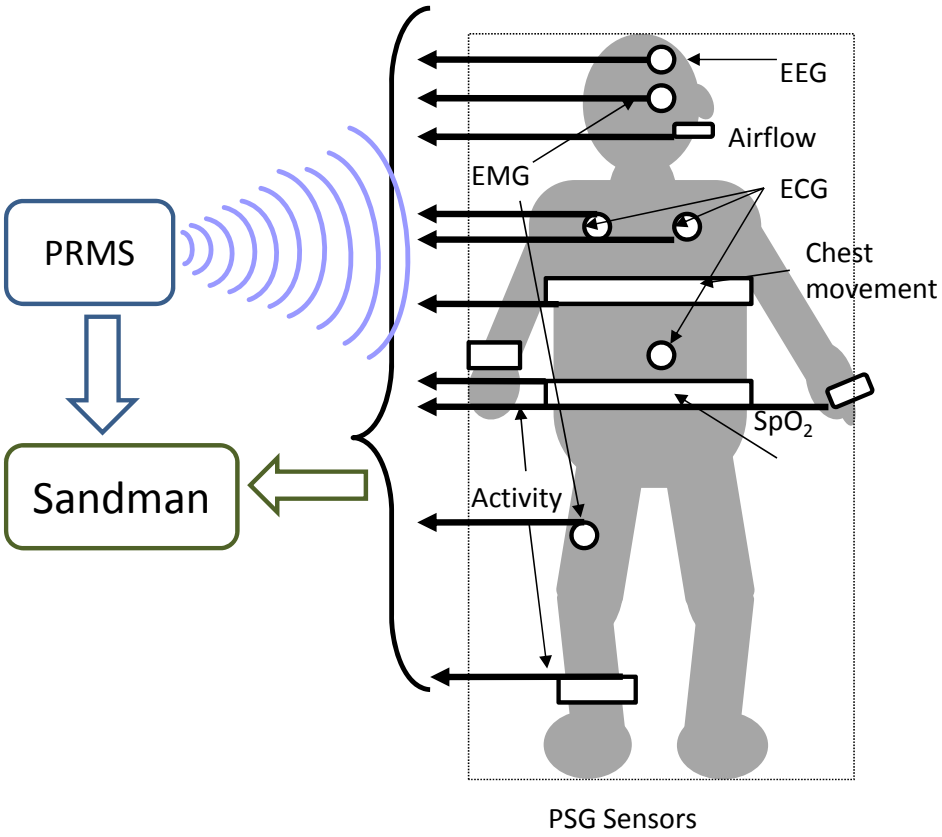

Figure 3-2 Integrating PRMS with Sandman

To use a system based on Doppler radar techniques for sleep disorder monitoring task various performance trade-offs and design factors must be taken into account. In the following sections design considerations and different possible architecture of PRMS will be explained which leads to the final architecture that was used in clinical studies.

3.4.1. Design consideration

When designing a PRMS that can be integrated with a clinical sleep monitoring system, many design factors must be considered. Some of these factors pertain to its physical design, while others pertain to the interface between PRMS and Sandman.

The PRMS must produce output waveforms and data in a format that can be read in real time by sleep assessment systems currently utilized in sleep centers. The PRMS also encounters a few design challenges such as the design of robust data output signals, low latency adequate for real-time readings, and a compact form factor.

This planned overnight sleep study will take place in a certified sleep study center at Queen's Medical Center in Honolulu, Hawaii. The size of the room will be approximately 5×6

m^2. Because the PRMS must be placed in the room without obstructing the normal movements of the subject, it should be compact. Careful placement of the radar is also critical as Doppler radar is most sensitive for motion that is orthogonal to the plane of its antenna. A sturdy physical structure is necessary to hold the radar and associated equipment in its proper position.

3.4.2. Selecting radar's architecture

3.4.2.1. Two transmitters, two receivers

During a normal breathing, the chest and abdomen movements are in phase together (Figure 3-3). As shown in Figure 3-3.b and Figure 3-3.c, this situation changes when an apnea or hypopnea event occurs. As a result of airway channel obstruction the chest and abdominal movement becomes out of phase. The phase change ranges from few degrees to 180 degree. In clinical sleep monitoring system chest and abdominal effort belts are used to measure the chest and abdomen movements Figure 3-4, Figure 3-5and Figure 3-6 show signals of chest and abdomen belt in normal, hypopnea and apnea breathing respectively.

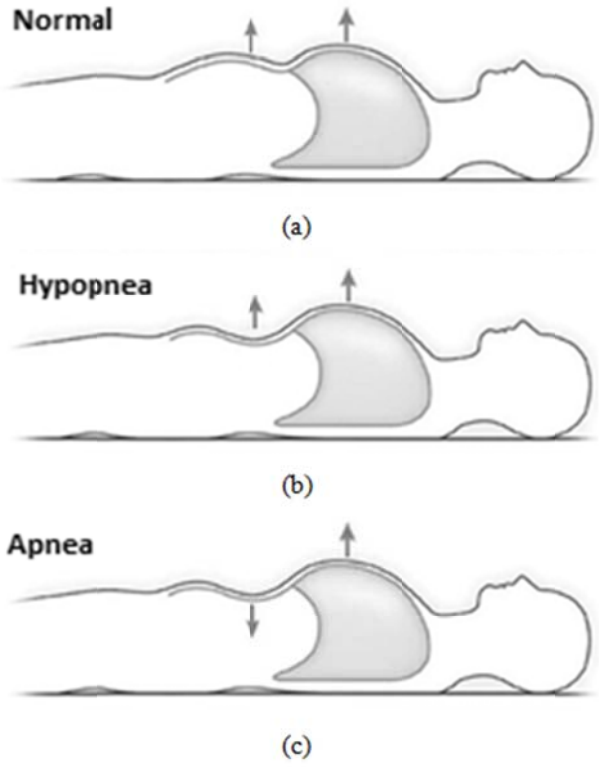

Figure 3-3 Phase difference in chest and abdominal movement during hypopnea and apnea events.

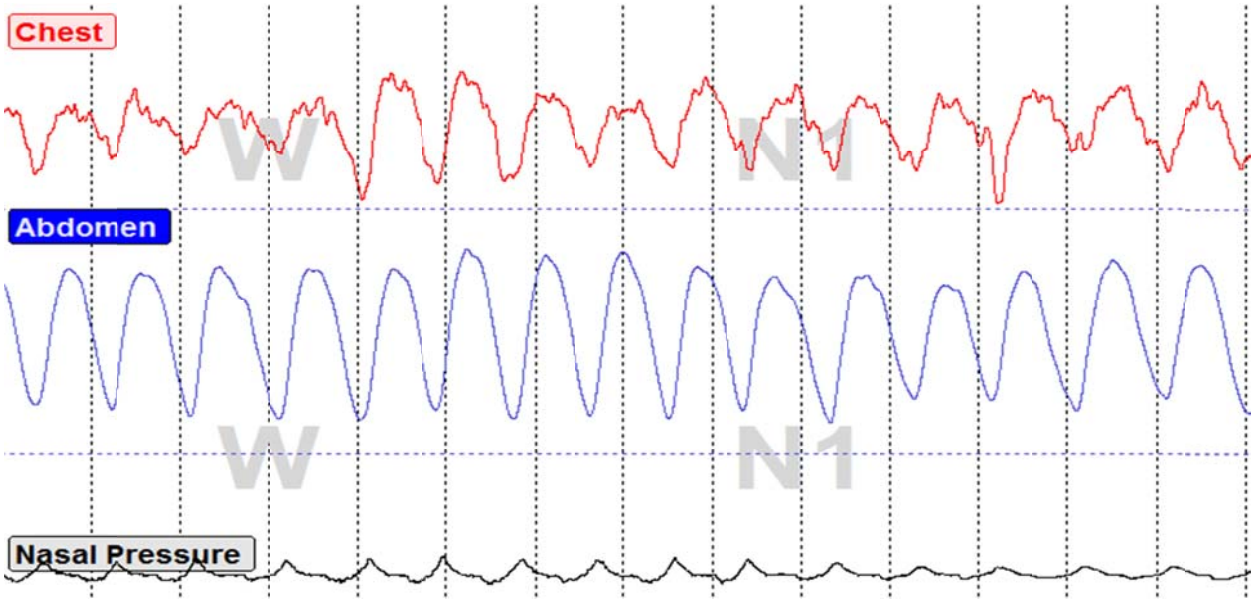

Figure 3-4 The effort belts shows in phase chest and abdominal movements in normal breathing.

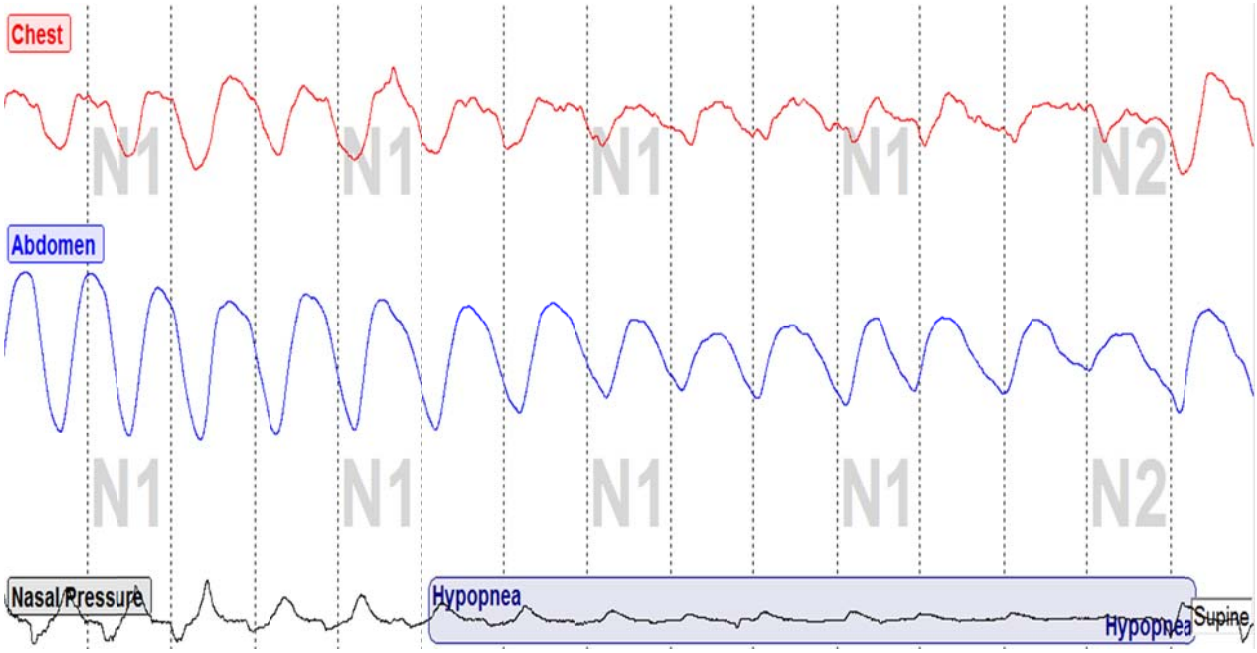

Figure 3-5 Phase difference in chest and abdomen chest belt's signals due to hypopnea event.

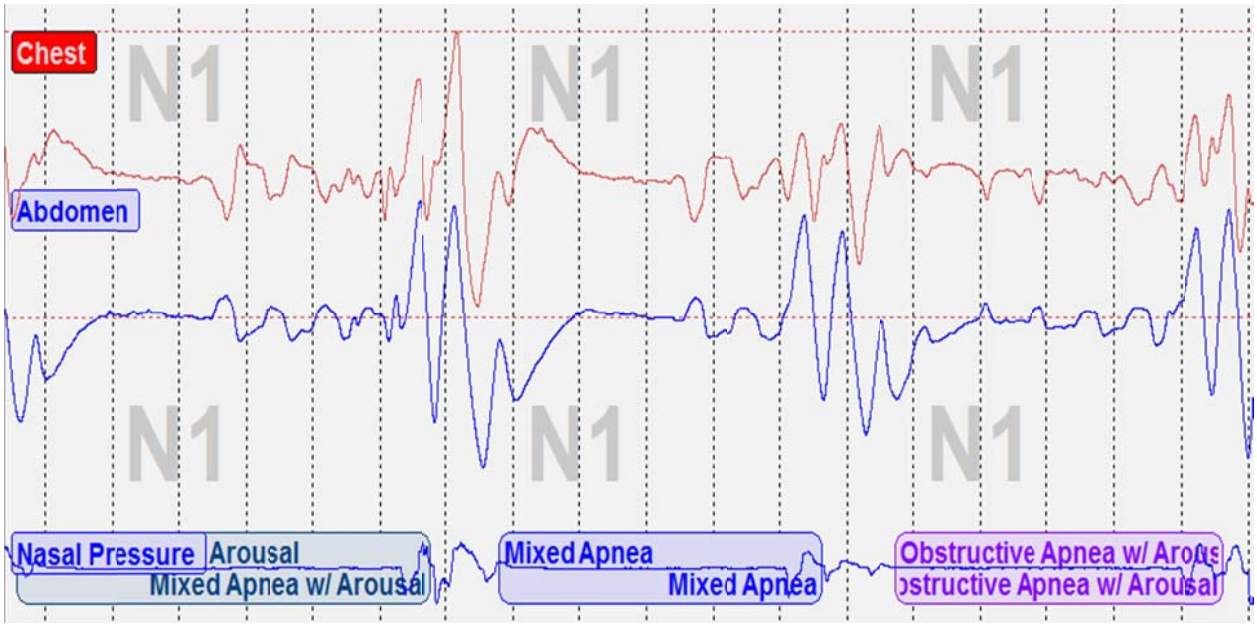

Figure 3-6 Effort belts shows out of phase chest and abdominal movements during apnea events.

The CW Doppler radars can measure a movement of a subject very accurately. Hence; at first glance it seems interested to use Doppler radar instead of effort belts to track the abdominal and chest movement. Two separate Doppler radar must be used for detecting chest and abdominal movement and the antennas beam must be narrow enough to cover only the chest or the abdomen of the subject. For this purpose, in the first step, we developed a quadrature Doppler radar with two transmitting and two receiving antennas. Figure 3-7 shows the block diagram of this architecture.

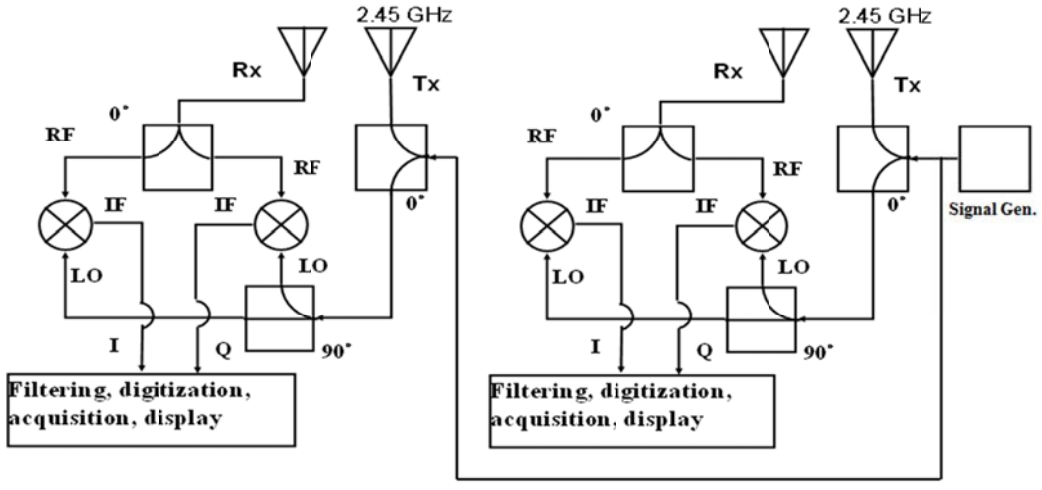

Figure 3-7 block diagram of an architecture with two Doppler radar to track chest and abdominal movement separately.

To test this architecture, a simulator was made with two programmable linear servo motors. One servo mimics the chest movement while the other imitates the abdominal movements. The simulator is shown in Figure 3-8

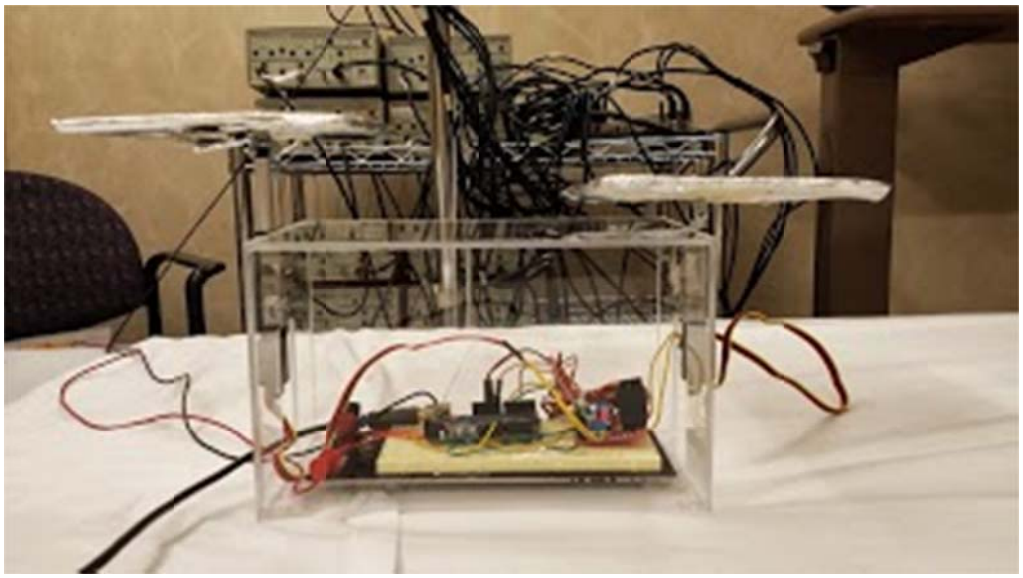

(a)

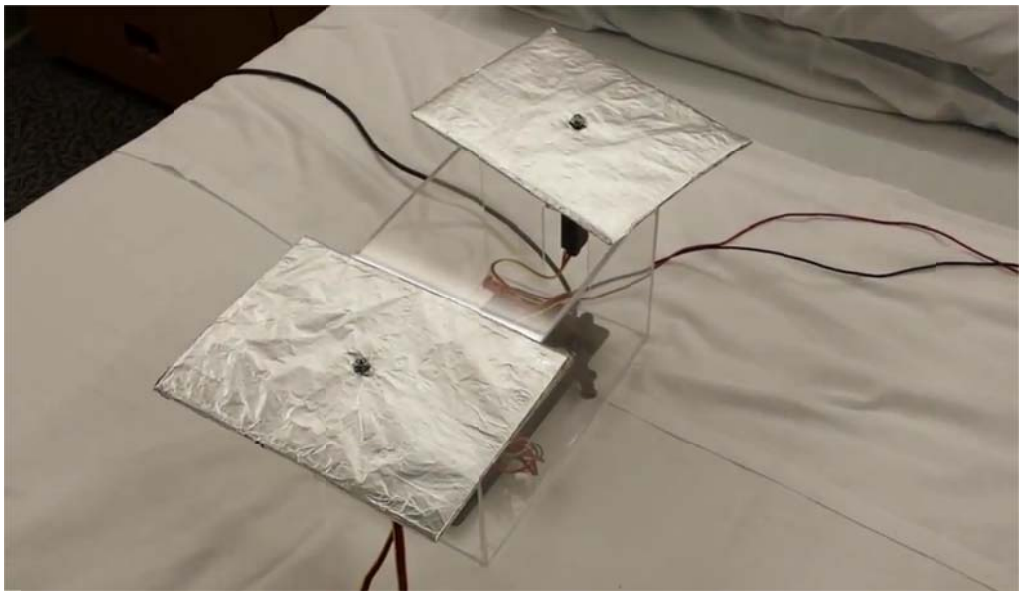

(b)

Figure 3-8 The programmable linear mover made by two servo motors. (a) Side (b) Top view

The radars was placed on top the simulator at 1 meter distance and the servos were programmed to have to move in-phase and then with 180 degree phase shift. Next the signals from two radars were recorded.

However, because the transmitters did not synchronize together the results were not correct and the signals were out of phase even in the situation were two servos moving in-phase.

3.4.2.1. One transmitter, two receivers

To eliminate the synchronization problem between two antennas a new architecture was developed with one common transmitter instead of two separate systems. The block diagram of this architecture is shown in Figure 3-9.

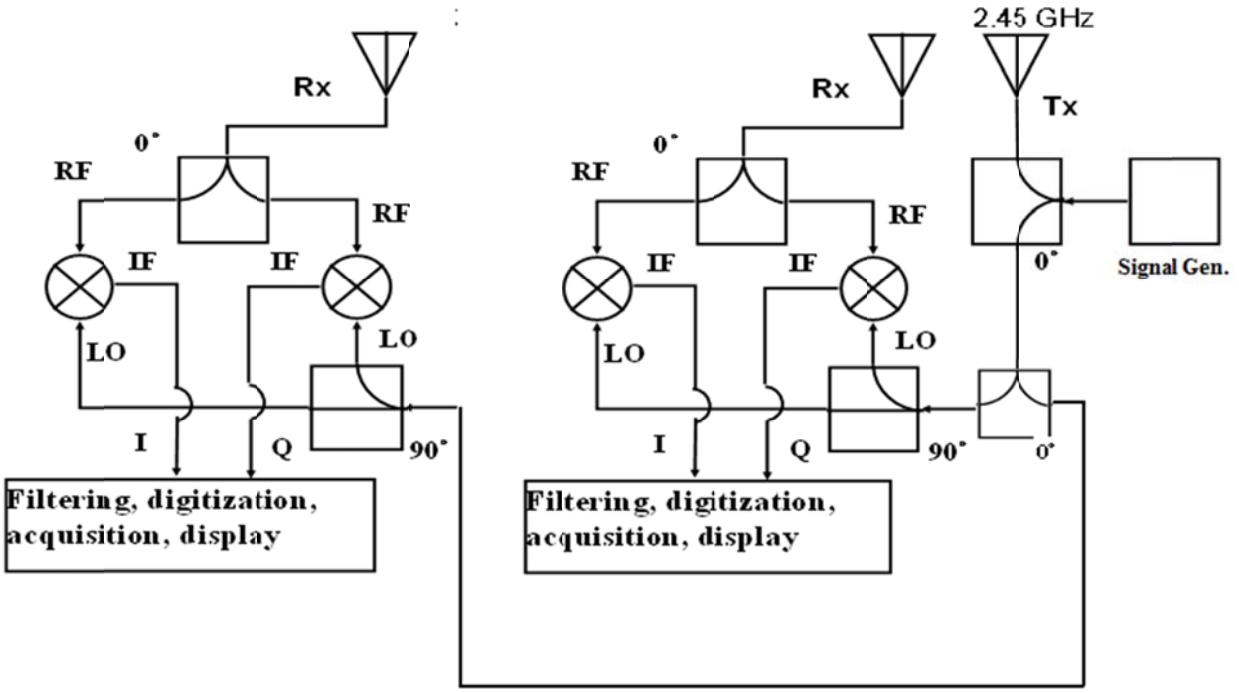

Figure 3-9 block diagram of a Doppler radar architecture with common transmitter and two receiver to track chest and abdominal movement.

Then the mover was programmed two move in-phase, 180^{o} out of phase and with a smaller phase shift to mimic normal, apnea and hypopnea breathing respectively. As shown in Figure 3-10 the signal recorded from two receivers can track the phase difference between two servos.

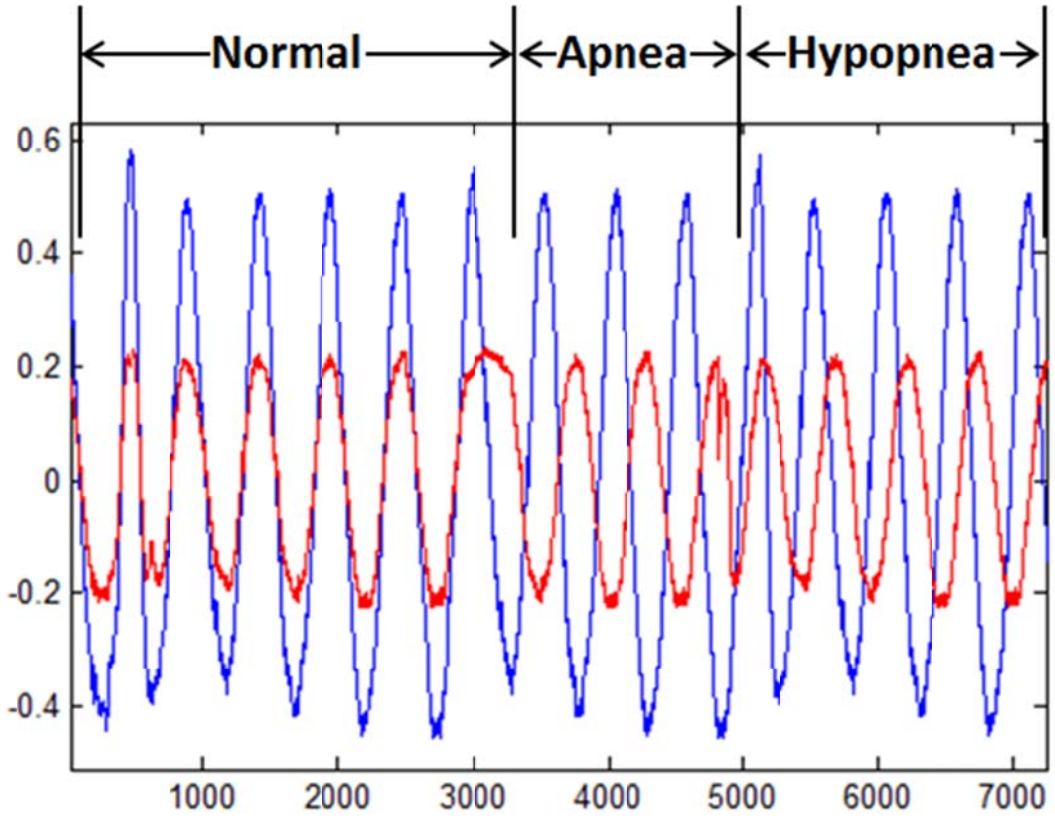

Figure 3-10 Signal recorded by two antenna receivers from a programmable mover with 2 servos when they move in-phase (Normal), 180^{o} out of phase (Apnea) and with a slight phase shift (Hypopnea).

However, recording the signals from a human subject did not show a noticeable difference because of the antenna pattern and subject position. The chest and abdominal movement are very complex and related to each other. Hence; to distinguish between two movements, the pattern of the antennas must be very narrow. This makes is very difficult to focus the field of view of the antennas on chest and abdomen of the subject. A small movement of either the subject or the radars will push the chest or abdomen out of the radars field of view. Using radars with wider pattern causes interfering that makes it impossible to distinguish between chest and abdominal movements.

As a result, the final PRMS architecture was developed with one receiver to cover both chest and abdominal movement. The second receiver was kept as a backup to insure recording high quality signals in any cases. Furthermore, the sensitivity of the Doppler radar to the motion sensitivity changes with the frequency of its operation. Finer resolution will be achieved using

higher frequencies (smaller wavelengths). The operating frequency also affects the radar cross section of the target. For example, [70] showed that detection of physiological motion using 2.4GHz provided a higher sensitivity to orientation whereas using 5.8GHz provided higher displacement resolution.

However, the benefits of using multiple Doppler radar systems should not come at the cost of a significant increase in size of the radar. This PRMS will have two quadrature Doppler radar systems transmitting at 2.45GHz and 24GHz integrated into a package 20cm×15cm×8cm in size (**Error! Reference source not found.**). The following section will explain this architecture in more detail.

3.4.2.2. PRMS architecture

Coaxial components [71, 72] were used to implement the Doppler radar with 2.45GHz. An oscillator with fixed power was used to generate the signal at 2.45GHz and the transmitter power was varied using a step attenuator [73] placed in the 2.4 GHz transmitter path. The ZFSC-2-2500 splitter [74] divides the source signal into the transmitter antenna and local oscillator paths with 90^{o} phase difference.Three ASPPT2988 panel antennas [75] was configured as one common transmitter and two receivers. The antenna pattern is shown in Figure 3-11. ZFM-4212 frequency mixer [76] was used to extract the baseband signal from RF input. Then the signal was fed to the differential input of the SR560 [77] low noise amplifier (see Figure 3-12) for DC cancellation, amplification and filtration.

The 24 GHz radar was a commercial off the shelf 24 GHz module K-MC1 from RF beam [78].This module has 24GHz K-band antenna with I/Q Mixer and IF-Preamplifiers. The antenna pattern is shown in Figure 3-13.

The outputs of 24GHz were also fed into SR560 low noise amplifier. Both radar outputs were amplified with the gain of 200 and filtered with a low pass frequency with the cut-off frequency at 30Hz.

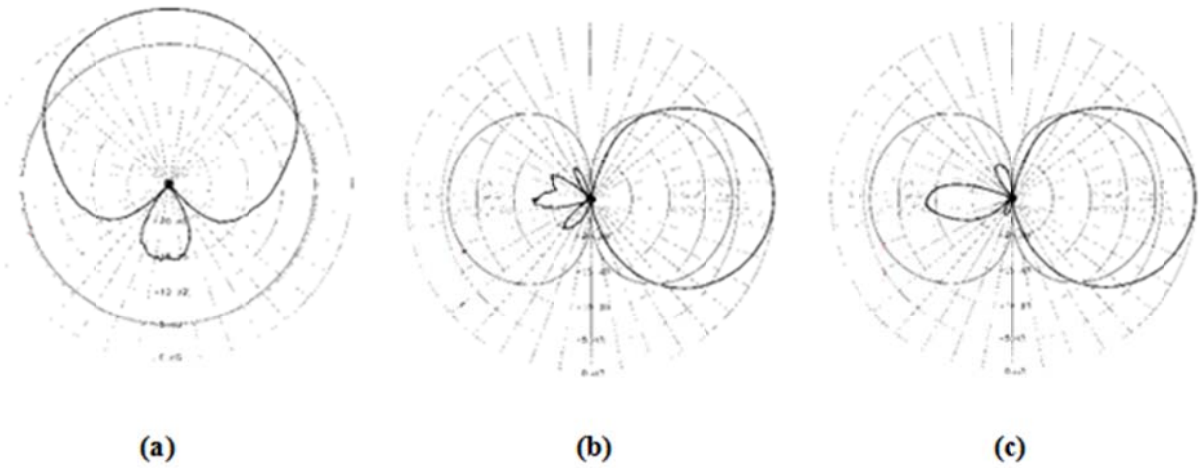

Figure 3-11 2.45GHz antenna pattern (a) H-Plane (80°) Dipole Reference (b) E-Plane (60°) Dipole Reference and (c) E-Plane (65°) Dipole Reference [75]

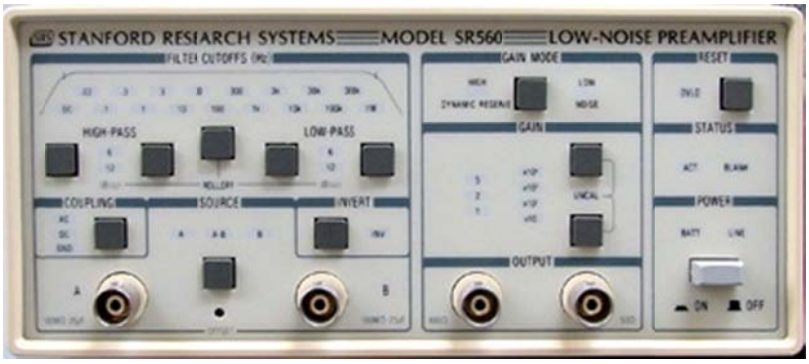

Figure 3-12 Pre amplifier

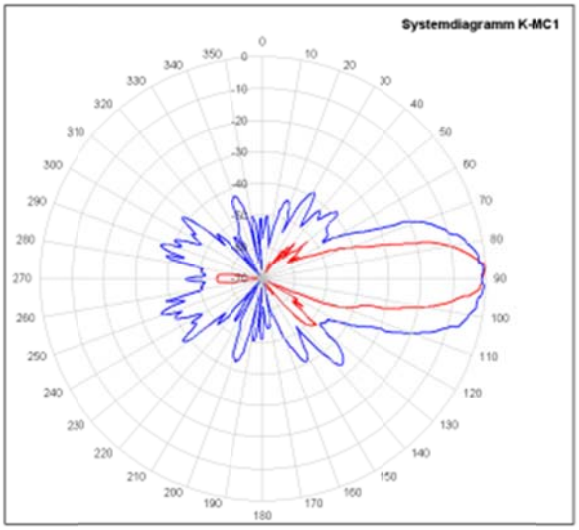

Figure 3-13 24Ghz antenna pattern [78]

Finally all the baseband outputs were converted from analog to digital using National instrument data acquisition module (NI-USB 6259 [79, 80]) and sent to MATLAB to be analyzed using sleep monitoring algorithm The same DAQ was used to send the algorithm outputs (as explained later) to Sandman. Figure 3-14show the input/output ports arrangement.

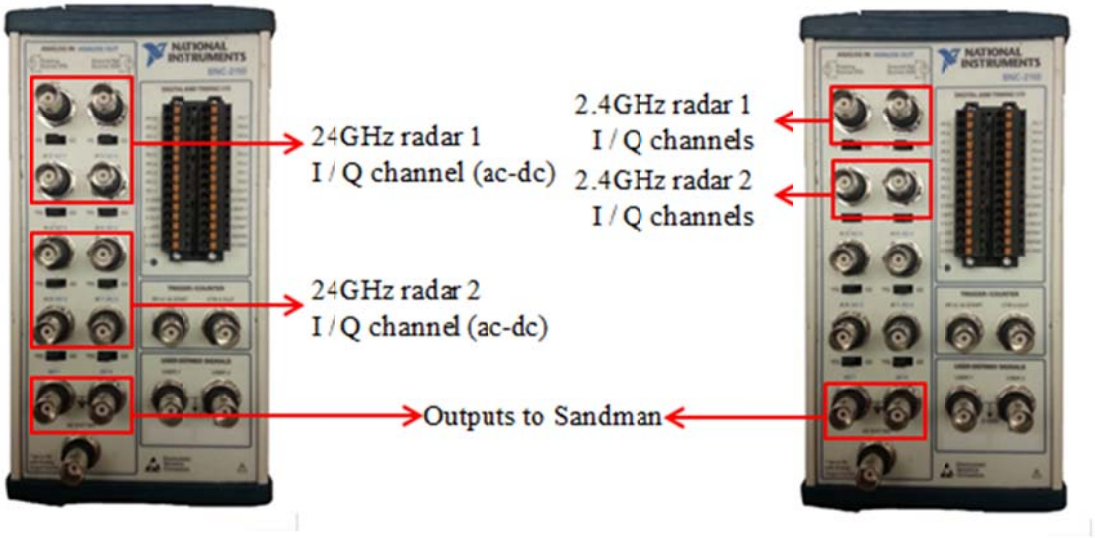

Figure 3-14 Analog inputs/outputs arrangement

The antennas board setup is shown in Figure 3-15.

Figure 3-15 Antenna board panel

3.4.3. Design evaluation

Preliminary experiments were carried out to assess the performance of PRMS systems using the programmable linear simulator (Figure 3-8). The mover was programmed to have a small periodic motion within 8mm range to imitate the chest and abdominal movement.

Figure 3-16 are shows the Q-component versus I-component for 2.45GHz and 24GHz radars. Comparing to the full circle in 24GHz, the outputs of 2.45GHz only forms a portion of a circle since the length of the arc (Q versus I) is inversely proportional to the radar wavelength which means it is directly proportional to the radar frequency. As a result 24GHz radar outputs form longer arc than 2.45GHz [45].

The multiple arcs formed by motion-modulated signal of 24GHz radar can be measured using an arctangent demodulation algorithm this gives us higher displacement resolution than 2.45GHz radar which has a simple arc. However, the circular trace is 24GHz have overlap with each other because of the DC drift of I and Q channel signals. This makes the arctangent demodulation very complex. In such situation as presented in [70] analysing the IQ signal can be performed using linear demodulation technique.

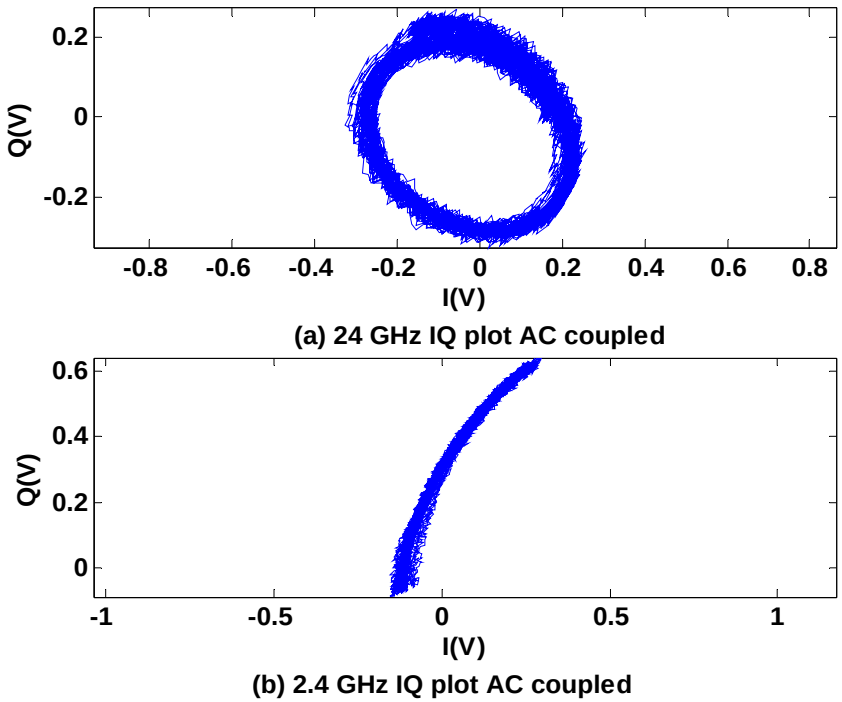

Figure 3-16 Q versus I channel signals plot on complex plane. (a) The arc of 24GHz radar is consisting 460.8˚ of a circle. (b) the arc for 2.45GHz radar is consisting 47.06˚ of a circle [45].

To measure the latency for integrating the PRMS into Sandman, an analog signal of 1 Hz, and 200 mV was generated from a signal generator to emulate the radar baseband output. The signal was converted from analog to digital using an NI-DAQ, processed in MATLAB and then converted back to analog signal using the same DAQ. Figure 3-17 shows the aligned original and converted signals. The delay between input and output is 130 ms which gives us an estimation of system latency [45].

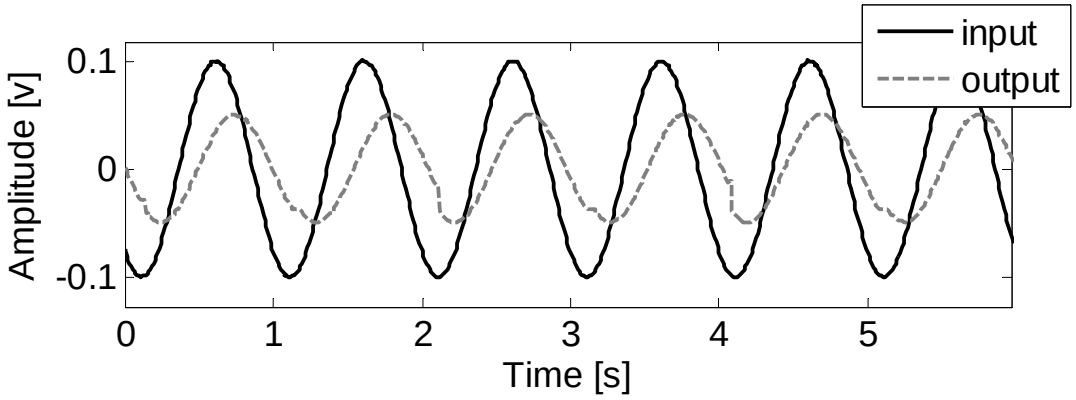

Figure 3-17 Latency between the original and converted analog signal [45].

These measurement results indicate the successful operation of the design PRMS. For a 8 hour sleep study applications, having a latency less than 500ms is acceptable. Hence; with an average of 130ms delay, the PRMS meets the requirement.

3.5. Adapting the PRMS to Sandman

From the description of the Sandman system the most conventional way to integrate the Doppler radar with the Sandman system seems to be connecting the processed outputs of radar as analog signals into the standard Sandman inputs. Sandman also provides a DC expansion Box for connecting unconventional signals from external devices such as pH, CPAP, and etc. After initial experimenting, it was found that dc box provided a more stable interface between the Doppler radar and Sandman.

To connect the radar, the radar outputs go first through an analog to digital (A/D) conversion using Data Acquisition system (NI DAQ). After that, they are processed using our sleep From the description of the Sandman system the most conventional way to integrate the Doppler radar with the Sandman system seems to be connecting the processed outputs of radar as

analog signals into the standard Sandman inputs. Sandman also provides a DC expansion Box for connecting unconventional signals from external devices such as pH, CPAP, and etc. After initial experimenting, it was found that dc box provided a more stable interface between the Doppler radar and Sandman.

To connect the radar, the radar outputs go first through an analog to digital (A/D) conversion using National instrument algorithm in MATLAB and the results are converted to from digital to analog (D/A) signals using the same DAQ).

These analog signals are then connected to Sandman using the DC expansion box. Four outputs which sent to Sandman are:

1. Respiration trace from Doppler radar
2. Respiration rate calculated by our algorithm
3. Paradoxical sleep indicator which shows the occurrence of apnea or hypopnœa based on the radar data.
4. Paradoxical sleep indicator 10s: This shows the occurrence of apnea and hypopnea that last for more than 10s.

To send the valid data to sandman, several parameters must sets carefully. We will discuss them in the following sections.

3.5.1. Sampling rate

The analog signals from DC box are sampled and appear in the Sandman software user interface as an independent channel. Sandman has two sampling rate: the first is the base sampling rate which is equal for all of the channels and the second one is individual channel sampling frequency which can be set based on the data that is shown on that channel. To avoid data mismatch between sandman and the Doppler radar, the output sampling rate of the radar DAQ must be equal to the channel sampling frequency of Sandman. If sandman sampling rate is higher than DAQ, it interpolates the data coming from the DAQ to match for its sampling rate. In our experiments the sampling rate is set to 128Hz for all of the four radar channels.

3.5.2. Underflow error with DAQ due to the lack of computer memory in long term monitoring.

The flowchart of the Physiologic Radar Monitoring System (PRMS) is shown in

Figure 3-18.

As shown in

Figure 3-18 the data are recorded from the radar in one second epoch format. In each reading cycle the new recorded data is appended to the previous recorded data which is saved in the RAM memory. The data is then analyzed using the sleep algorithm and one second of the results is put in the DAQ output channel s to be send to Sandman. Hence; to send the valid data to Sandman the DAQ output buffer must be updated on each second. Otherwise the underflow error would happen and the last sample in the DAQ output buffer is send repeatedly to Sandman until new data arrive (Figure 3-19).

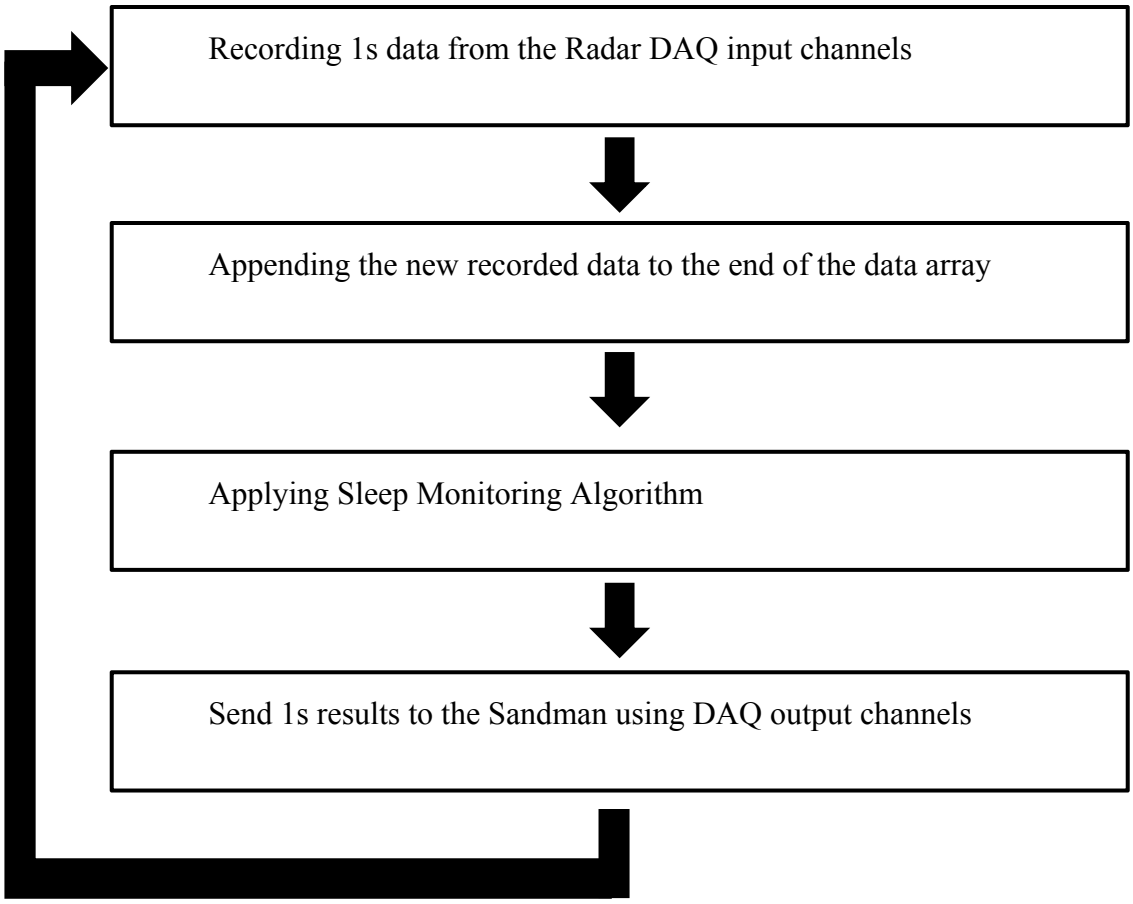

Figure 3-18. The flowchart of Radar Sleep Disorder Monitoring System

This problem arises in long-term monitoring in which the big amount of data from radar are recorded in the RAM memory which fill up and eventually causes the delay more than one second in processing the data and updating the DAQ output buffer and as a result underflow error will happen

To prevent such a problem, we free the RAM memory in each 30 minutes by saving the data to the hard disk.

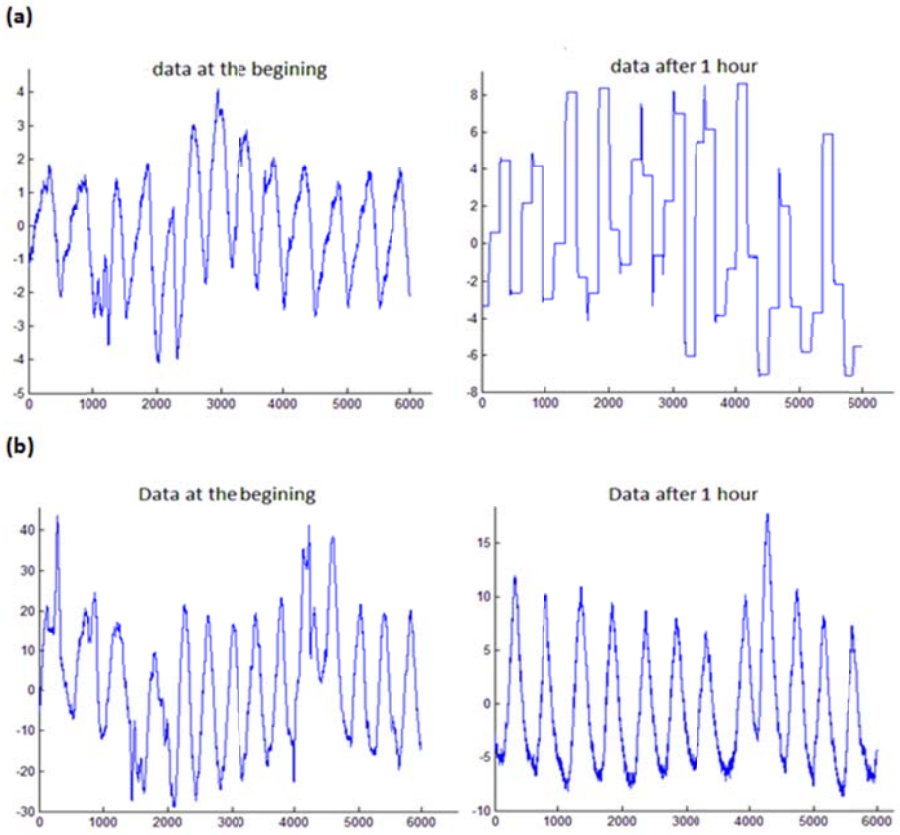

Figure 3-19 (a) Underflow Error happens after 1 hour of receiving data because of the memory lack. The output channel of the DAQ does not updated on-time causing the several transmitting of some of the samples to Sandman. (b) Resolving the problem by freeing the RAM to the hard disk every 30 minutes.

3.6. Sleep Disorder Monitoring Algorithm

To develop the sleep disorder monitoring algorithm, two set of nap studies were performed and offline analysis on the results were carried out. The sleep algorithm is then improved based on the comparison between the radar data and scored data acquired from Sandman. Finally the algorithm is modified to analyze the data and send the real-time result to

Sandman. The data recorded from the radar are processed by our sleep monitoring algorithm to detect apnea and hypopnea. The steps of the algorithm which is shown in Figure 3-20 are:

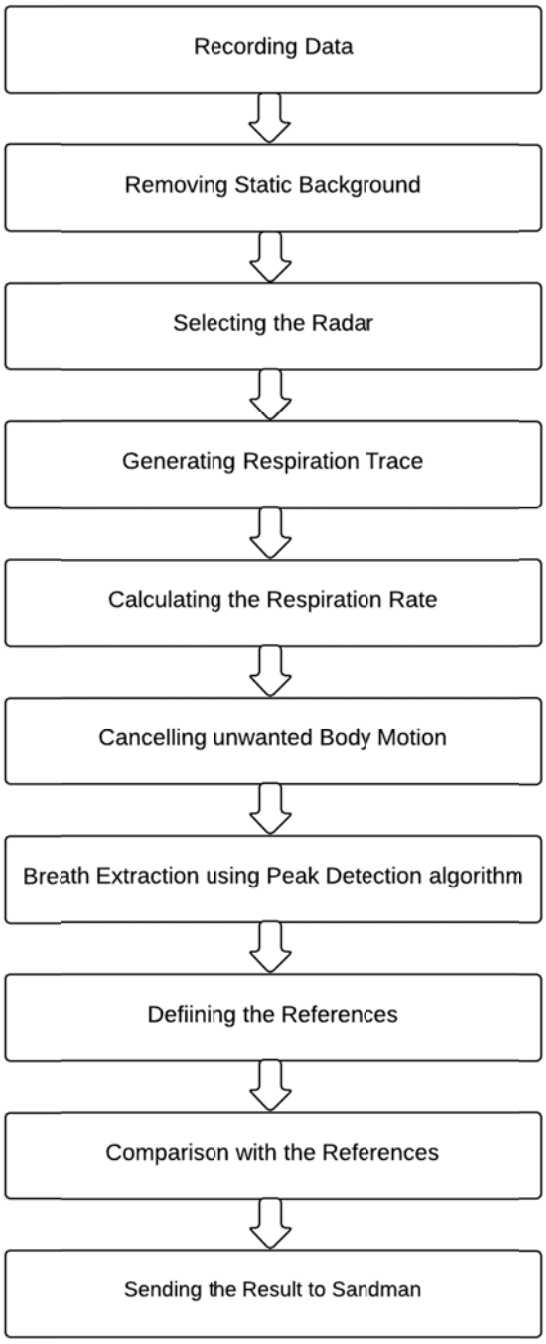

Figure 3-20 Sleep Disorder Monitoring Algorithm

1. **Recording data**: The data were recorded from two 2.4GHz Doppler radar. The subject lies down on the bed and the antenna is suspended on top of his chest. The distance between antenna and the subject is on meter.
2. **Removing static background:** The static background was removed by subtracting the average of the data from each channel:

$$x(t) = r(t) - \frac{1}{n}\sum_{k=0}^{n} r(t) \quad (3\text{-}1)$$

3. **Selecting the radar:** The data were acquired from two Doppler radar and based on the patient position to the radars; the data received from one radar has higher quality than the other radar. To select the radar, the variance of the data for the first 30s were calculated from:

$$\sigma^2 = \frac{1}{n-1}\sum_{k=0}^{n}(x_k - \bar{x})^2 \quad (3\text{-}2)$$

Where $\bar{x} = \frac{1}{n}\sum_{k=0}^{n} x_k$ and n is the number of elements in the signal. The channel consists respiratory data has higher variance and is selected for further data analyzing.

A sample of two radar signals and their variances are show in Figure 3-21.

4. **Generating respiration trace:** Respiration trace was acquired by combining I and Q-component of baseband data from the quadrature radar using linear demodulation. In this method, the input data were multiplied by the transpose of the matrix of eigenvectors of the covariance matrix. As a result, the Q-component is always in an optimum point (and the I-component always in a null point) [81], and were considered as a demodulated signal.

   The baseband signals and respiration trace are shown in Figure 3-22

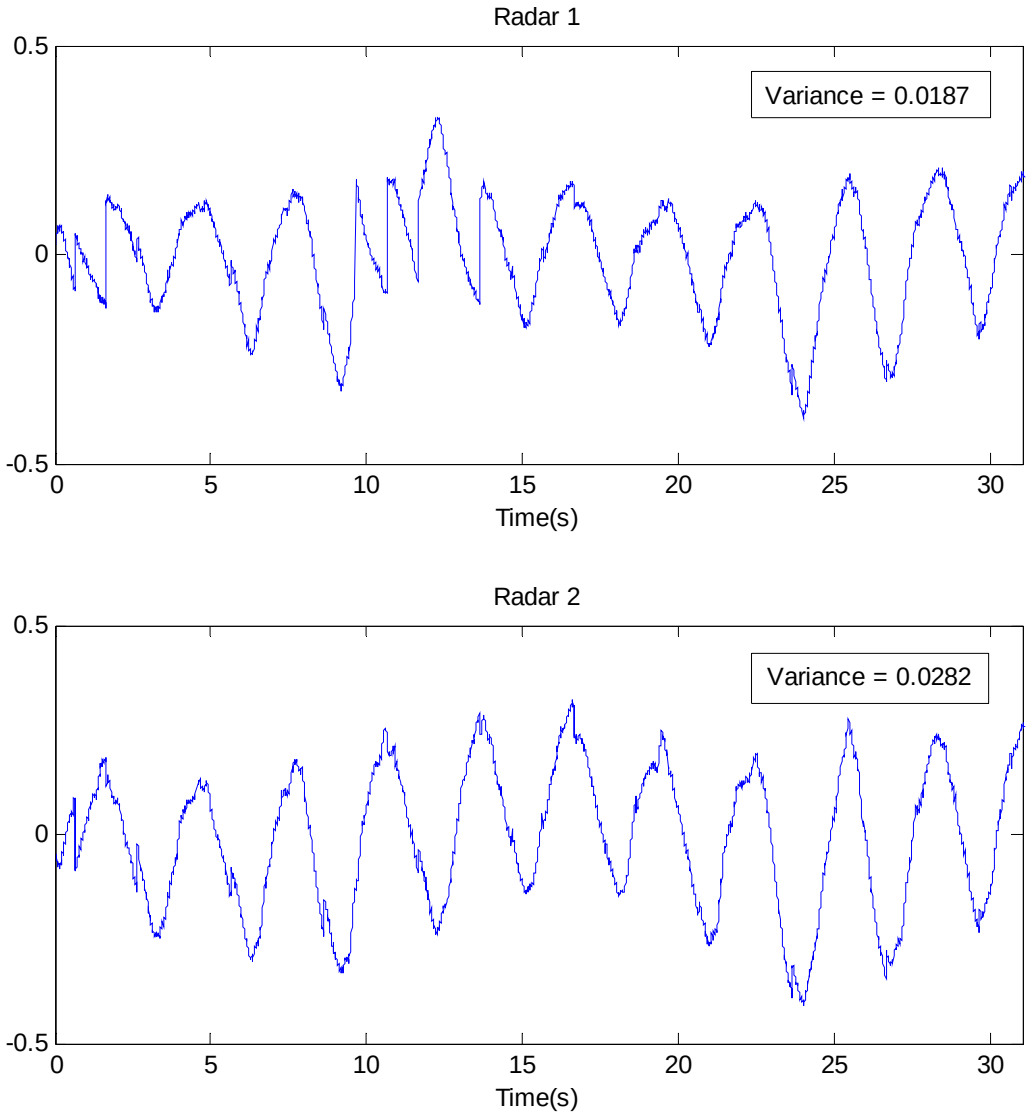

Figure 3-21 Selecting the radar. Radar 2 is selected since its variance is higher than radar 1

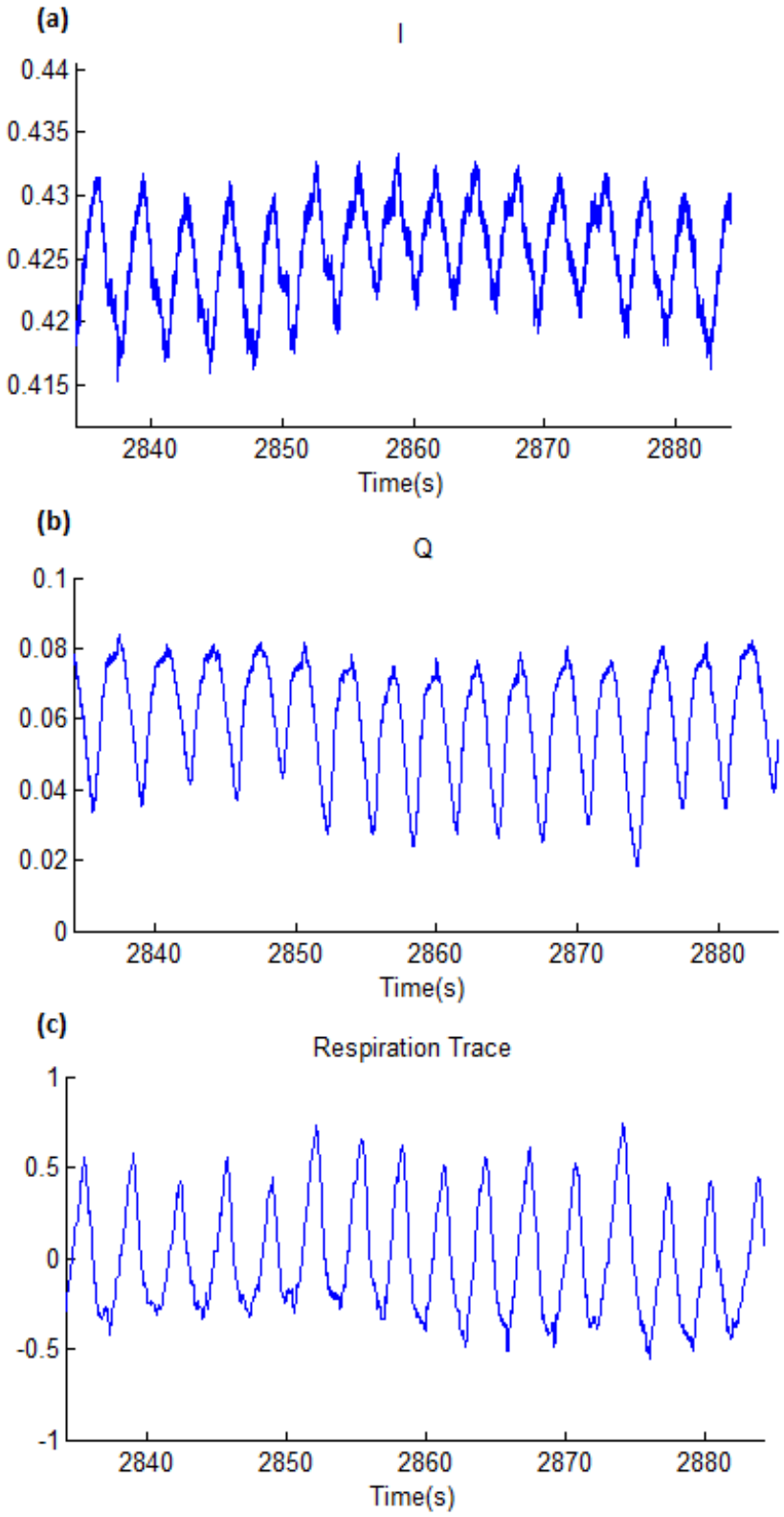

Figure 3-22 Generating respiration Trace(c) from baseband signal (a) and (b) using linear demodulation method

5. **Calculating respiration rate:** The respiration rate was calculated by taking an average from the rates acquired by two methods: a) The Fourier transform of the signal is calculated and the frequency of the peak in the frequency spectrum was selected as a respiration rate. b) In time domain, the local maxima were detected using peak detection algorithm and the time between two consecutive maxima was defined as one breath. The respiration rate then was the total number of breath per minutes. The available range in sandman is between -5 and 5 V. Hence; the calculated respiration rate (breath per minute) was divided by 10 and send to the Sandman. In case of paradoxical breathing the respiration rate was shown with a minus sign. Figure 3-23 shows a sample of calculated respiration rate.

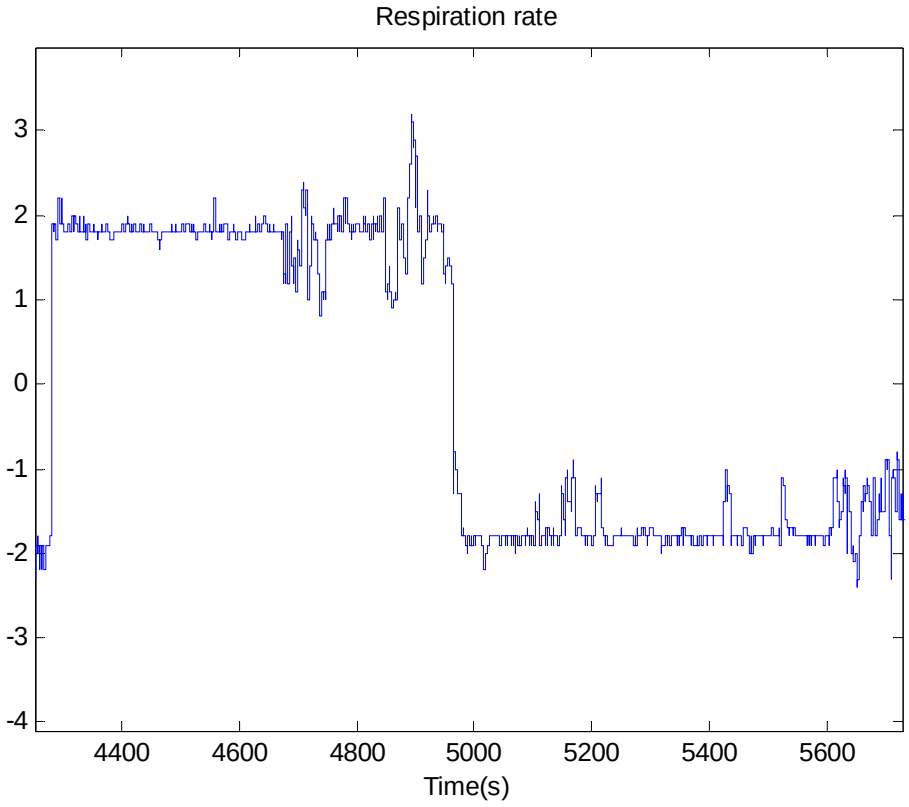

Figure 3-23 Respiration rate trace. Minus rate after 5000s shows the occurrence of paradoxical breathing.

6. **Cancelling unwanted body motion:** To remove the artifacts from unwanted body motion, the motion artifact detection algorithm uses different thresholds for

motion when switching off the rate and sleep apnea detection and reinitializing it. The algorithm indicates unwanted motion in Doppler signal if there is a sudden increase in amplitude and/or a sudden change in the rate of more than the normal value for respiration rate. Figure 3-24 shows the radar data when the patient moves his hand.

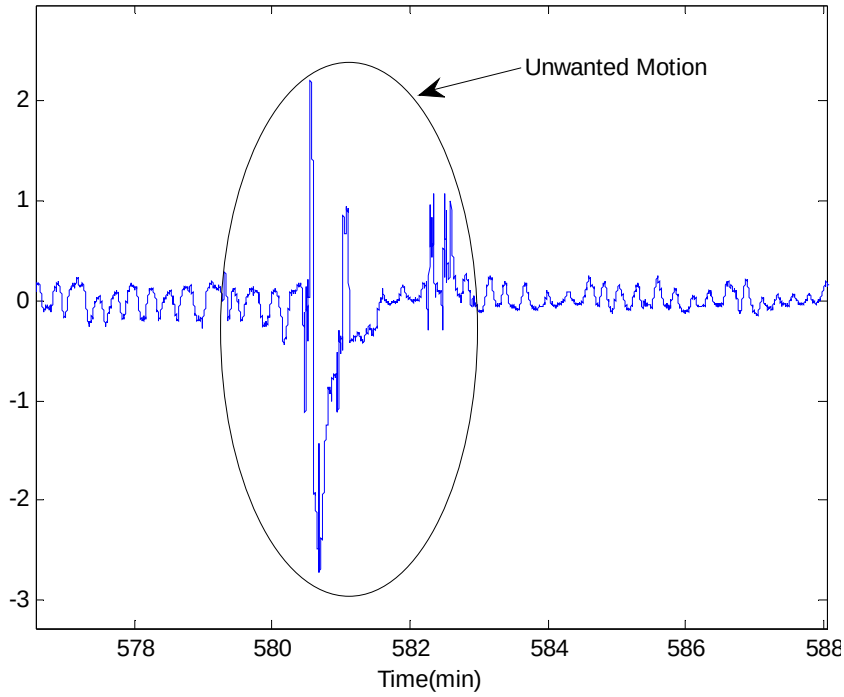

Figure 3-24 Unwanted hand movement causes a sudden increase in amplitude

7. **Breath extraction using peak detection algorithm:** The data between two local maxima was considered as a complete breath. Hence; for breath extraction a local maximum detect algorithm must develop. The first approach was to detect the zero passing points and find the peak between two zeros. However this method has two serious draw back. First, the signal may not pass the zero if paradoxical breathing happens and second, it may pass the zero several times because of the noise. We addressed this problem by proposing a local peak detection algorithm the spes of the algorithm are:

a. Smoothing the signal by applying a moving average filter. A moving average filter.

b. Subtracting each samples of the signal from the previous sample:

$$dif(i) = s(i) - x(i-1) i = 2,3,\dots,N \quad (3\text{-}3)$$

c. Determining the sign

$$sgn(i)\begin{cases} +1, & d\,if(i) \geq 0 \\ -1, & dif(i) < 0 \end{cases} \quad (3\text{-}4)$$

d. Subtracting each samples of the *sgn* from previous sample.

$$d(i) = sgn(i) - sgn(i-1)\ \ i = 2,3,\dots,N-1 \quad (3\text{-}5)$$

e. Appending a zero at the beginning to match the index

f. Detecting the local maxima and minima

$$\begin{cases} \text{d is local min,} & \text{if d (i)} > 0 \\ \text{d is local max,} & \text{if d(i)} < 0 \\ \text{other} & \text{if d(i)} = 0 \end{cases} \quad (3\text{-}6)$$

Figure 3-25 shows the algorithm steps for a sample signal.

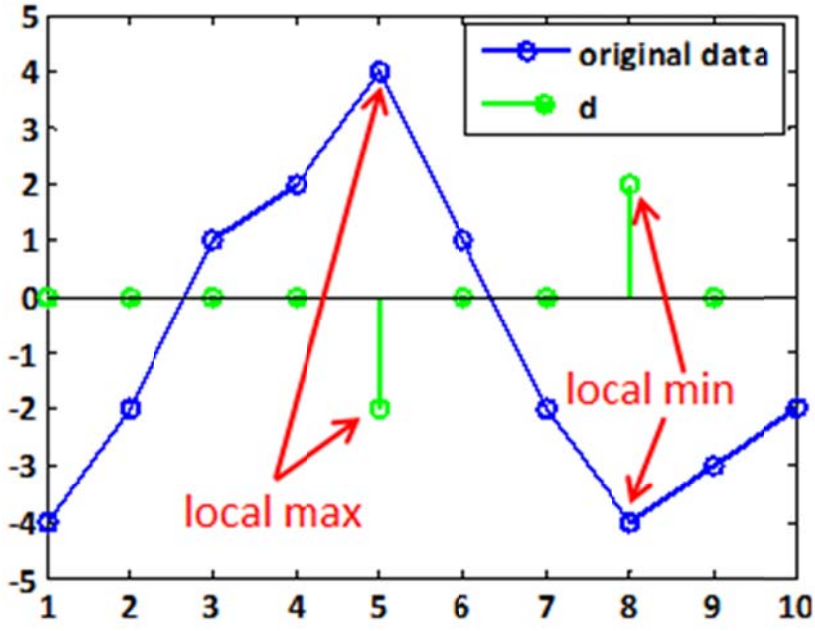

Figure 3-25. Peaks detection algorithm. The index of negative points in d matches to the local maxima in the signal.

In actual respiration signal, the existence of the noise generates wrong local maxima or minima in the signal in random places (Figure 3-26.a). To remove this wrong exterma, and additional criteria is added to the algorithm: two consecutive minima without a maxima is considered as one and vice versa. Figure 3-26b shows the result of the algorithm after this step.

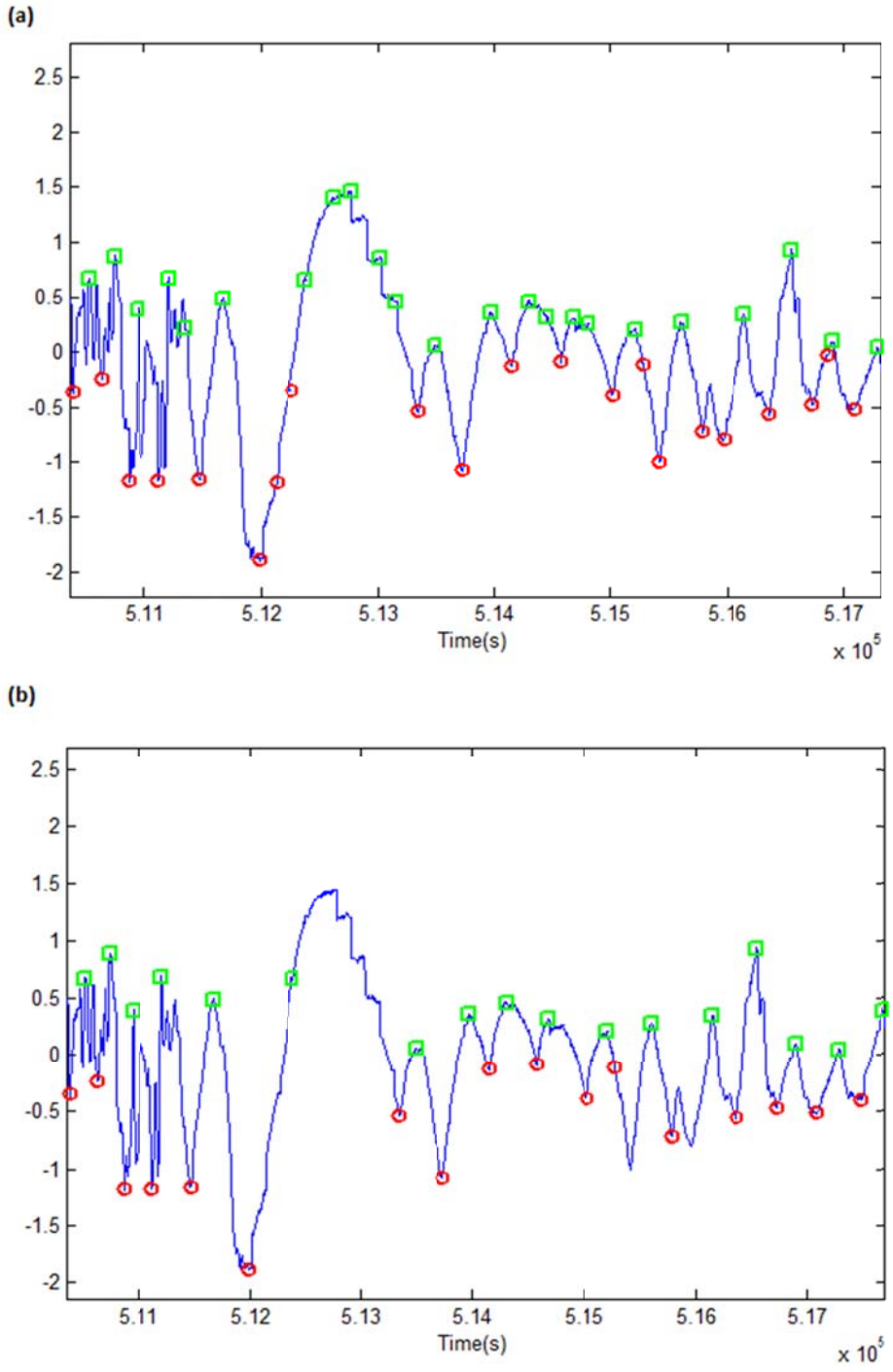

Figure 3-26 Peak detection algorithm. (a) Before (b) After removing wrong exterma

8. **Defining the References:** Two types of references were considered. In **Static threshold** mode it is considered that the patient breaths normally during the first 30s of data. The following parameter is calculated for comparison:

a. The average of energy of each breath. The energy of a signal is calculated by:

$$E = \sum_{k=0}^{n} {x_k}^2 \quad (3\text{-}7)$$

b. The average of duration of each breath.

c. The average area of the arcs of each breath. The arc is determined by plotting the Q-component of the radar data for each breath versus its I-component.

In **Dynamic threshold** mode the references is updated continuously using the last four normal breaths.

9. **Comparison with the References**; Comparing the radar data of nap studies with the sleep technician scored data from Sandman shows the signal amplitude falls under 80% and 60% of the reference for apnea and hypopnea respectively because of decreasing the respiration depth. Figure 3-27 and Figure 3-28 shows a sample of the signal changes when an apnea and hypopnea occurs.

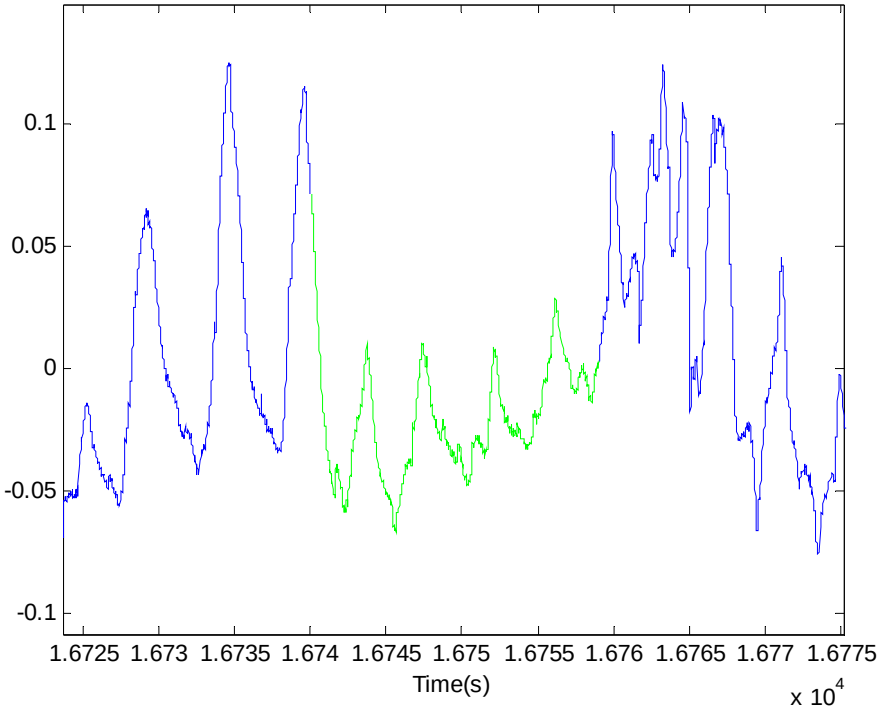

Figure 3-27 60% drop in signal amplitude during a hypopnea

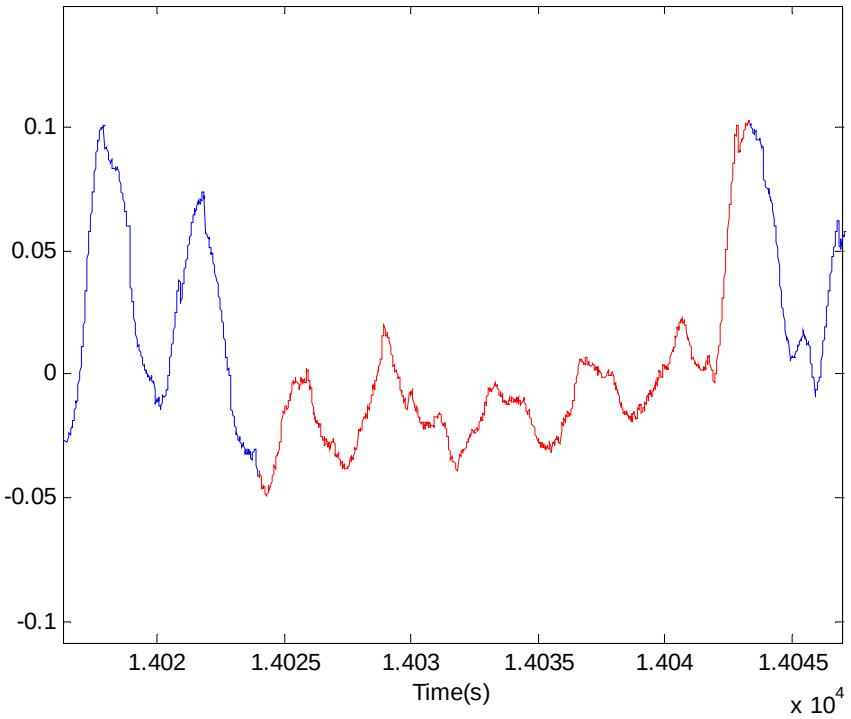

Figure 3-28 80% drop in signal amplitude during a hypopnea

Moreover, the duration of each breath during paradoxical breathing is 40% and 20% longer or shorter than normal breathing for apnea and hypopnea respectively.

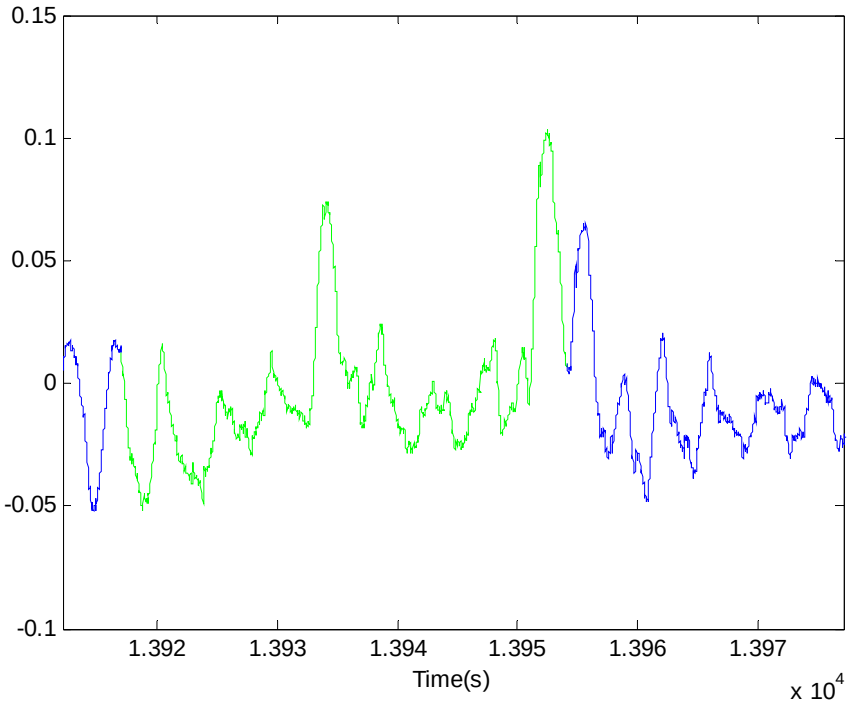

Figure 3-29 Changing the shape and breathing interval during a hypopnea

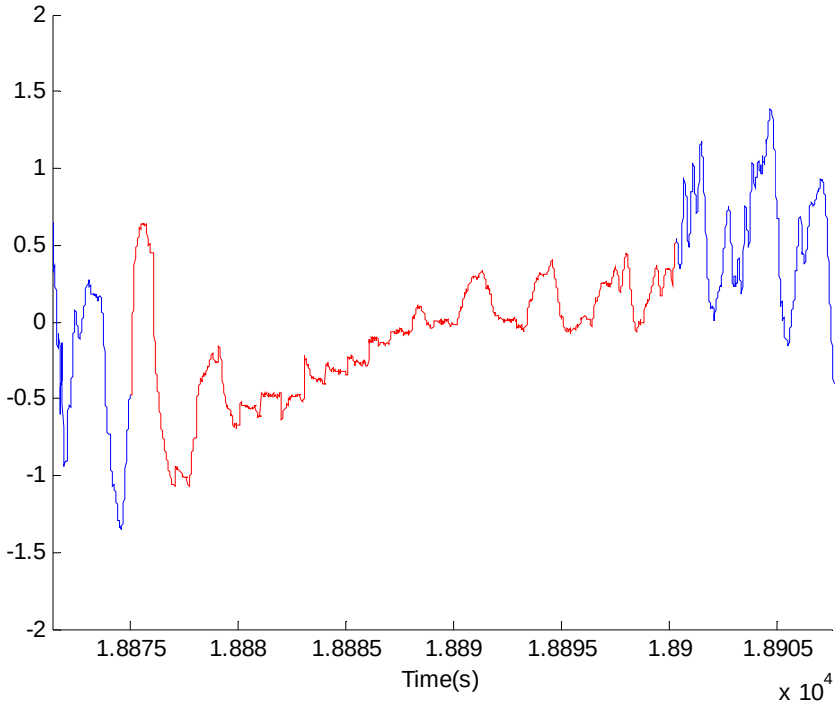

Figure 3-30 Changing the shape and breathing interval during an apnea

Figure 3-32 shows the arc forming due to I and Q channels for a normal breath (from a local minimum to the next local minimum) and apnea. As shown in Figure 3-32, the area of the arc increases as a result of apnea.

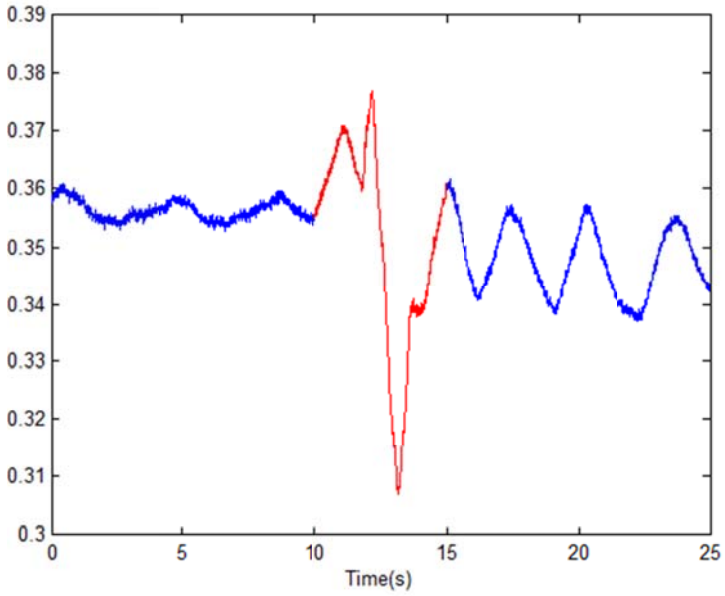

Figure 3-31 An apnea lasting for 5 seconds

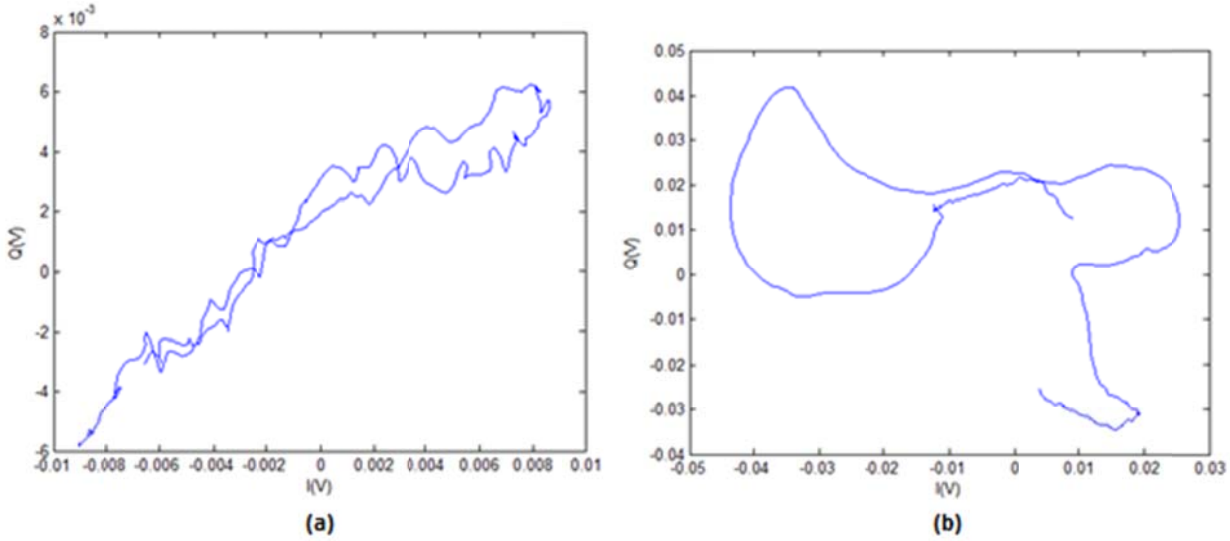

Figure 3-32 Arc formed due to I and Q channels (a) A normal breathing (b) Apnea Breathing

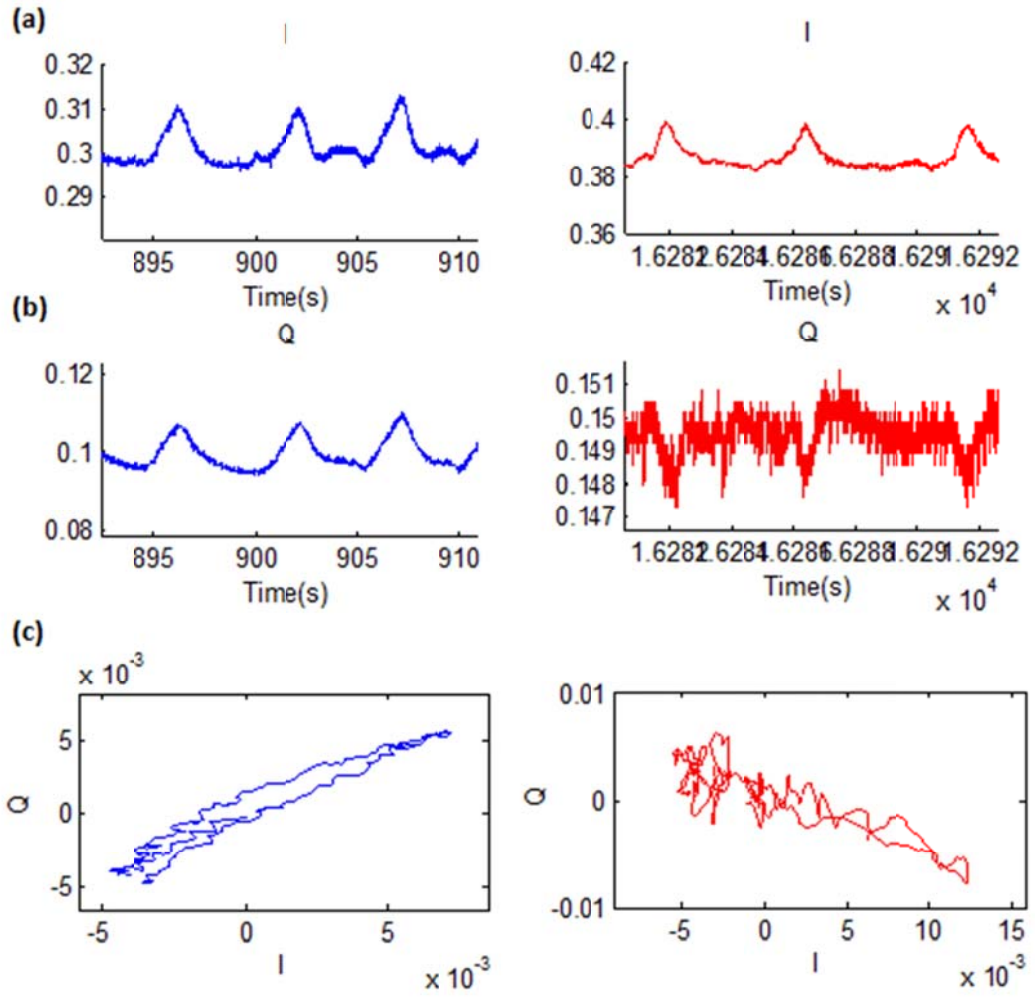

Figure 3-33 Normal (right column) versus apnea (left column) (a) I (b) Q and (c) the I-Q plot for one breath. The area of the arc increases from 1.0227e-05 to 2.1737e-05 in apnea situation.

Two decisions were made and sent to the output based on the comparison. The first output is the result of comparison for each breath. It becomes one or two if hypopnea or apnea has happened. Hence; the delay for this output is equal to duration of one breath. The second output is set when the apnea or hypopnea lasts more than 10s. So it has 10s delay relative to respiration trace.

10. **Sending the Result to Sandman:** as explained earlier, the respiration trace, respiration rate, comparison result for each breath (actigraphy 3) and 10s comparison (actigraphy 10) were send to Sandman as a results of sleep disorder monitoring algorithm Figure 3-34.

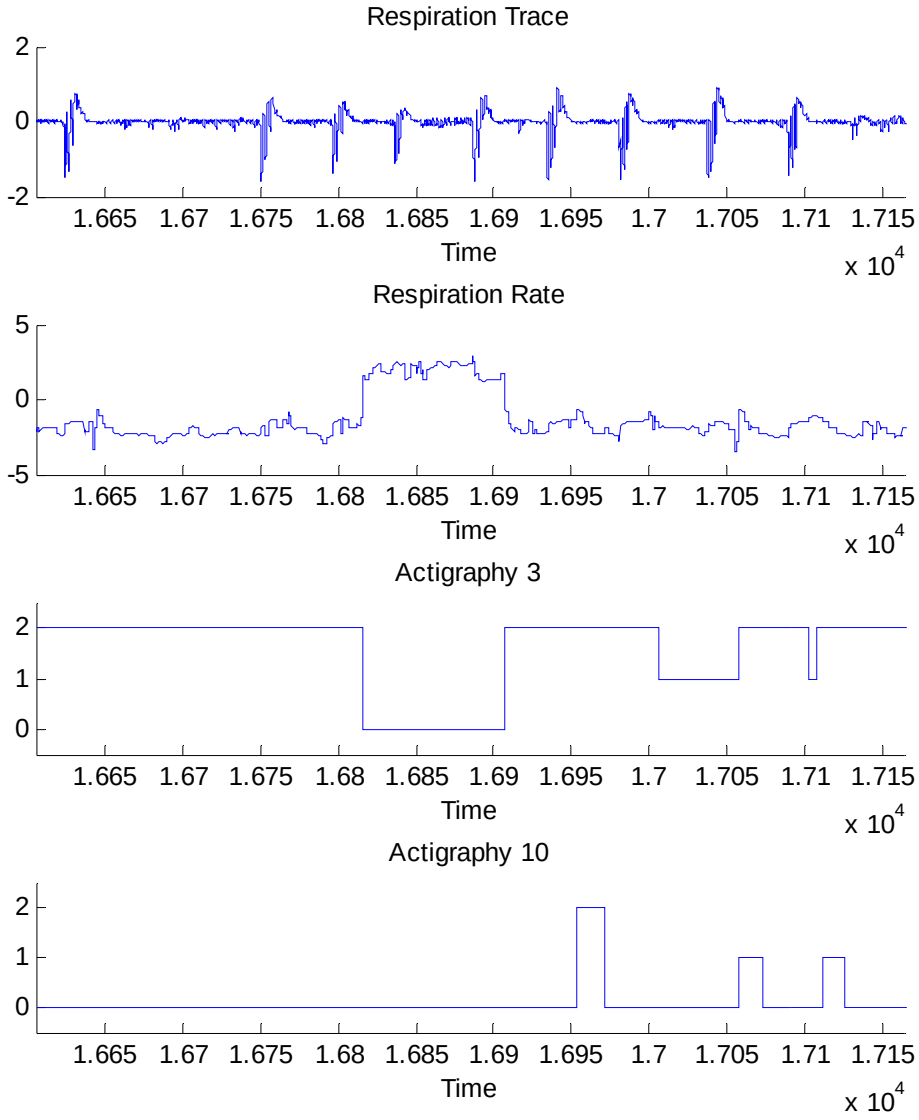

Figure 3-34 - A snapshot of the outputs that are sent to Sandman

Chapter 4

PRMS in Clinical Study

The PRMS system was developed for monitoring a human target during sleep, measuring the respiration rate, the respiration depth and detecting sleep disorders including different kinds of apnea and hypopnea.

In this chapter, the experimental setup and protocol for using PRMS in clinical studies along with Sandman system as gold standard is explained. The information about the population under studies is also outlined in this chapter.

4.1. Experiment Setup

The overnight sleep studies were carried out in a certified sleep study center at Queen's Medical Center in Hawaii. The size of the room is approximately 5 by 6 m^2. The PRMS must be compact because it shouldn't obstruct the movement of the subject. Careful placement of radar is essential as Doppler radar would give most sensitivity for motion that is orthogonal to the plane of the antenna. Hence; the transceiver antennas were installed vertically on top of the chest of the lying patient using a camera stand in a way that the chest and abdomen movements are to the plane of the antenna. The target lies comfortably on his back such that the Doppler radar monitors the front of the body. The distance between antenna board and the patient's chest is 1 meter. This is the nearest safe distance without obstructing the patient movement. The antenna board installation is shown in Figure 4-1.

Figure 4-1 Antenna board installation for sleep disorder monitoring.

The I and Q outputs of two 2.4GHz radar and 7 Outputs of 24GHz radar were converted from analog to digital using Ni DAQ and analyzed using sleep monitoring algorithm in MATLAB. The results are then converted back from digital to analog using the same DAQ to be connected to the Sandman system as a reference.

4.2. Gold Standard

The Sandman system was used as a gold standard. Multiple physiological variables are continuously recorded. These variables include sleep staging using the electroencephalogram, electromyogram, electrooculogram, respiration (flow, effort, oxygen saturation), and snoring. The movement of the chest and abdomen of the patient is tracked using a chest and abdomen effort belts. The patient is monitored by a nurse using a camera the whole night. Using these signals, it is possible to precisely quantified the distorted breath as well as its effect on sleep and blood oxygen saturation level.

Figure 4-2 shows the complete experiment setup. A snapshot from Sandman sleep software which includes all signals is shown in Figure 5.3.

Figure 4-2 Experiment setup for sleep disorder monitoring

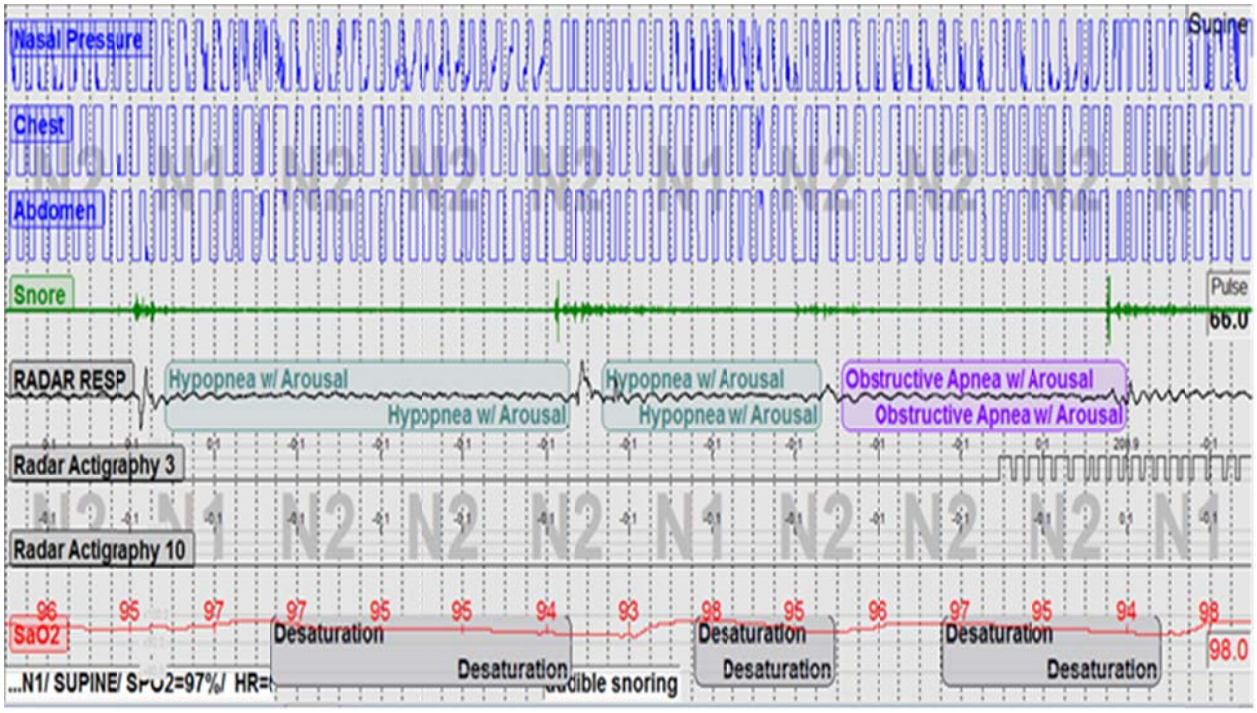

Figure 4-3 A snapshot from Sandman sleep software. The PRMS signals are shown in black.

4.1. Subject Physical Characteristics

4.1.1. Body Mass Index

The body mass index (BMI) of an individual is defined as the body weight divided by the square of the height. The formula in SI units is as follows:

$$BMI = \frac{Weight}{Height^2} \ (Kg/m^2) \tag{4-1}$$

This formula is very commonly used in medicine to estimate the ideal healthy weight of a person based on their height. While it ignores body fat percentage, it is a crude, easy to understand, and generally accurate measurement of whether a person is underweight (BMI < 19), normal weight (19-25), overweight (25-30), or obese (30-39). Each individual subject in the tests was weighed using a strain-gauge based digital scale and height measured. The BMI was then calculated using these measurements.

4.1.2. Neck circumference

A measuring tape is wrapped around the neck of the subject in a horizontal plane and at the middle of the neck.

4.1.3. Chest circumference

By wrapping the measuring tape around the chest, the circumference is measured at maximum inhalation and maximum exhalation. The variation of the chest and breadths circumferences with respiration is an indication on the volume of air flowing into the body during inhalation.

4.1.4. Abdomen circumference

A measuring tape is wrapped around the abdomen of the subject in a horizontal plane and at the level of natural waist. Maximum and minimum circumferences are measured at maximum inhalation and exhalation, respectively. The average abdomen circumference with respect to height represents another mean to assess body obesity.

The physical characteristics obtained for the population of subjects are shown in Table 4-1. Four women and six men were studied. The ages range from 34 to 67 years with an average of 49 years, the average weight-228 pounds with the maximum and minimum of 134 and 322 pounds, the body mass index with the average of 36.7 varies from 24.5 to 53.6 kg/m^2. The averages of neck, chest and abdominal circumference are 17.2 (range: 12.2-20.7), 46.5 (range: 38-55.2) and 45.9 (range: 33.5-56.5) respectively (Table 4-2).

Table 4-1 Subjects physical characteristics

Subject ID	Weight (lb)	Height (inches)	BMI	Neck Circumference (inches)	Chest Circumference (inches)	Abdominal Circumference (inches)
1	257.8	65	42.89548	20.7	52.5	50.2
2	297	70	42.61041	18	49.7	51.2
3	322	65	53.57775	20	53	51.7
4	237.4	67	37.17804	19	49	47.2
5	177.6	65	29.55096	16	41.5	41
6	337.8	70	48.46396	20.5	55.2	56.5
7	134.6	58.5	27.64959	12.2	38	33.5
8	253.4	71	35.33827	17.5	45.2	48.5
9	250	64	42.90771	15.2	51.2	48
10	235.9	75	29.48226	17	44	46

Table 4-2 Overview of subjects physical characteristics

Variable	N	Mean	Std Dev	Minimum	Maximum
Weight (lb)	10	215.2	72.5	107	322
Height (inches)	10	65.9	4.5	58.5	75
BMI	10	35.1	11.4	13.4	53.6
Neck circumference (inches)	10	17	2.7	12.2	20.7
Chest circumference (inches)	10	46.6	5.7	38	53
Abd circumference (inches)	10	45.3	6.6	33.5	51.7

4.2. Procedure of the experiments

As the volunteering subject was welcomed in the sleep lab, he was guided to the test room to have an explanation about the experiment procedure and the equipment used. Questions were allowed before the experiment to provide a learning experience for those who are interested. The subject was then directed to another room to go over the consent form and sign it.

In the test room, a nurse connect all the sandman leads (chest and abdomen belts, EEG leads, etc.) to the subject and then the subject lies down on the bed and the antenna is suspended on top of his chest. The subject stays for the whole night and his breathing is monitored during the sleep. He was not allowed to use CPAP since it prevents happening the paradoxical breathing.

During the time while the test is running, the subject is the only person present in the room. For control and monitoring purposes, a computer outside the test room is controlling the DAQ and the radar inside the room. The data from all subjects are analyzed real-time using the sleep monitoring algorithm. The baseband signals, the respiration trace resulting from combining the I/Q as well as the respiration rate and algorithms results (i.e. Atigraphy s and 10) are plotted real-time while being recorded Figure 4-4.

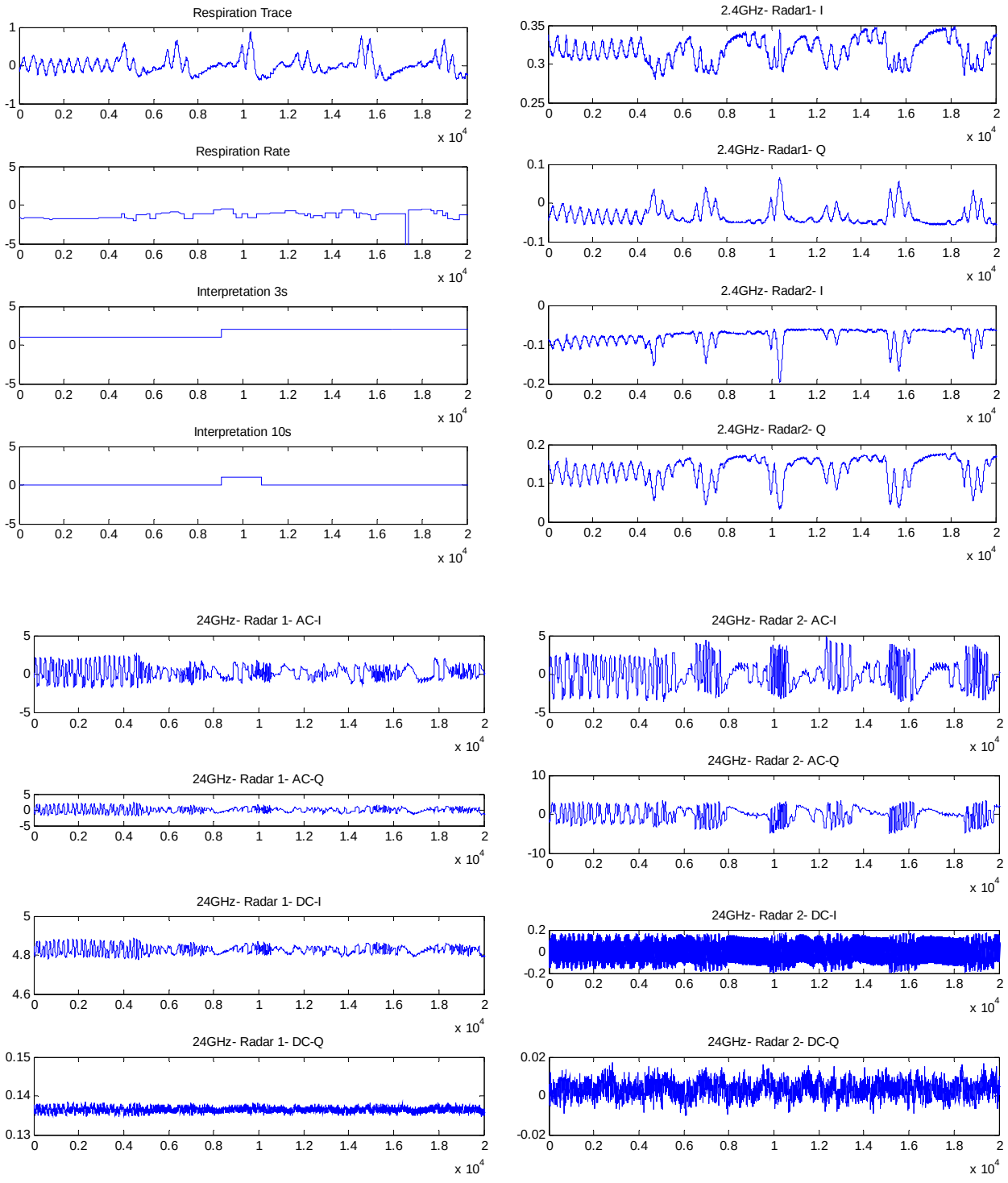

Figure 4-4 An snapshot of real time recording in MATLAB

Chapter 5

Evaluation of Physiological Radar Sleep monitoring system

To evaluate the possibility of integrating the PRMS into a conventional sleep monitoring system, scoring rules were developed to identify normal breathing, hypopnea and apneas. The output of the gold standard system and PRMS were scored separately by two blinded technologists and organized using the Sandman software. The PRMS scored results was then compared to the gold standard.

In this chapter the scoring rules for gold standard system and PRMS are explained more in detail. Then the scoring results of two system is preented following by the comparison result.

5.1. Gold standard scoring rules

The gold standard data was scored using respiratory rules for adults stated in AASM manual for the scoring of sleep (2007). In this manual, it is recommended to use an oronasal thermal sensor to detect absence of airflow for apnea detection. For hypopnea detection, the sensor is a nasal air pressure transducer with or without square root transformation of the signal. The respiratory effort is detected either by esophageal manometry, or by calibrated or uncalibrated inductance plethysmography. A pulse oximetr with a maximum acceptable signal averaging time of 3 seconds is recommended for detection of blood oxygen [82].

5.1.1. Apnea Rules

A respiratory event is scored as an apnea when the following criteria are met [82] (Figure 5-1):

1. There is a drop in the peak thermal sensor excursion by ≥90% of baseline
2. The duration of the event lasts at least 10 seconds.

3. At least 90% of the event's duration meets the amplitude reduction criteria for apnea

The scored apneas are then classified in an adult based on following rules [82].

1. An apnea event is scored as an obstructive apnea if it meets the above apnea criteria and is associated with continued or increased inspiratory effort throughout the entire period of absent airflow [82].
2. A respiratory event is scored as a central apnea if it meets the above apnea· criteria and is associated with absent inspiratory effort throughout the entire period of absent airflow [82].
3. A respiratory event is scored as a mixed apnea if it meets the above apnea criteria and is associated with absent inspiratory effort in the initial portion of the event, followed by resumption of inspiratory effort in the second portion of the event [82].

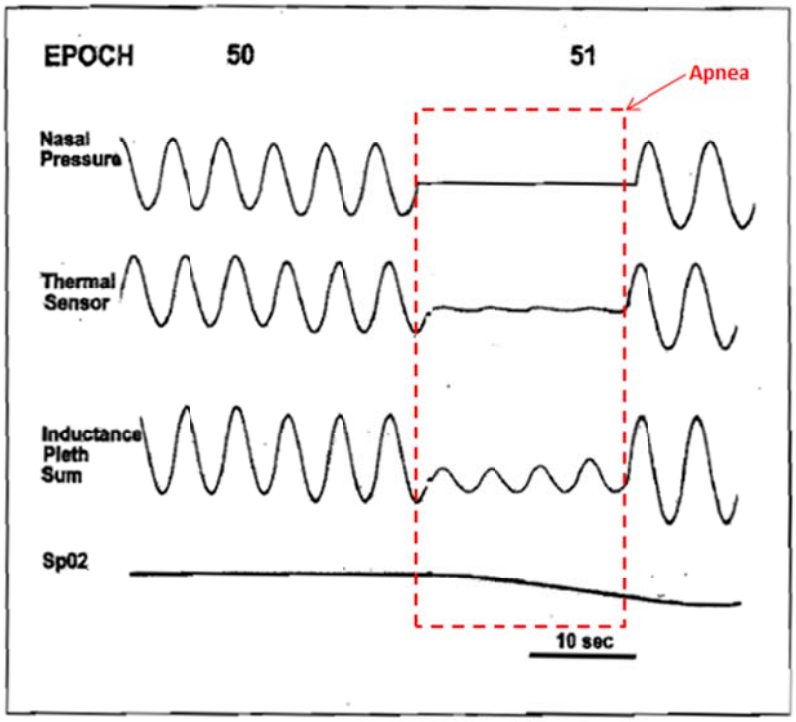

Figure 5-1 Apnea rules [82]

5.1.2. Hypopnea Rules

The recommended criteria for detecting a hypopnea are (Figure 5-2) [82].

1. The drop of the nasal pressure signal excursions by more than 30% of baseline
2. The nasal pressure signal drop lasts at least 10 seconds
3. More than 4% desaturation occurs from pre-event baseline
4. Amplitude reduction of criteria for hypopnea happens in at least 90% of the event's duration.

Alternatively a respiration event is scored as a hypopnea if following criteria are met [82].

1. The drop of the nasal pressure signal excursions by more than 50% of baseline
2. The nasal pressure signal drop lasts at least 10 seconds
3. More than 3% desaturation occurs from pre-event baseline or the event is associated with arousal
4. Amplitude reduction of criteria for hypopnea happens in at least 90% of the event's duration.

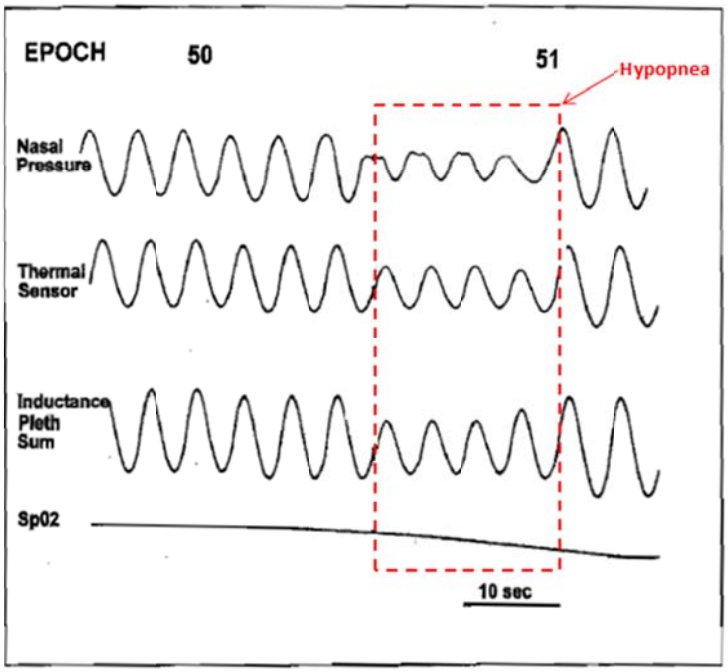

Figure 5-2 Hypopnea rules

5.2.PRMS scoring rules

The following rules were used for scoring PRMS respiration trace. The data were scored using only these channels

- Radar respiration
- Radar respiration Rate
- Radar actigraphy 3
- Radar actigraphy 10
- SpO2
- Video

The scoring rules were as follows:

1. Actigraphy 3 & 10:

(0) = Symmetrical movement,

(1) = Phase delay,

(2) = Paradoxical effort,

(-4) =Unwanted movement

2. Apneas:

Actigraphy shows (1) or (2) - paradoxical or phase delay with reduction in, or flat respiratory excursion channel, and with or without 4% oxygen desaturation.

3. Hypopneas:

Actigraphy shows (0) or (1) -symmetrical or phase delay with normal or reduced respiratory excursion, and with a 4% desaturation.

4. Apneas and hypopneas will be at least 10 seconds in duration (The AASM Manual for the Scoring of Sleep and Associated Events 2007).

5.3. Scoring parameters

For each subjects, the following parameters are calculated after scoring.

1. Total Recording Time(TRT)

This parameter shows the total time of recording signals using the sleep monitoring systems.

2. Total Sleep Time (TST)

This number shows the total time that the subject was sleeping. The state of wakefulness are determine using electroencephalogram (EEG).

3. Sleep efficiency:

The Sleep efficiency is calculated as the ratio between the total sleep time and the total recording time

4. WASO

Wake time after sleep onset (WASO) defines as the amount of time spent awake after sleep has been initiated and before final awakening [83]. Increasing WASO will decrease in sleep efficiently

5. REM latency

Once a person sleep, he progresses through four stages of increasingly deep, dreamless sleep and into a fifth stage during which dreaming occurs. This fifth stage is called Rapid Eye Movement (REM) sleep and it is characterized by the rapid and random movement of the eyes, low muscle tone and a rapid, low-voltage EEG [84].

The REM latency is defined as the time span between the beginning of the sleeping and the first onset of REM sleep[85].

6. Central Apneas (CSA)

It shows the total number of CSA happening during one recording. Central sleep apnea (CSA) happens when the effort to breathe is diminished or absent. It usually lasts for 10 to 30 seconds and links with a reduction in blood oxygen saturation [86]. It is a collective term referring to two breathing disorders: Cheyne-Stokes respiration (an abnormal pattern of breathing characterized by progressively deeper and sometimes faster breathing)and periodic breathing [87].

7. Obstructive sleep apnea (OSA)

It is defined as the total number of obstructive sleep apnea happening in one recording.

Obstructive sleep apnea (OSA) happens as a result of obstruction of the upper airway and is characterized by repetitive pauses in breathing during sleep in spite of the effort to breathe. Blood oxygen saturation usually reduces during OSA.

8. Mixed apneas

This parameter shows the total number of mixed apnea that happens in one recording.

Mixed apnea is the combination of both types. The central apnea is developed as a result of severe and longstanding episode of obstructive apnea [49].

9. Hypopneas

This parameter shows the total number of hypopnea that happens in one recording.

Hypopnea is characterized by reduction in but not complete cessation of airflow to less than 50% of normal. Blood oxygen saturation also usually reduces during hypopnea [3].

10. Total apneas

This is the total number of apneas including obstructive, central and mixed apneas.

11. Apnea + hypopnea

This parameter shows the total number of apnea and hypopnea happening during one recording.

12. Central apnea index

This number shows the frequency of central apnea per hour of sleep.

13. OBS apnea index

This parameter is defined as the number of obstructive apnea episode per hour of sleep.

14. Mixed apnea index

This number shows the frequency of mixed apnea per hour of sleep.

15. Hypopnea index

This number shows the frequency of hypopnea per hour of sleep.

16. Total apnea index

This parameter is defined as the number of apnea episode per hour of sleep.

17. apnea–hypopnea index(AHI)

Apnea–hypopnea index is an index of sleep apnea severity. It is defined as the frequency of apneas and hypopneas per hour of sleep [3].

18. Max SPO2

This number shoes the maximum level of blood oxygen saturation level measured by a pulse oximeter during the recording.

19. Min SPO2

This number shoes the minimum level of blood oxygen saturation level measured by a pulse oximeter during the recording.

20. Max SPO2

This number shoes the average level of blood oxygen saturation level measured by a pulse oximeter during the recording.

21. Max HR

This parameter shows the maximum measured heart rate in one recording.

22. Min HR

This parameter shows the minimum measured heart rate in one recording.

23. Mean HR

This parameter shows the average measured heart rate in one recording.

5.4.Scoring Result

The results of scoring gold standard and PRMS data for 10 subjects are shown in Table 5-1 and Table 5-2 respectively.

Table 5-1 Scoring result for gold standard

Subject ID	TRT Gold	TST Gold	Sleep efficiency	WASO	REM latency	SPON arousals
1	400.4	353	88.1	47.5	82.5	26
2	431.9	315.5	73	65	188	10
3	406.9	375.5	92.3	26	158.5	29
4	456.4	93	20.4	299	216	46
5	425.4	298	70	123	188.5	15
6	452.9	410	90.5	42	215.5	66
7	438.4	345	78.7	89.5	145	57
8	361.9	266	73.5	43.5	124.5	44
9	377.9	298.5	79	21.5	63.5	11
10	432.9	342.5	79.1	51	109.5	47

Table 5-1. Scoring result for gold standard (continued)

Subject ID	Central apneas	OBS apneas	Mixed apneas	Hypopneas	Total apneas	Apnea + hypopnea
1	0	28	0	204	28	232
2	13	150	191	103	354	457
3	0	1	0	88	1	89
4	23	18	7	14	48	62
5	0	202	3	76	205	281
6	0	0	0	12	0	12
7	0	21	0	113	21	134
8	0	3	0	107	3	110
9	0	0	0	60	0	60
10	4	3	1	136	8	144

Table 5-1. Scoring result for gold standard (continued)

Subject ID	Central apnea index	OBS apnea index	Mixed apnea index	Hypopnea index	Total apnea index	Apnea hypopnea index
1	0	4.8	0	34.7	4.8	39.4
2	2.5	28.5	36.3	19.6	67.3	86.9
3	0	0.2	0	14.4	0.2	14.2
4	14.8	11.6	4.5	9	31	40
5	0	40.7	0.6	15.3	41.3	56.6
6	0	0	0	1.8	0	1.8
7	0	3.7	0	19.7	3.7	23.3
8	0	0.7	0	24.1	0.7	24.8
9	0	0	0	12.1	0	12.1
10	0.7	0.5	0.2	23.8	1.4	25.2

Table 5-1. Scoring result for gold standard (continued)

Subject ID	Max SPO2	Min SPO2	Mean SPO2	PLMS	PLMS arousals	PLMS arousal index	Max HR	Min HR	Mean HR
1	99	66	89.4	67	1	0.2	85	43	61
2	100	72	90.2	33	0	6.3	84	48	61.2
3	99	85	94.2	0	0	0	101	61	77.7
4	100	76	96.7	0	0	0	76	45	55.3
5	100	63	91.9	0	0	0	93	62	72.5
6	100	88	93.9	0	0	0	88	63	72.6
7	99	85	95.4	0	0	0	102	60	73.8
8	100	93.4	76	0	0	0	77	40	56.4
9	100	86	97	0	0	0	57	38	46.4
10	99	82	94.1	0	0	0	83	47	63.8

Table 5-2 Scoring result for PRMS

Subject ID	Central apneas	OBS apneas	Mixed apneas	Hypopneas	Total apneas	Apnea + hypopnea
1	0	116	0	94	116	210
2	0	382	0	21	382	403
3	0	54	0	28	54	82
4	0	80	0	4	80	84
5	0	1	0	14	1	15
6	0	60	0	80	60	140
7	0	81	0	43	81	124
8	0	55	0	20	55	75
9	0	114	0	39	114	153
10	0	81	0	43	81	124

Table 5-2 Scoring result for PRMS (continued)

Subject ID	Central apnea index	OBS apnea index	Mixed apnea index	Hypopnea index	Total apnea index	Apnea hypopnea index
1	0	19.7	0	16	19.7	35.7
2	0	72.7	0	4	72.7	76.6
3	0	8.6	0	4.5	8.6	13.1
4	0	56.1	0	2.8	56.1	58.9
5	0	19.3	0	30.6	19.3	49.9
6	0	0.1	0	2	0.1	2.2
7	0	10.4	0	13.9	10.4	24.3
8	0	18.3	0	9.7	18.3	28
9	0	11.1	0	4	11.1	15.1
10	0	20	0	6.8	20	26.8

Table 5-2 Scoring result for PRMS (continued)

Subject ID	Max SPO2	Min SPO2	Mean SPO2
1	99	66	89.4
2	100	72	90.2
3	99	85	94.2
4	100	76	96.7
5	100	63	91.9
6	100	88	93.9
7	99	85	95.4
8	100	76	93.4
9	100	86	97
10	99	82	94.1

5.5.Scoring comparison

The overall results of gold standard and PRMS are depicted in Table 5-3 and Table 5-4.

Table 5-3 Gold standard overall scoring results

Variable	N	Mean	Std Dev	Minimum	Maximum
Total recording time (min)	10	418.5	31.2	361.9	456.4
Total sleep time (min)	10	309.7	86.8	93	410
Sleep efficiency (min)	10	74.4	20.5	20.4	92.3
Central apnea index	10	1.8	4.6	0	14.8
Obstructive apnea Index	10	9.1	14.2	0	40.7
Mixed apnea index	10	4.2	11.4	0	36.3
Hypopnea index	10	17.5	9.1	1.8	34.7
Total apnea index	10	15.0	23.5	0	67.3
Apnea hypopnea index	10	32.4	24.8	1.8	86.9
Minimum SpO2	10	79.6	10.0	63	93.4
Mean SpO2	10	91.9	6.1	76	97
Max heart rate	10	84.6	13.1	57	102
Minimum heart rate	10	50.7	9.8	38	63
Mean heart rate	10	64.1	9.9	46.4	77.7

Table 5-4 PRMS overall scoring results

Variable	N	Mean	Std Dev	Minimum	Maximum
Central apnea index	10	0	0	0	0
Obstructive apnea index	10	23.6	22.7	0.1	72.7
Mixed apnea index	10	0	0	0	0
Hypopnea index	10	9.4	8.8	2	30.6
Total apnea index	10	23.6	22.7	0.1	72.7
Apnea hypopnea index	10	33.1	22.7	2.2	76.6

5.5.1. Peason Correlation Coefficient

To measure of the strength of the linear relationship between the gold standard and PRMS results, Pearson Correlation Coefficients was calculated between two system using Eq.6.1. The result is shown in Table 5-5.

$$\rho_{X,Y} = \frac{cov(X,Y)}{\sigma_X \sigma_Y} = \frac{E[(X-\mu_X)(Y-\mu_Y)]}{\sigma_X \sigma_Y} \quad (5\text{-}1)$$

where, *cov* is the covariance, σ_X is the standard deviation of X , μ_X is the mean of X , and *E* is the expectation.

Table 5-5 Pearson Correlation Coefficients, r (p value), N=10 between the PRMS and Gold Standard

PRMS noncontact sensors			
Gold standard contact sensors	**Obstructive apnea index**	**Hypopnea index**	**Apnea/hypopnea index**
Obstructive apnea index	0.52366 (0.12)		
Hypopnea index		0.37 (0.29)	
Apnea/hypopnea index			0.95 (<0.0001)

The fit plot for each parameter is plotted in Figure 5-3, Figure 5-4 and Figure 5-5. Moreover, the degrees of freedom for error (Error DF), Mean Square Error (MSE), coefficient of determination (R-square) and adjusted R-square are calculated for each plot.

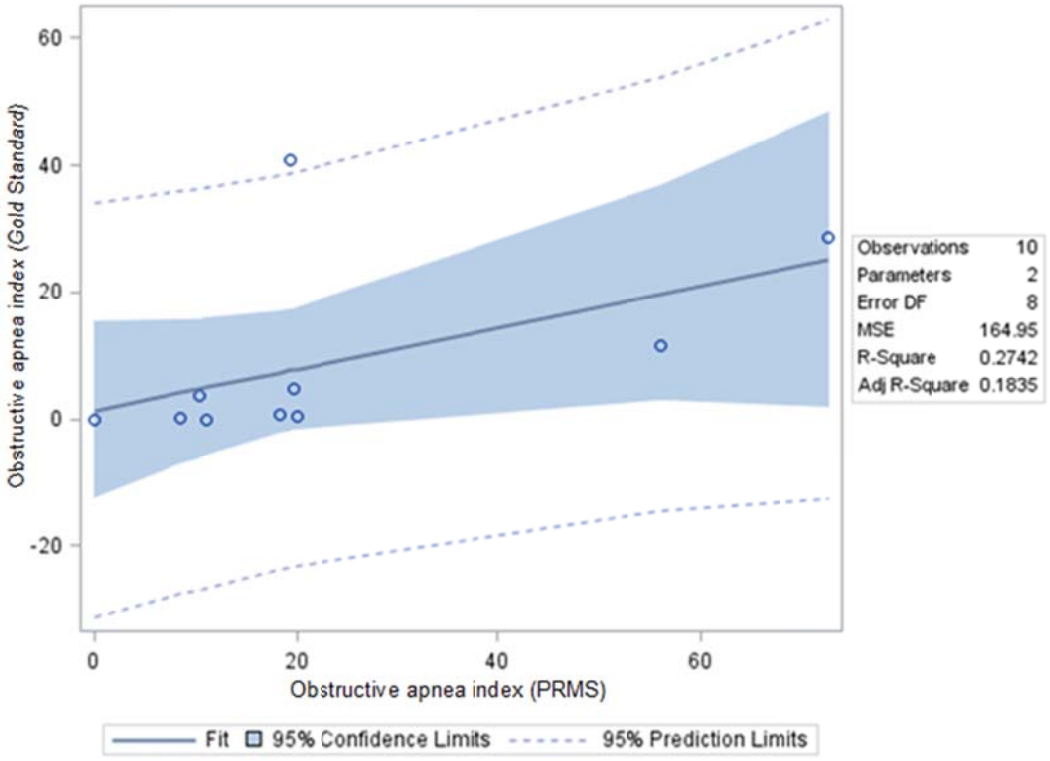

Figure 5-3 Fit plot for obstructive apnea index

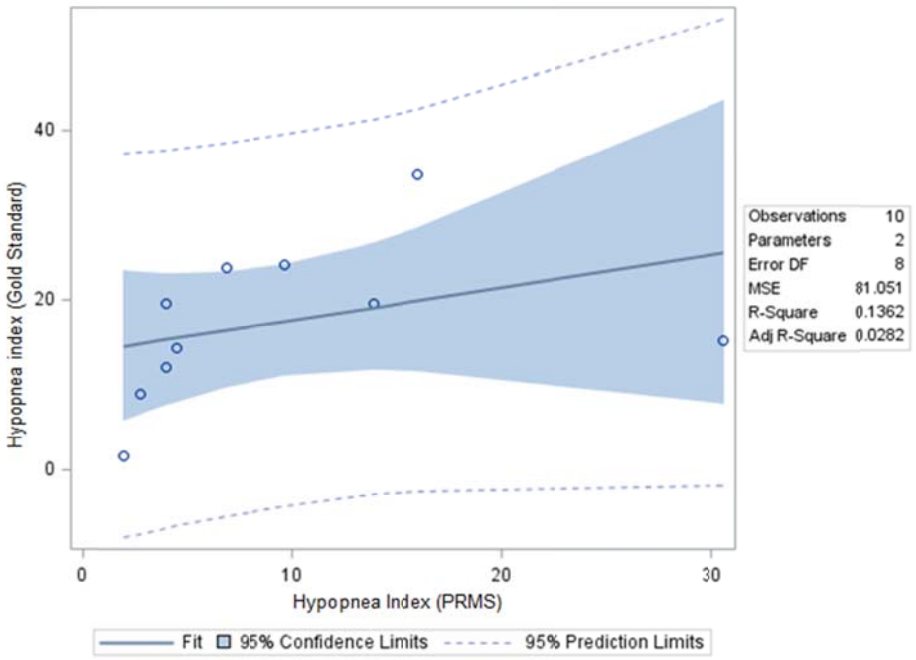

Figure 5-4 Fit plot for hypopnea index

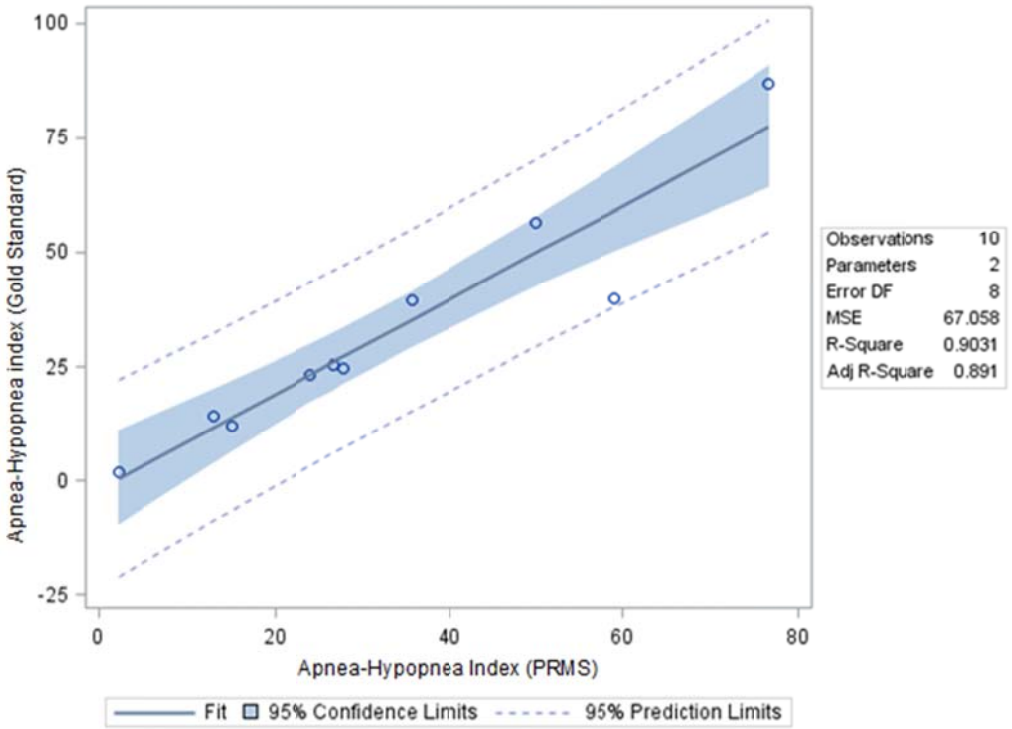

Figure 5-5 Fit plot for apnea-hypopnea index

5.5.2. Sensitivity, Specificity and Accuracy

To determine the reliability and goodness of the PRMS in detecting apnea and hypopnea three situations were considered:

1. Detecting the paradoxical breathing (Apnea + hypopnea).
2. Detecting Apnea.
3. Detecting Hypopnea

For each situation using the scoring data each breath is classify into one of true positive, true negative, false positive and false negative; and the confusion matrix [88] was formed as shown in Table 5-6 . Then the following parameters were calculated [89] for each subject in three above situation. The results are shown in Table 5-7, Table 5-8and Table 5-9.

Table 5-6 Confusion matrix

PRMS noncontact sensors		
Gold standard contact sensors	**Apnea(Hypopnea)**	**Normal**
Apnea(Hypopnea)	True positive (TP)	False positive (TP)
Normal	False Negative (FN)	True negative (TN)

- Sensitivity

Sensitivity or true positive rate (TPR) shows the percentage of apnea (hypopnea) that was detected correctly with PRMS.

$$TPR = \frac{TP}{TP + FN} \tag{5-2}$$

- Specificity

Specificity (SPC) or true negative rate shows the percentage of normal events that was correctly identified by PRMS.

$$SPC = \frac{TN}{TN + FP} \tag{5-3}$$

- Precision

Precision or positive predictive value (PPV) shows the percentage of apnea (hypopnea) that was detected correctly with PRMS.

$$PPV = \frac{TP}{TP + FP} \tag{5-4}$$

- Negative predictive value

Nositive predictive value (NPV) shows the percentage of apnea (hypopnea) that was detected correctly with PRMS.

$$NPV = \frac{TN}{TN + FN} \tag{5-5}$$

- Fall-out

Fall-out or false positive rate (FPR) shows the percentage of apnea (hypopnea) that was detected correctly with PRMS.

$$FPV = \frac{FP}{TN + FP} = 1 - SPC \tag{5-6}$$

- False discovery rate

False discovery rate (FDR) shows the percentage of apnea (hypopnea) that was detected correctly with PRMS.

$$FPV = \frac{FP}{TP + FP} = 1 - PPV \tag{5-7}$$

- Accuracy

Accuracy (ACC) shows how accurately PRMS was identified the apnea or normal event.

$$ACC = \frac{TP + TN}{TP + FN + TN + FP} \tag{5-8}$$

- F1 score

F1 score was calculated as a harmonic mean or a weighted average of precision and sensitivity [90].

$$F1 = \frac{2TP}{2TP + FN + FP} \tag{5-9}$$

- Mathews correlation coefficient

Matthews correlation coefficient (MCC) considers true and false positives and negatives to give a balanced measure to show how successful the method was to predict the correct states (apnea or normal). The MCC ranges between -1 to +1 where +1 shows a perfect prediction while -1 presents the complete disagreement. 0 shows the prediction was no better than random [91, 92].

$$MCC = \frac{TP \times TN - FP \times FN}{\sqrt{(TP + FP)(TP + FN)(TN + FP)(TN + FN)}} \tag{5-10}$$

The sensitivity, precision, specificity, accuracy and F1 score of three situations are shown in Figure 5-6 to Figure 5-10 respectively.

Table 5-7 Statistical parameter for detecting apnea-hypopnea with PRMS

Subject ID	TPR	SPC	PPV	NPV	FPR	FDR	ACC	F1 score	MCC
1	82.16	82.97	64.70	92.45	17.03	35.30	82.75	72.39	0.61
2	73.27	97.57	37.76	99.45	2.43	62.24	97.09	49.83	0.51
3	91.35	84.84	85.90	90.65	15.16	14.10	88.11	88.54	0.76
4	91.61	89.11	86.41	93.36	10.89	13.59	90.19	88.93	0.80
5	91.28	92.06	64.28	98.54	7.94	35.72	91.96	75.43	0.72
6	61.50	93.93	41.62	97.20	6.07	58.38	91.80	49.64	0.46
7	84.68	89.05	79.84	91.90	10.95	20.16	87.57	82.19	0.73
8	88.15	94.90	60.00	98.93	5.10	40.00	94.36	71.40	0.70
9	83.47	91.36	67.36	96.28	8.64	32.64	89.97	74.55	0.69
10	84.14	90.32	59.37	97.13	9.68	40.63	89.43	69.62	0.65
Mean	83.16	90.61	64.72	95.59	9.39	35.28	90.32	72.25	0.66
STD	9.43	4.43	16.55	3.22	4.43	16.55	3.91	13.66	0.11
Min	61.50	82.97	37.76	90.65	2.43	13.59	82.75	49.64	0.46
Max	91.61	97.57	86.41	99.45	17.03	62.24	97.09	88.93	0.80

Table 5-8 Statistical parameter for detecting apnea with PRMS

Subject ID	TPR	SPC	PPV	NPV	FPR	FDR	ACC	F1 score	MCC
1	89.40	81.13	11.84	99.63	18.87	88.16	81.36	20.91	0.28
2	70.67	97.56	30.11	99.55	2.44	69.89	97.17	42.23	0.45
3	42.16	85.53	62.21	72.35	14.47	37.79	69.87	50.26	0.31
4	39.43	89.49	62.88	76.59	10.51	37.12	73.91	48.47	0.34
5	44.44	92.97	8.27	99.15	7.03	91.73	92.28	13.95	0.17
6	0.00	93.30	0.00	99.98	6.70	100.00	93.28	0.00	0.00
7	83.60	82.56	61.00	93.91	17.44	39.00	82.81	70.53	0.60
8	NaN	91.45	0.00	100.00	8.55	100.00	91.45	0.00	NaN
9	84.21	84.33	3.58	99.87	15.67	96.42	84.33	6.87	0.15
10	95.00	86.54	2.76	99.98	13.46	97.24	86.57	5.36	0.15
Mean	60.99	88.49	24.27	94.10	11.51	75.73	85.30	25.86	0.27
STD	31.47	5.32	27.47	10.56	5.32	27.47	8.71	25.07	0.18
Min	0.00	81.13	0.00	72.35	2.44	37.12	69.87	0.00	0.00
Max	95.00	97.56	62.88	100.00	18.87	100.00	97.17	70.53	0.60

Table 5-9 Statistical parameter for detecting hypopnea with PRMS

Subject ID	TPR	SPC	PPV	NPV	FPR	FDR	ACC	F1 score	MCC
1	43.48	95.51	76.13	83.69	4.49	23.87	82.62	55.35	0.48
2	53.85	99.88	70.00	99.76	0.12	30.00	99.65	60.87	0.61
3	44.86	73.63	21.92	89.00	26.37	78.08	69.55	29.45	0.14
4	45.29	76.48	20.68	91.17	23.52	79.32	72.76	28.39	0.16
5	66.00	95.84	68.66	95.34	4.16	31.34	92.23	67.30	0.63
6	26.48	98.64	57.74	95.04	1.36	42.26	93.92	36.31	0.36
7	7.77	98.37	32.72	91.26	1.63	67.28	89.97	12.56	0.12
8	30.98	99.23	77.71	94.31	0.77	22.29	93.78	44.30	0.47
9	24.68	98.19	73.57	86.49	1.81	26.43	85.76	36.96	0.37
10	33.91	97.84	71.82	90.10	2.16	28.18	88.89	46.06	0.44
Mean	37.73	93.36	57.09	91.62	6.64	42.91	86.91	41.76	0.38
STD	16.51	9.77	22.93	4.69	9.77	22.93	9.55	16.54	0.19
Min	7.77	73.63	20.68	83.69	0.12	22.29	69.55	12.56	0.12
Max	66.00	99.88	77.71	99.76	26.37	79.32	99.65	67.30	0.63

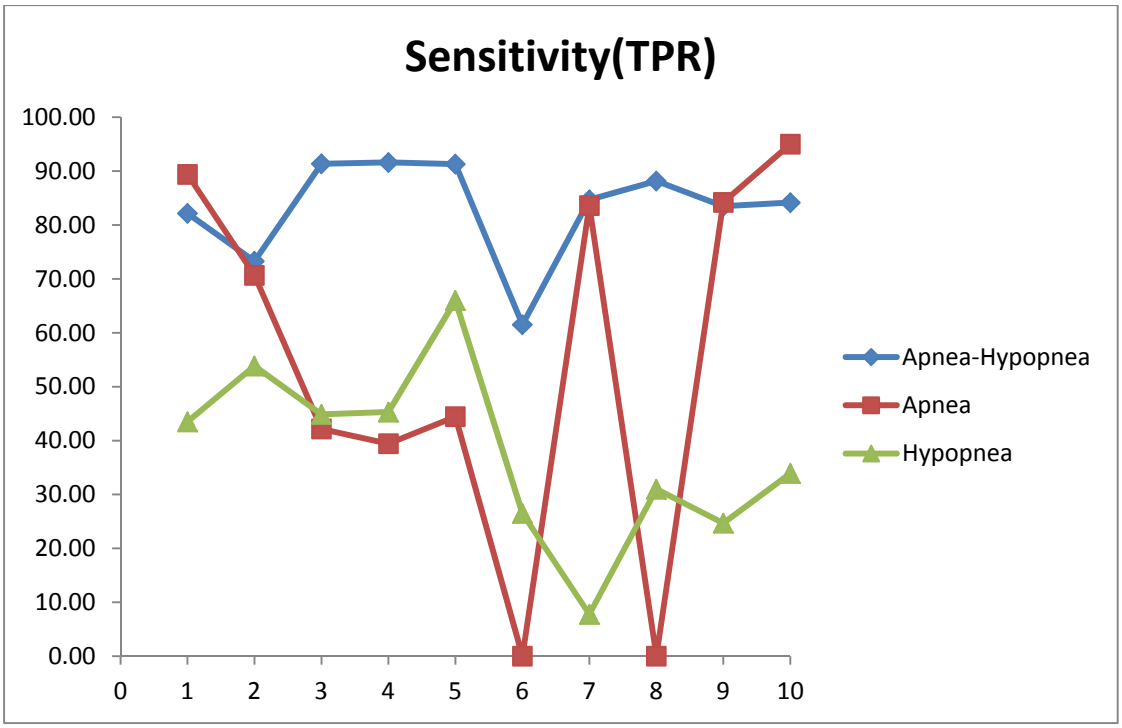

Figure 5-6 Sensitivity of PRMS method in detecting apnea, hypopnea and all paradoxical events.

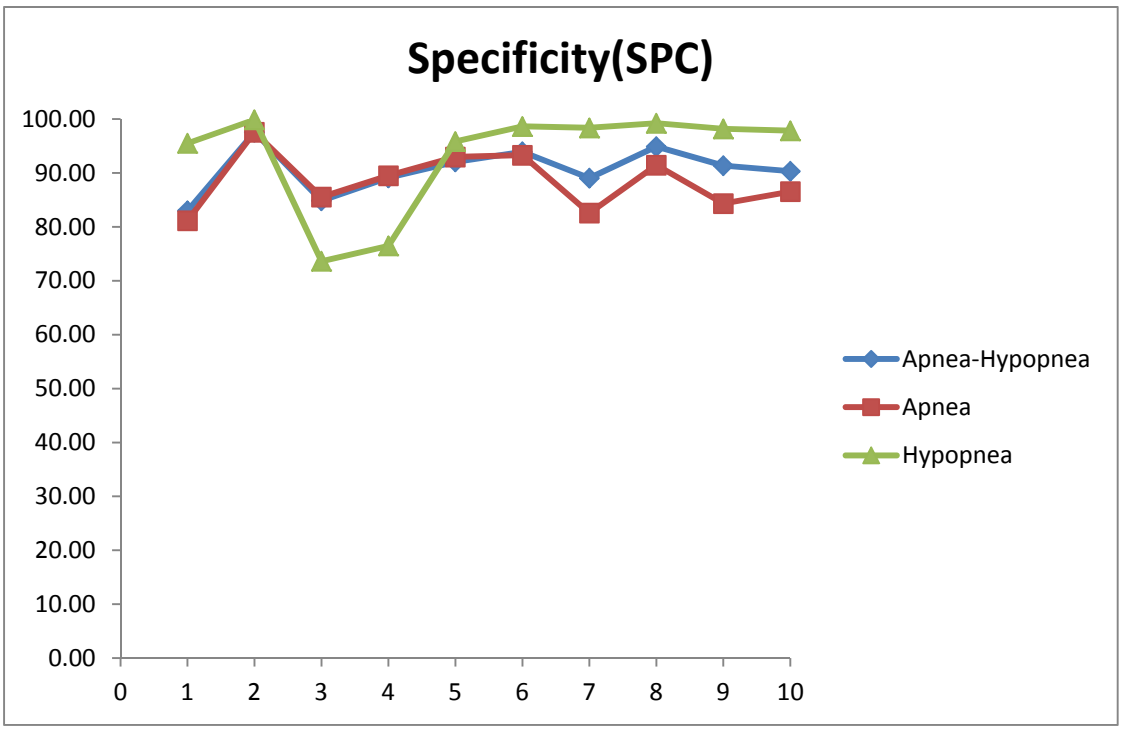

Figure 5-7 Sensitivity of PRMS method in detecting apnea, hypopnea and all paradoxical events

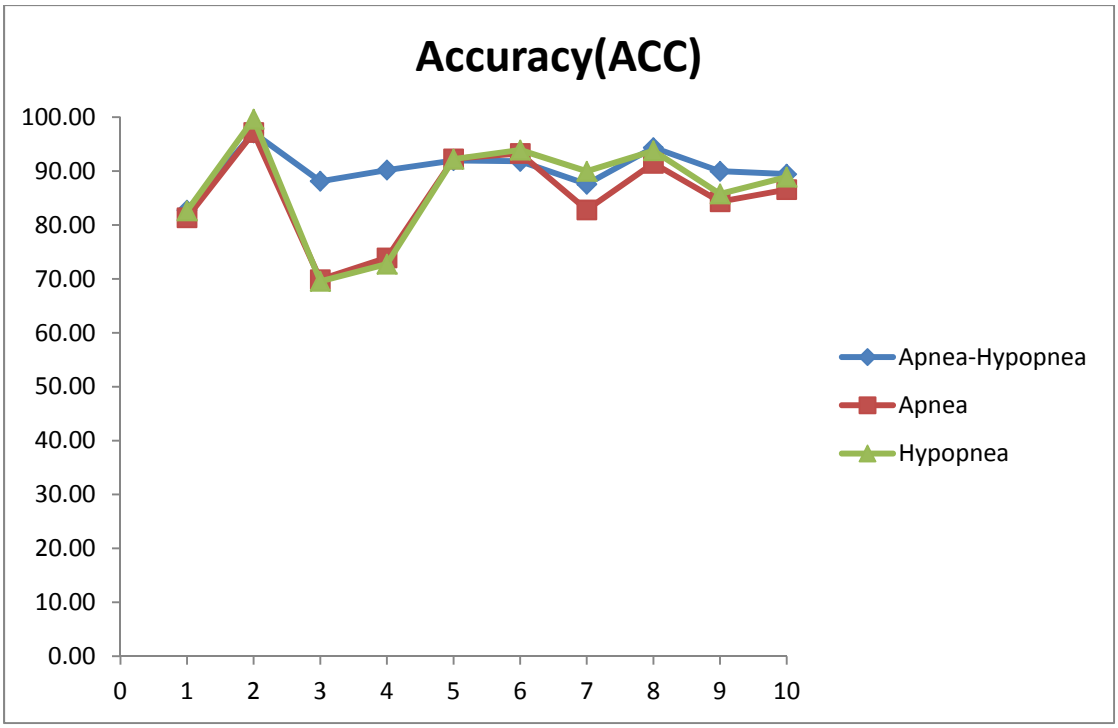

Figure 5-8 Accuracy of PRMS method in detecting apnea, hypopnea and all paradoxical events

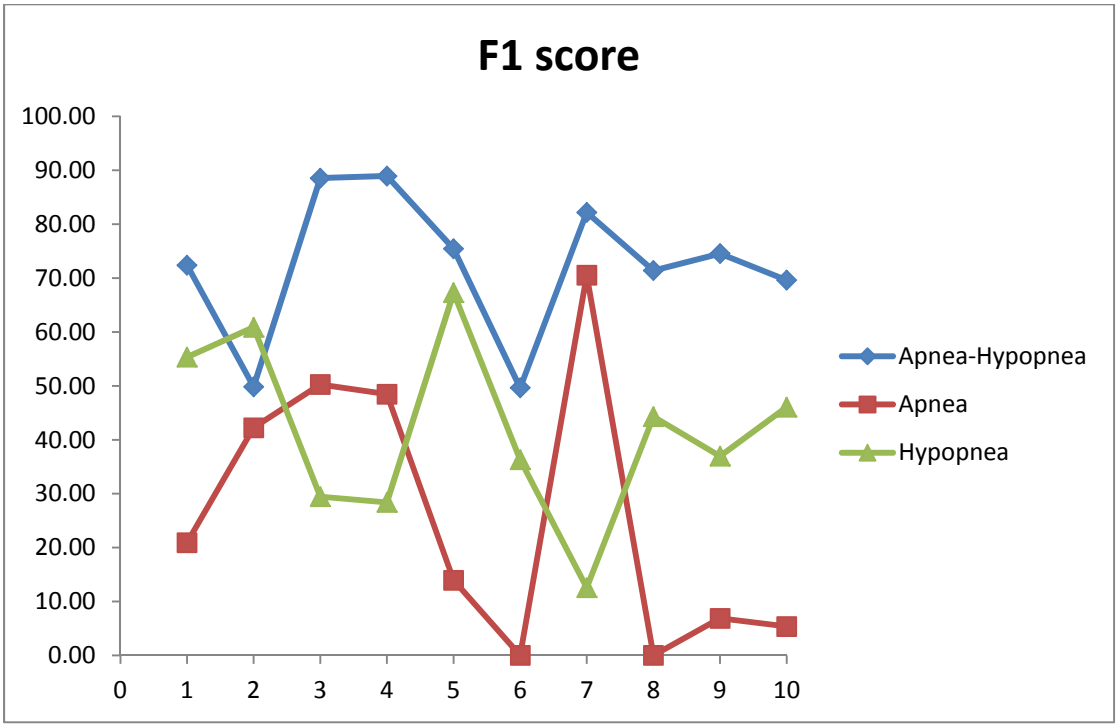

Figure 5-9 F1 score of PRMS method in detecting apnea, hypopnea and all paradoxical events

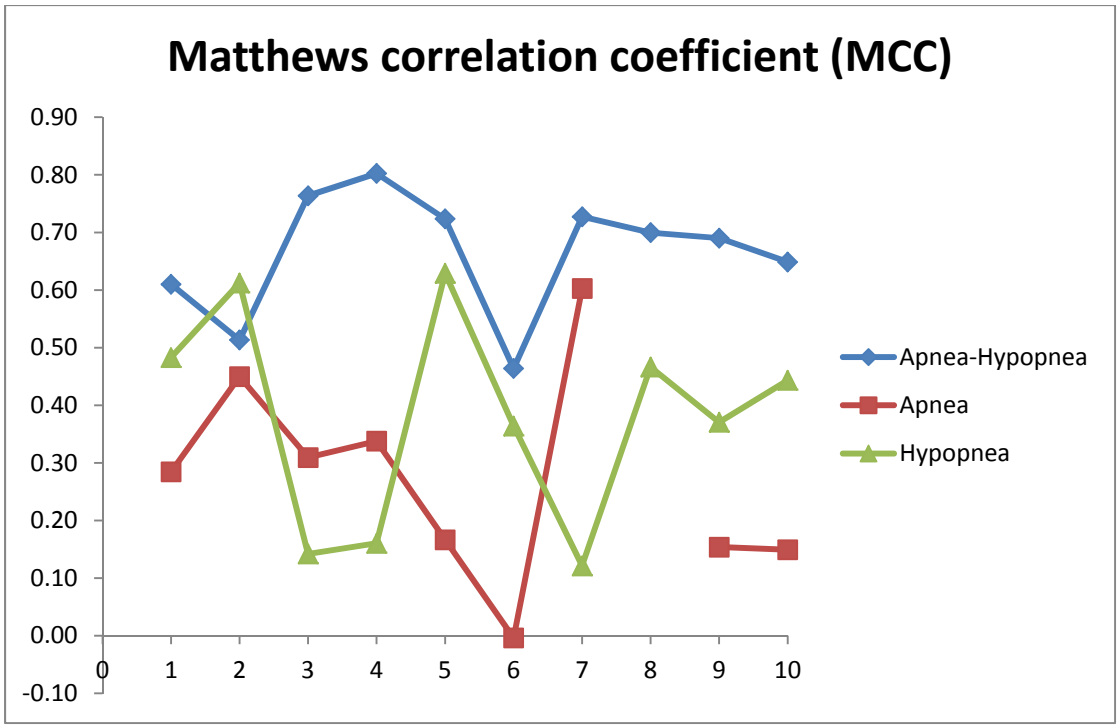

Figure 5-10 Matthews correlation coefficient of PRMS method in detecting apnea, hypopnea and all paradoxical events

Chapter 6

Summary and Future works

Sleep disorder monitoring is commonly done with contact sensors. The ability of Doppler radar to measure motion-based physiological parameters makes it suitable for the design of a non-contact sleep monitoring system. In this thesis, a physiological radar monitoring system (PRMS) based on CW Doppler radar is designed and studied for the detection of apneas and hypopneas. The hardware for the system includes radar with two different frequencies. A 2.4 GHz radar provides higher sensitivity to respiratory motion patterns while the additional 24 GHz radar provides a higher displacement resolution for small motion such as that due to heartbeat. A real time sleep monitoring software program was developed to be used with the hardware. The system has can be integrated with a "gold standard" monitoring system by sending its measurement and analysis outputs as analog signals to conventional sensor inputs on the gold standard system. The system was first tested on a programmable linear mover respiratory-disorder phantom and then on human subjects in a sleep lab. Analog outputs indicating torso displacement, respiratory rate, and respiratory distress determined by the PRMS were integrated to the sleep lab's Sandman Elite gold standard PSG system. A PRMS scoring rule was developed to identify normal breathing, apneas and hypopneas. Two evaluate the system, the data recorded using PRMS and gold standard monitoring system (Sandman) was scored separately for blind analysis by two technologists. The population under study was previously diagnosed with obstructive sleep apnea and were not allowed to use CPAP during the tests. The result demonstrated the ability of a PRMS to detect paradoxical breathing in a population with different characteristics. The PRMS accurately measured the apnea/hypopnea index in this small population of patients. However, the PRMS overestimated the apnea index and underestimated the hypopnea index.

6.1. Summary

A general introduction to the research problem and the motivation behind this thesis has been given in Chapter.1. It is estimated than over 18 million American have sleep apnea. However, around 10 million of them remain undiagnosed. Hence, it is critical to investigate new methods of diagnosing sleep apnea which are affordable and convenient for patients.

The theory behind Doppler radar and its application in physiological monitoring was explained in Chapter 2. The effect of the radar's parameters on the accuracy of measurement in physiological monitoring was investigated and the optimum design for sleep monitoring application was selected. The power level must be set to the minimum level required needed for the system to operate in order to meet FCC requirements. Our experiments showed that higher frequency radar has a better sensitivity for detecting smaller motions but demodulation is complicated for large motions. The linear displacement of the torso during respiration (~1cm) can be successfully estimated using linear demodulation for 2.45 GHz, while much more complicated demodulation methods must be used to measure the same displacement for 24 GHz radar. Narrow beam antennas allow for a longer range of measurement for a given transmitter power level. However, the narrowness of the beam makes it difficult to pinpoint the target. As a result, wider pattern antennas are superior to the narrowest patterns for long range or low power applications.

Chapter 3 starts with sleep terminology and sleep disorder monitoring methods that exist in the literature. Next, a PRMS based on a Doppler radar structure is presented to be integrated with Embla Sandman Elite, which is used as a gold standard sleep monitoring system. A new sleep disorder monitoring algorithm is implemented in Matlab which can to track the respiratory motion trace and detect apnea and hypopnea using the Doppler radar. The algorithm reads the baseband I and Q channel from the radar and generates the respiration trace using the linear demodulation method. Next, the static background is removed from the signal. After that, by assuming normal breathing in first 30 seconds of the data, three references are calculated to compare the energy, duration and area of the arc for each breathing cycle. In dynamic threshold mode, the references are updated using the last four normal breaths. In the last step of the algorithm four outputs are converted to analog signals and sent to Sandman Elite software. The four outputs are respiration trace, respiration rate, thoraco-abdominal actigraphy 3, which shows the comparison result for each breath, and actigraphy 10, which shows the apneas or hypopneas

that last for at least 10 seconds. In sending the output to Sandman two points must be considered first the frequency of sending data must be same as Sandman input channels rate and second the radar data recorded in Matlab must be saved to hard disk and the RAM of system must be freed to avoid underflow Error with DAQ.

The experiments setup and protocol as well as subjects physical characteristics are explained in Chapter 5 following the results of using the PRMS along with Sandman Elite system as a gold standard to detect apnea and hypopnea.

To evaluate the PRMS, scoring rules for gold standard and PRMS were developed and the data was blindly scored by two technologists. The results are shown in Chapter 6. Although the Pearson correlation coefficients and the *p* values show an overestimation of the apnea index and underestimation of hypopnea, the PRMS measurements of the apnea-hypopnea index (AHI) are very accurate.

In summary, this work shows the possibility of using PRMS as a sleep monitoring system as a compliment to PSG or as a stand-alone screening device. However more work must be done to refine the PRMS technology and to create accurate scoring rules.

6.2. Future work

This study on human subjects has shown that the PRMS system has a great potential to be of use for sleep disorder monitoring. Considering the experimental results and knowledge acquired from this work, some areas that could be investigated in the future are presented in the following sections.

6.2.1. Detecting the type of the apnea

The current sleep monitoring algorithm is only able to identify happening of an apnea or hypopnea event without separating the different types of apneas. Figure 6-1show the respiration trace generated by PRMS.

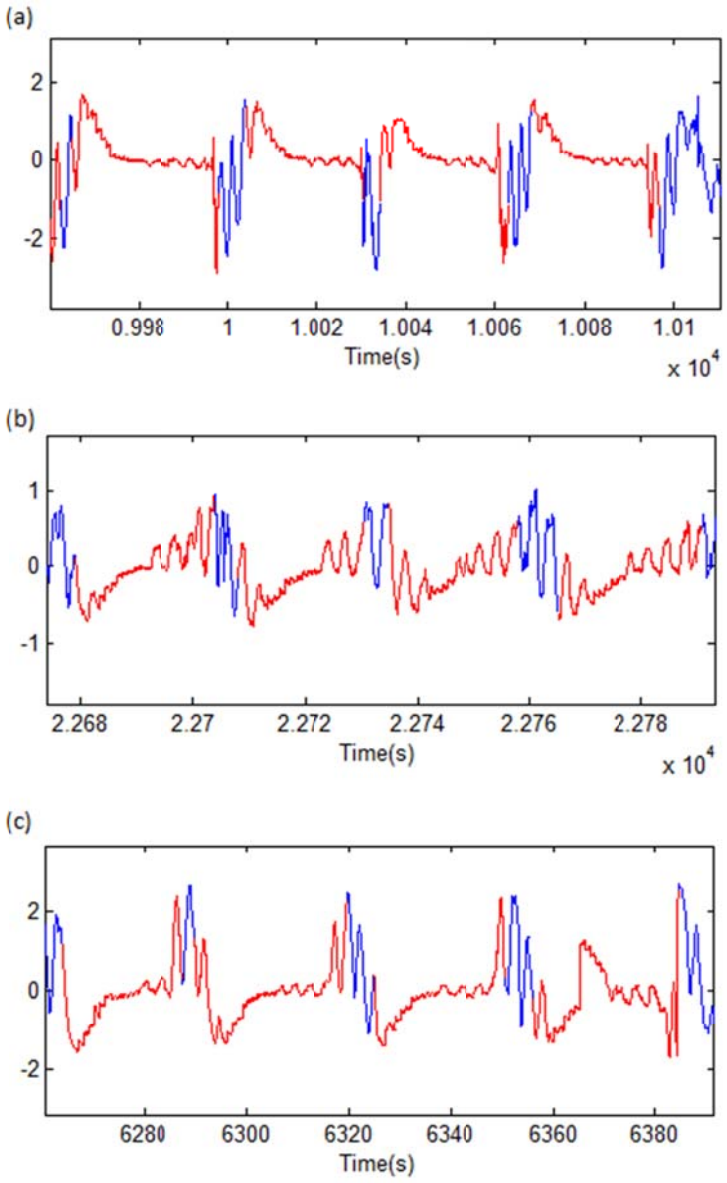

Figure 6-1 Different Pattern in (a) Obstructive apnea (b) Central apnea and (c) Mixed apnea

As shown in Figure 6-1. The pattern of the radar signal is different in obstructive and central apnea. Hence; an interesting work to pursue could be developing an algorithm to identify the type of the apnea using pattern recognition methods.

6.2.2. Improving the peak detection algorithm

The result of the algorithm is mainly based on separating the breaths correctly using local peak detection algorithms. The accuracy of the peak detection algorithm presented in this thesis can be affected by the noise (Figure 6-2). Hence; having an algorithm which is more robust to the noise could improve the detection results.

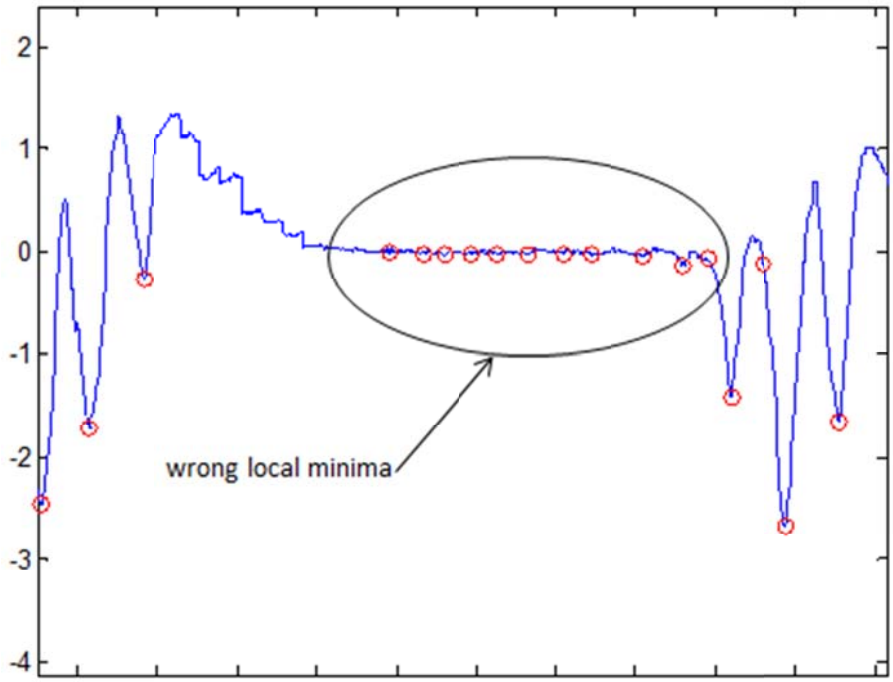

Figure 6-2 Detecting a wrong local minima because of the noise

References

[1] Centre for Technology and Aging. (2010). *Technologies for remote patient monitoring for older adults*. Available: http://www.thehealthwell.info/node/13181 [Accessed: July 20, 2014]

[2] V. K. Somers, D. P. White, R. Amin, W. T. Abraham, F. Costa, A. Culebras*, et al.*, "Sleep Apnea and Cardiovascular DiseaseAn American Heart Association/American College of Cardiology Foundation Scientific St atement From the American Heart Association Council for High Blood Pressure Research Professional Education Committee, Council on Clinical Cardiology, Stroke Council, and Council on Cardiovascular Nursing In Collaboration With the National Heart, Lung, and Blood Institute National Center on Sleep Disorders Research (National Institutes of Health)," *Journal of the American College of Cardiology,* vol. 52, pp. 686-717, 2008.

[3] T. D. Bradley and J. S. Floras, "Sleep Apnea and Heart Failure: Part II: Central Sleep Apnea," *Circulation,* vol. 107, pp. 1822-1826, April 8, 2003 2003.

[4] D. J. Eckert, A. S. Jordan, P. Merchia, and A. Malhotra, "Central sleep apnea: Pathophysiology and treatment," *Chest,* vol. 131, pp. 595-607, Feb 2007.

[5] L. J. Olson and V. K. Somers, "Sleep apnea: implications for heart failure," *Curr Heart Fail Rep,* vol. 4, pp. 63-9, Jun 2007.

[6] S. M. Caples, R. Wolk, and V. K. Somers, "Influence of cardiac function and failure on sleep-disordered breathing: evidence for a causative role," *J Appl Physiol (1985),* vol. 99, pp. 2433-9, Dec 2005.

[7] S. Javaheri, "Heart failure and sleep apnea: emphasis on practical therapeutic options," *Clin Chest Med,* vol. 24, pp. 207-22, Jun 2003.

[8] S. M. Caples, A. S. Gami, and V. K. Somers, "Obstructive sleep apnea," *Ann Intern Med,* vol. 142, pp. 187-97, Feb 1 2005.

[9] J. D. Lattimore, D. S. Celermajer, and I. Wilcox, "Obstructive sleep apnea and cardiovascular disease," *J Am Coll Cardiol,* vol. 41, pp. 1429-37, May 7 2003.

[10] A. Malhotra and D. P. White, "Obstructive sleep apnoea," *Lancet,* vol. 360, pp. 237-45, Jul 20 2002.

[11] T. D. Bradley and J. S. Floras, "Sleep apnea and heart failure: Part I: obstructive sleep apnea," *Circulation,* vol. 107, pp. 1671-8, Apr 1 2003.

[12] S. M. Caples, A. Garcia-Touchard, and V. K. Somers, "Sleep-disordered breathing and cardiovascular risk," *Sleep,* vol. 30, pp. 291-303, Mar 2007.

[13] S. Kapa, F. H. Sert Kuniyoshi, and V. K. Somers, "Sleep apnea and hypertension: interactions and implications for management," *Hypertension,* vol. 51, pp. 605-8, Mar 2008.

[14] D. P. Baraglia, M. J. Berryman, S. W. Coussens, Y. Pamula, D. Kennedy, A. J. Martin*, et al.*, "Automated sleep scoring and sleep apnea detection in children," 2005, pp. 60390T-60390T-12.

[15] J. C. Lin, "Noninvasive microwave measurement of respiration," *Proceedings of the IEEE,* vol. 63, pp. 1530-1530, 1975.

[16] X. Yanming, L. Jenshan, O. Boric-Lubecke, and V. M. Lubecke, "A Ka-Band Low Power Doppler Radar System for Remote Detection of Cardiopulmonary Motion," in *Engineering in Medicine and Biology Society, 2005. IEEE-EMBS 2005. 27th Annual International Conference of the*, 2005, pp. 7151-7154.

[17] L. Changzhi, L. Jenshan, O. Boric-Lubecke, V. M. Lubecke, A. Host-Madsen, and P. Byung-Kwon, "Development of Non-contact Physiological Motion Sensor on CMOS Chip and Its Potential Applications," in *ASIC, 2007. ASICON '07. 7th International Conference on*, 2007, pp. 1022-1027.

[18] L. Changzhi, L. Jenshan, and X. Yanming, "Robust Overnight Monitoring of Human Vital Signs by a Non-contact Respiration and Heartbeat Detector," in *Engineering in Medicine and Biology Society, 2006. EMBS '06. 28th Annual International Conference of the IEEE*, 2006, pp. 2235-2238.

[19] V. M. Lubecke, O. Boric-Lubecke, A. Host-Madsen, and A. E. Fathy, "Through-the-Wall Radar Life Detection and Monitoring," in *Microwave Symposium, 2007. IEEE/MTT-S International*, 2007, pp. 769-772.

[20] J. Geisheimer and E. F. Greneker, Iii, "A non-contact lie detector using radar vital signs monitor (RVSM) technology," *Aerospace and Electronic Systems Magazine, IEEE,* vol. 16, pp. 10-14, 2001.

[21] J. Muehlsteff, J. Thijs, R. Pinter, G. Morren, and G. Muesch, "A handheld device for simultaneous detection of electrical and mechanical cardio-vascular activities with synchronized ECG and CW-Doppler Radar," in *Engineering in Medicine and Biology Society, 2007. EMBS 2007. 29th Annual International Conference of the IEEE*, 2007, pp. 5758-5761.

[22] K. Mostov, E. Liptsen, and R. Boutchko, "Medical applications of shortwave FM radar: Remote monitoring of cardiac and respiratory motion," *Medical Physics,* vol. 37, pp. 1332-1338, 2010.

[23] D. Qiao, T. He, B. Hu, and Y. Li, "Non-contact physiological signal detection using continuous wave Doppler radar," *Bio-Medical Materials and Engineering,* vol. 24, pp. 993-1000, 01/01/ 2014.

[24] A. Droitcour, V. Lubecke, L. Jenshan, and O. Boric-Lubecke, "A microwave radio for Doppler radar sensing of vital signs," in *Microwave Symposium Digest, 2001 IEEE MTT-S International*, 2001, pp. 175-178 vol.1.

[25] A. D. Droitcour, O. Boric-Lubecke, V. M. Lubecke, and L. Jenshan, "0.25 /spl mu/m CMOS and BiCMOS single-chip direct-conversion Doppler radars for remote sensing of vital signs," in *Solid-State Circuits Conference, 2002. Digest of Technical Papers. ISSCC. 2002 IEEE International*, 2002, pp. 348-349 vol.1.

[26] A. D. Droitcour, O. Boric-Lubecke, V. M. Lubecke, J. Lin, and G. T. A. Kovacs, "Range correlation effect on ISM band I/Q CMOS radar for non-contact vital signs sensing," in *Microwave Symposium Digest, 2003 IEEE MTT-S International*, 2003, pp. 1945-1948 vol.3.

[27] A. D. Droitcour, O. Boric-Lubecke, V. M. Lubecke, L. Jenshan, and G. T. A. Kovacs, "Range correlation and I/Q performance benefits in single-chip silicon Doppler radars for noncontact cardiopulmonary monitoring," *Microwave Theory and Techniques, IEEE Transactions on,* vol. 52, pp. 838-848, 2004.

[28] M. I. Skolnik, *Introduction to radar systems*: McGraw-Hill, 1962.

[29] W. Massagram, A Study of Feasibility in Long-term Cardiopulmonary Monitoring Via Doppler Radar: University of Hawai'i at Manoa, 2008.

[30] M. I. Skolnik, *Introduction to Radar Systems*: Tata McGraw Hill, 2003.

[31] S. Kingsley and S. Quegan, *Understanding Radar Systems*: Institution of Engineering and Technology, 1999.

[32] M. I. Skolnik, *Radar handbook*: McGraw-Hill, 1990.

[33] D. Kissinger, Millimeter-Wave Receiver Concepts for 77 GHz Automotive Radar in Silicon-Germanium Technology: Springer, 2012.

[34] A. D. Droitcour, Non-contact measurement of heart and respiration rates with a single-chip microwave Doppler radar, 2006.

[35] J. Lin, Electromagnetic Interaction with Biological Systems: Springer US, 2012.

[36] P. Byung-Kwon, O. Boric-Lubecke, and V. M. Lubecke, "Arctangent Demodulation With DC Offset Compensation in Quadrature Doppler Radar Receiver Systems," *Microwave Theory and Techniques, IEEE Transactions on,* vol. 55, pp. 1073-1079, 2007.

[37] D. Smardzija, O. Boric-Lubecke, A. Host-Madsen, V. M. Lubecke, T. Sizer, Ii, A. D. Droitcour*, et al.*, "Applications of MIMO techniques to sensing of cardiopulmonary activity," in *Wireless Communications and Applied Computational Electromagnetics, 2005. IEEE/ACES International Conference on*, 2005, pp. 618-621.

[38] P. Byung-Kwon, S. Yamada, O. Boric-Lubecke, and V. Lubecke, "Single-channel receiver limitations in Doppler radar measurements of periodic motion," in *Radio and Wireless Symposium, 2006 IEEE*, 2006, pp. 99-102.

[39] L. Changzhi and L. Jenshan, "Complex signal demodulation and random body movement cancellation techniques for non-contact vital sign detection," in *Microwave Symposium Digest, 2008 IEEE MTT-S International*, 2008, pp. 567-570.

[40] A. M. Vergara and V. M. Lubecke, "Data Acquisition System for Doppler Radar Vital-Sign Monitor," in *Engineering in Medicine and Biology Society, 2007. EMBS 2007. 29th Annual International Conference of the IEEE*, 2007, pp. 2269-2272.

[41] A. Singh, "Subject isolation and non stationary clutter rejection using RF Backscatter -- tag radar," 3569109 Ph.D., University of Hawai'i at Manoa, Ann Arbor, 2012.

[42] J. Proakis, Digital Signal Processing: Principles, Algorithms, And Applications, 4/E: Pearson Education, 2007.

[43] A. V. Oppenheim and R. W. Schafer, *Discrete-Time Signal Processing: Pearson New International Edition*: Pearson Education, Limited, 2013.

[44] M. Baboli, A. Singh, N. Hafner, and V. Lubecke, "Parametric study of antennas for long range Doppler radar heart rate detection," in *Engineering in Medicine and Biology Society (EMBC), 2012 Annual International Conference of the IEEE*, 2012, pp. 3764-3767.

[45] A. Singh, M. Baboli, G. Xiaomeng, E. Yavari, B. Padasdao, B. Soll*, et al.*, "Considerations for integration of a physiological radar monitoring system with gold standard clinical sleep monitoring systems," in *Engineering in Medicine and Biology Society (EMBC), 2013 35th Annual International Conference of the IEEE*, 2013, pp. 2120-2123.

[46] "Sleep-related breathing disorders in adults: recommendations for syndrome definition and measurement techniques in clinical research. The Report of an American Academy of Sleep Medicine Task Force," *Sleep,* vol. 22, pp. 667-89, Aug 1 1999.

[47] T. Young, P. E. Peppard, and D. J. Gottlieb, "Epidemiology of Obstructive Sleep Apnea," *American Journal of Respiratory and Critical Care Medicine,* vol. 165, pp. 1217-1239, 2002/05/01 2002.

[48] P. V. Tishler, E. K. Larkin, M. D. Schluchter, and S. Redline, "Incidence of sleep-disordered breathing in an urban adult population: The relative importance of risk factors in the development of sleep-disordered breathing," *JAMA,* vol. 289, pp. 2230-2237, 2003.

[49] Mayo Clinic. (2006). *Mayo Clinic Discovers New Type Of Sleep Apnea.* Available: www.sciencedaily.com/releases/2006/09/060901161349.htm [Accessed: July 20,2014]

[50] L. Almazaydeh, "An interactive, real-time, high precision and portable monitoring system of obstructive sleep apnea," 3571495 Ph.D., University of Bridgeport, Ann Arbor, 2013.

[51] P. De Chazal, T. Penzel, and C. Heneghan, "Automated detection of obstructive sleep apnoea at different time scales using the electrocardiogram," *Physiol Meas,* vol. 25, pp. 967-83, Aug 2004.

[52] P. De Chazal, C. Heneghan, and W. T. Mcnicholas, "Multimodal detection of sleep apnoea using electrocardiogram and oximetry signals," *Philos Trans A Math Phys Eng Sci,* vol. 367, pp. 369-89, Jan 28 2009.

[53] A. Yilmaz and T. Dundar, "Home recording for pre-phase sleep apnea diagnosis by Holter recorder using MMC memory," in *Virtual Environments Human-Computer Interfaces and Measurement Systems (VECIMS), 2010 IEEE International Conference on*, 2010, pp. 126-129.

[54] L. Almazaydeh, K. Elleithy, and M. Faezipour, "Detection of obstructive sleep apnea through ECG signal features," in *Electro/Information Technology (EIT), 2012 IEEE International Conference on*, 2012, pp. 1-6.

[55] M. O. Mendez, D. D. Ruini, O. P. Villantieri, M. Matteucci, T. Penzel, S. Cerutti*, et al.*, "Detection of Sleep Apnea from surface ECG based on features extracted by an Autoregressive Model," in *Engineering in Medicine and Biology Society, 2007. EMBS 2007. 29th Annual International Conference of the IEEE*, 2007, pp. 6105-6108.

[56] L. Derong, P. Zhongyu, and S. R. Lloyd, "A Neural Network Method for Detection of Obstructive Sleep Apnea and Narcolepsy Based on Pupil Size and EEG," *Neural Networks, IEEE Transactions on,* vol. 19, pp. 308-318, 2008.

[57] T. Sugi, F. Kawana, and M. Nakamura, "Automatic EEG arousal detection for sleep apnea syndrome," *Biomedical Signal Processing and Control,* vol. 4, pp. 329-337, 10// 2009.

[58] R. Lin, R.-G. Lee, C.-L. Tseng, H.-K. Zhou, C.-F. Chao, and J.-A. Jiang, "A New Approach For Identifying Sleep Apnea Syndrome Using Wavelet Transform And Neural Networks," *Biomedical Engineering: Applications, Basis and Communications,* vol. 18, pp. 138-143, 2006.

[59] A. L. Coito, D. Belo, T. Paiva, and J. M. Sanches, "Topographic EEG brain mapping before, during and after Obstructive Sleep Apnea Episodes," in *Biomedical Imaging: From Nano to Macro, 2011 IEEE International Symposium on*, 2011, pp. 1860-1863.

[60] Z. Yuxia, Z. Haixiu, L. Wenlong, and D. Shuxue, "A snoring detector for OSAHS based on patient's individual personality," in *Awareness Science and Technology (iCAST), 2011 3rd International Conference on*, 2011, pp. 24-27.

[61] U. R. Abeyratne, S. D. Silva, C. Hukins, and B. Duce, "Obstructive sleep apnea screening by integrating snore feature classes," *Physiological Measurement,* vol. 34, p. 99, 2013.

[62] S. K. Asela, R. A. Udantha, and H. Craig, "Multi-feature snore sound analysis in obstructive sleep apnea–hypopnea syndrome," *Physiological Measurement,* vol. 32, p. 83, 2011.

[63] H. Yeh-Liang, C. Ming-Chou, C. Chih-Ming, and W. Chang-Huei, "Development of a portable device for home monitoring of snoring," in *Systems, Man and Cybernetics, 2005 IEEE International Conference on*, 2005, pp. 2420-2424 Vol. 3.

[64] A. K. Ng, T. S. Koh, E. Baey, T. H. Lee, U. R. Abeyratne, and K. Puvanendran, "Could formant frequencies of snore signals be an alternative means for the diagnosis of obstructive sleep apnea?," *Sleep Med,* vol. 9, pp. 894-8, Dec 2008.

[65] A. K. Ng, T. S. Koh, E. Baey, and K. Puvanendran, "Speech-like Analysis of Snore Signals for the Detection of Obstructive Sleep Apnea," in *Biomedical and Pharmaceutical Engineering, 2006. ICBPE 2006. International Conference on*, 2006, pp. 99-103.

[66] W. Yaqi, Z. Zhao, Q. Kun, X. Zhiyong, and X. Huijie, "Analysis of Long Duration Snore Related Signals Based on Formant Features," in *Information Technology and Applications (ITA), 2013 International Conference on*, 2013, pp. 91-95.

[67] M. A. Al-Abed, P. Antich, D. E. Watenpaugh, and K. Behbehani, "Upper airway occlusion detection using a novel ultrasound technique," in *Engineering in Medicine and*

Biology Society (EMBC), 2012 Annual International Conference of the IEEE, 2012, pp. 5650-5653.

[68] M. Cabrero-Canosa, E. Hernandez-Pereira, and V. Moret-Bonillo, "Intelligent diagnosis of sleep apnea syndrome," *Engineering in Medicine and Biology Magazine, IEEE,* vol. 23, pp. 72-81, 2004.

[69] G. Schlotthauer, L. E. Di Persia, L. D. Larrateguy, and D. H. Milone, "Screening of obstructive sleep apnea with empirical mode decomposition of pulse oximetry," *Medical Engineering & Physics,* vol. 36, pp. 1074-1080, 8// 2014.

[70] J. E. Kiriazi, O. Boric-Lubecke, and V. M. Lubecke, "Radar cross section of human cardiopulmonary activity for recumbent subject," in *Engineering in Medicine and Biology Society, 2009. EMBC 2009. Annual International Conference of the IEEE*, 2009, pp. 4808-4811.

[71] *minicircuits. [Online]*. Available: http://www.minicircuits.com/ [Accessed:

[72] *broadwavetechnoligies.* Available: http://www.broadwavetechnologies.com/ [Accessed:

[73] W. Xiaoyue, C. Mingqui, L. Macchiarulo, and O. Boric-Lubecke, "Fully-Integrated Heart Rate Variability Monitoring System with an Efficient Memory," in *Engineering in Medicine and Biology Society, 2006. EMBS '06. 28th Annual International Conference of the IEEE*, 2006, pp. 5064-5067.

[74] Mini Circuits. *Coaxial Power Splitter/Combiner*. Available: http://www.minicircuits.com/pdfs/ZFSC-2-2500.pdf [Accessed: July 20, 2014]

[75] Datasheet Archive. (2014). *ASPPT2988 data sheet*. Available: http://www.datasheetarchive.com/ASPPT2988-datasheet.html [Accessed:

[76] Mini Circuits. *ZFM-4212 Coaxial Fequency Mixer*. Available: http://www.minicircuits.com/pdfs/ZFM-4212+.pdf [Accessed: July 20, 2014]

[77] Stanford Research Systems. *Preamplifier SR560*. Available: http://www.thinksrs.com/products/SR560.htm [Accessed:

[78] Rf Beam Microwave Gmbh. (2014). *K-MC1 Radar Transceiver*. Available: http://www.rfbeam.ch/products/k-mc1-transceiver/ [Accessed: 2014]

[79] National Instruments. (2014). *NI USB-6259 Screw Terminal*. Available: http://sine.ni.com/nips/cds/view/p/lang/en/nid/202803 [Accessed: July 20, 2014]

[80] National Instruments. (2014). *NI BNC-2110 Shielded Connector Block* [Accessed: July 20, 2014]

[81] P. Byung-Kwon, V. Lubecke, O. Boric-Lubecke, and A. Host-Madsen, "Center Tracking Quadrature Demodulation for a Doppler Radar Motion Detector," in *Microwave Symposium, 2007. IEEE/MTT-S International*, 2007, pp. 1323-1326.

[82] Iber C, Ancoli-Israel S, J. Chesson Al, and Q. Sf, "The AASM manual for the scoring of sleep and associated events: rules, terminology and technical specifications," 1 ed. American Academy of Sleep Medicine, 2007.

[83] B. Peters. (2014). *Definition of WASO*. Available: http://sleepdisorders.about.com/od/sleepglossarypz/g/WASO.htm [Accessed: July 20,2014]

[84] V. M. Koval'zon, "Central mechanisms of the sleep-wakefulness cycle control," *Human Physiology,* vol. 37, pp. 500-508, 2011/07/01 2011.

[85] Gale Encyclopedia of Medicine. (2008). *REM latency. (n.d.)* Available: http://medical-dictionary.thefreedictionary.com/REM+latency [Accessed: July 20, 2014]

[86] Kendra Becker and Jeanne M Wallace. (2010). *Central Sleep Apnea* Available: http://emedicine.medscape.com/article/304967-overview [Accessed:

[87] Parveen Kumar and Micheal Clark, *Clinical Medicine*, 6 ed.: Elsevier Saunders, 2005.

[88] S. V. Stehman, "Selecting and interpreting measures of thematic classification accuracy," *Remote Sensing of Environment,* vol. 62, pp. 77-89, 10// 1997.

[89] T. Fawcett, "An introduction to ROC analysis," *Pattern Recognition Letters,* vol. 27, pp. 861-874, 6// 2006.

[90] Wikipedia. (2014). *Sensitivity and specificity*. Available: http://en.wikipedia.org/wiki/Sensitivity_and_specificity#cite_note-Fawcelt2006-1 [Accessed: July 21, 2014]

[91] Wikipedia. (2014). *Matthews correlation coefficient*. Available: http://en.wikipedia.org/wiki/Matthews_correlation_coefficient [Accessed: July 21, 2014]

[92] B. W. Matthews, "Comparison of the predicted and observed secondary structure of T4 phage lysozyme," *Biochimica et Biophysica Acta (BBA) - Protein Structure,* vol. 405, pp. 442-451, 10/20/ 1975.